

Generalized, sublethal damage-based mathematical model for improved prediction of clonogenic survival curve flattening upon hyperthermia, radiotherapy, and beyond

Adriana M. De Mendoza^{1,2,+,*}, Soňa Michlíková^{2,3,+}, Steffen Lange^{2,4}, Paula S. Castro⁵,
Anni G. Muñoz¹, Lisa Eckhardt^{2,6,7}, and Leoni A. Kunz-Schughart^{2,8,*}

¹Pontificia Universidad Javeriana, Physics Department, Bogotá, 110231, Colombia

²OncoRay—National Center for Radiation Research in Oncology, Faculty of Medicine and University Hospital Carl Gustav Carus, TUD Dresden University of Technology, Helmholtz-Zentrum Dresden — Rossendorf, 01307 Dresden, Germany

³Helmholtz-Zentrum Dresden-Rossendorf, Institute of Radiooncology - OncoRay, 01328 Dresden, Germany

⁴DataMedAssist Group, HTW Dresden—University of Applied Sciences, 01069 Dresden, Germany

⁵Universidad Distrital - Francisco José de Caldas, Bogotá, 111611, Colombia

⁶Core Unit for Molecular Tumor Diagnostics (CMTD), National Center for Tumor Diseases Dresden (NCT/UCC), Germany: German Cancer Research Center (DKFZ), 69120 Heidelberg, Germany; TUD Dresden University of Technology, Helmholtz-Zentrum Dresden — Rossendorf (HZDR), 01307 Dresden, Germany

⁷German Cancer Consortium (DKTK), Partner site Dresden, and German Cancer Research Center (DKFZ), 69192 Heidelberg, Germany

⁸National Center for Tumor Diseases Dresden (NCT/UCC), Germany: German Cancer Research Center (DKFZ), 69120 Heidelberg, Germany; TUD Dresden University of Technology, Helmholtz-Zentrum Dresden — Rossendorf (HZDR), 01307 Dresden, Germany

* Author to whom correspondence should be addressed

+ These authors contributed equally to this work

ABSTRACT

Mathematical modeling can offer valuable insights into the behavior of biological systems upon treatment. Different mathematical models (empirical, semi-empirical, and mechanistic) have been designed to predict the efficacy of either hyperthermia (HT), radiotherapy (RT), or their combination. However, mathematical approaches capable of modeling cell survival from shared general principles for both mono-treatments alone and their co-application are rare. Moreover, some cell cultures show dose-dependent saturation in response to HT or RT, manifesting in survival curve flattenings. An advanced survival model must, therefore, appropriately reflect such behavior. We propose a cell survival model to predict the effect of both treatments based on the general principle of sublethal damage (SLD) accumulation for the induction of cell death and irreversible proliferation arrest. Our approach extends Jung's model on heat-induced cellular inactivation by incorporating dose-dependent recovery rates that delineate changes in SLD restoration. The resulting unified model (Umodel) accurately describes not only HT but also RT survival outcomes, is applicable to simultaneous thermoradiotherapy modeling, and particularly suited to reproduce and predict survival curve flattening phenomena. We demonstrate the Umodel's robust performance ($R^2 \gtrsim 0.95$) based on numerous clonogenic cell survival data sets from the literature and our experimental studies.

Introduction

Radiotherapy (RT) continues to be the second most common medical intervention prescribed to more than half of the patients diagnosed with cancer^{1,2}. Even though RT is very potent in reducing the tumor mass, the dose required to cure the patient can often not be applied due to high radiotoxicity in the adjacent normal tissues. Therefore, combining RT with local or selective radiosensitizing moieties can be crucial for better (curative) therapeutic outcomes. Heat is one of the most potent radiosensitizers, achieving thermal enhancement ratios (TER) as high as 8.0 in *in vivo* studies³⁻⁶. A growing number of recent topic-related publications and, to this date, 55 reported active or completed clinical trials evidence the revival of thermoradiotherapy (TRT) in cancer research and treatment⁷, mainly motivated by state-of-the-art advances in a localized, spatially, and temporally controlled heat application⁸⁻¹⁴.

Tumor response to treatment and prediction of patient survival are both based on cell survival models, which are translated by mathematical approaches or simulations into tumor control probabilities (TCPs)¹⁵⁻¹⁷. Different mathematical models (empirical, semi-empirical, and mechanistic) have been designed to predict the efficacy of RT, HT, and their combination. Only mechanistic models allow the development of new therapeutic approaches based on a hypothesis-driven understanding of synergistic biological effects. Furthermore, as soon as biological treatment planning is integrated into the clinical routine of TRT, suitable and valid mechanism-based mathematical models are required for a personalized treatment design. The accuracy of such models will then be of critical importance. On the one hand, underestimation of cell killing can lead to overtreatment with unnecessarily high radiation doses, resulting in unwanted side effects and other related problems. On the other hand, if the model overestimates cell killing, the treatment will be planned with radiation doses accompanied by side effects but insufficient to control the malignancy, thus resulting in tumor relapse and, most probably, progression of the disease.

For ionizing radiation, the LQ model offers one of the most robust approaches to predicting the survival fraction in RT treatments¹⁸. It was initially developed as an empirical approach, which later gained mechanistic interpretations related to the probabilities of radiation-induced DNA damage¹⁹. The validity of these interpretations is still a matter of debate. Most importantly, however, the LQ model is not suited for mechanistically describing the effects of hyperthermia, as DNA breaks are usually not induced by conventional HT regimes (40-50 °C)²⁰. Likewise, other mechanistic approaches, such as the Repair-Misrepair model²¹, the Local Effect Model (LEM)²², and the Giant Loop Binary Lesion model²³, are also explicitly suited for RT. Similarly, the various mathematical strategies to model HT-induced cell killing are not readily applicable to RT responses, and there is poor consensus on the underlying biology²⁴⁻²⁸.

Regarding TRT, a component reflecting the HT-induced radiosensitization has to be implemented in addition to the cumulative cell killing by the two individual therapies. Several proposed models provide good empirical approximations ($R^2 \geq 0.95$), as summarized in our previous publication²⁹. A comprehensive overview of the major mathematical approaches currently available for modeling cell survival upon RT, HT, and TRT is given in the supplemental information (section SI.1) Tables SI.1a-c. Evidentially, mathematical approaches capable of modeling cell survival from shared general principles for both mono-treatments alone and for their co-application are rare, in particular, mechanical models that can contribute to a better understanding of the synergistic effects of the combined therapy. Notably, many of the models referenced above encounter limitations at low-survival or high-dose regimes, where the cell kill is overestimated, e.g., at the tail of the logarithmic survival curves, which are typically straight for mono-RT³⁰. Some alternative mathematical models deal with this issue³¹⁻³⁴. Still, these models poorly reproduce those clonogenic survival curves that are severely affected by thermal or radiation-dose dependent changes in cell population recovery, e.g., among others, due to alterations in the kinetics of DNA repair, protein refolding, metabolic adaptations, or the existence of resistant subpopulations. Such effects are expressed as further straightening or flattening of the clonogenic cell survival curves and occur in various cell types subjected to ionizing photon or heavy ion radiation and upon moderate HT. The phenomenon of survival curve flattening has, for example, been observed in the radiation response of lymphocytes^{35,36}, a gold standard *in-vitro* assay for determining individual radiosensitivities in humans. Therefore, an advanced survival model must appropriately reflect such behavior.

We advocate that a meaningful mechanistic model must allow the accumulation of sublethal damage (SLD) to encompass the effects of heat and irradiation in mono- and combination treatments. Only a few models incorporate this feature^{25,27,33}. However, these models are suited only for combined TRT and cannot emulate the respective mono-therapies. The same is true for our recently introduced model for simultaneous TRT, which is based on thermodynamic principles, where radiosensitization is defined as an accumulation of HT-induced SLD²⁹. In the present study, we propose Jung's model as a coherent basis to (i) describe the effect of RT, HT, and TRT from shared underlying principles and (ii) reproduce survival curves presenting saturation of the cell-killing effect with increasing dose. Jung's model stipulates that cells lose their reproductive capacity due to damage accumulation in discrete stages without reliance based on general mechanistic principles. This assumption provides the advantage to illuminate the harm induced by any therapy (i.e., ionizing radiation or heat). As we demonstrate, Jung's model very well describes clonogenic cell survival under HT and RT mono-treatments. However, it does not contain components delineating changes in SLD restoration rates. Hence, it can neither reflect the effects of HT on the repair of RT-induced DNA damage, a fundamental phenomenon in HT-induced radiosensitization, nor the flattening of the survival curve.

In the newly presented approach, we modified Jung's model²⁵ by incorporating a dose-dependent rate of SLD recovery. The recovery rate is modeled as an effective enzymatic reaction, accounting for all possible restoration mechanisms of accumulated non-lethal damage at the cellular or the population level. The radiosensitizing effect of HT is mathematically implemented by reducing the repair rates for the RT-induced damage upon HT. These modifications improve the accuracy in predicting dose-response relationships. We conducted a thorough and comprehensive testing of our "unified" model (Umodel) on various cell survival data from the literature and our experimental data in a panel of human head and neck squamous cell carcinoma (HN-

SCC) cell lines, where HT and RT were applied individually and in combination. In the mono-treatment cases, we compare the goodness-of-fit of the Umodel to the standard LQ, the LQC, and Jung's models, yielding comparable or, in selected cases, preferable results. The latter is particularly noticed when therapeutic phenomena such as thermal adaptation or high-dose radioresistance are observed. Here, we demonstrate the ability of the Umodel to predict straightening and flattening survival curves with superior fidelity. The LQC model often performs slightly better in data fitting but is not plausible for prediction. Our findings, therefore, support using the Umodel for plausible predictions of cell survival upon TRT in biological treatment planning. The report concludes by discussing the advantages and limitations of the newly developed Umodel, providing an outlook, and suggesting possible future uses and improvements.

The key biological terms used in this work are specified as follows (adapted from De Mendoza et al. 2021²⁹):

- **Sublethal cell damage:** Any non-lethal deterioration of cellular processes, regardless of origin and kinetics, that advances the cell toward a dead state. In the Umodel, the sublethal damage accumulates with rate r .
- **Sublethal damage repair:** Any cellular process, regardless of underlying biological mechanism and kinetics, leading to restoration of the sublethal damage. In the Umodel, repair is defined only as a rate $q(t)$ with which the cell 'returns' to the previous compartment.
- **Cell kill (“dead state/compartment”):** From the radiotherapeutic perspective, cells are considered to be dead (killed) when they have lost their reproductive capacity, i.e., they are no longer able to divide and become replication-incompetent. It encompasses cells losing their membrane integrity and cells truly dying by apoptosis, necrosis, or other mechanisms, but also living cells undergoing terminal differentiation, permanent cell cycle arrest, or senescence. This type of cell kill leads to the control of a malignant disease, independent of the underlying process. In the Umodel, the dead state is a final compartment reached when a cell cannot accumulate more sublethal damage.
- **Cell survival (“alive state/compartment”):** A cell is considered to survive if it remains replication-competent, i.e., when retaining reproductive capacity after treatment. In the Umodel, the cell is alive in all compartments (n) from $n = 0$ to n_{\max} .

Methods

Development of the “Umodel”

Original Jung's model

Jung's model considers an infinite number of SLD accumulation stages, also called compartments. At the n -th stage, a fraction of surviving cells endures n non-lethal lesions. The probability that the cell is in the n -th compartment, also reflecting the fraction of cells in the compartment, is given by the solution of the detailed balance equation

$$\frac{dP_n(t)}{dt} = -rP_n(t) - ncP_n(t) + rP_{n-1}(t), \quad (1)$$

which is a time-continuous Markov chain. It describes the time evolution of the probability at the n -th compartment in a way that cells can advance in a sequence of SLD with a rate r , or escape to death with a rate nc , proportional to the stage of non-lethal damage accumulation (Figure 1). Here, r is defined as the rate of SLD accumulation, and c is the rate of damage fixation, which refers to processes that prevent further damage repair in a non-reversible manner. Thus, the state of the cell population is given by the probability vector $\vec{P}(t) = (P_0(t), P_1(t), P_2(t), \dots, P_n(t), \dots)^T$, whose n -th element is the probability that the cell is in the n -th compartment at time t . Jung's original approach, initially proposed to model the effect of heat on *Chinese hamster ovary* (CHO) cells *in vitro*, very well reproduces the HT outcome²⁵. In this case, the advance rate r between consecutive compartments in the chain of non-lethal damage is constant.

Equation (1) is solved under the following boundary conditions:

1. In the first compartment ($n = 0$), cells are in their initial undamaged state, a pivotal starting point. They are only damaged and move forward after the onset of the treatment $\frac{dP_0(t)}{dt} = -r_0P_0(t)$.
2. At $t = 0$, immediately before the start of treatment, $P_{n=0}(0) = 1$ and $P_n(0) = 0$ (for $n \geq 1$). Accordingly, the initial condition can be written as the state vector $\vec{P}(t=0) = (1, 0, 0, 0, \dots, 0)^T$.

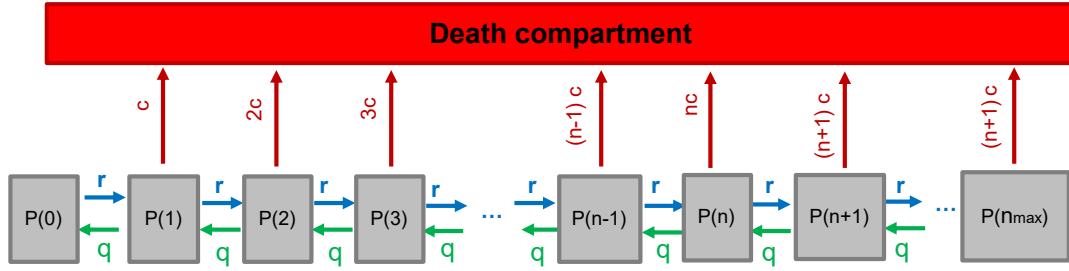


Figure 1. Compartment model of cell killing by HT. The original Jung's model²⁵ is represented by the scheme without regression rates q (green arrows). Our proposed modification called Umodel includes regression rates q (green arrows). In the Umodel (as in Jung's), compartments constitute a basis of possible states of the cell population, and $P(n)$ is the proportion (probability) of the population in the n -th state.

3. The concept of cell killing is straightforward: it requires damage. Hence, the cell undergoes at least one stage of damage before dying.

Furthermore, the evolution of the state vector is expressed as $\frac{d\vec{P}(t)}{dt} = \hat{A}\vec{P}(t)$, where the elements of the transition matrix \hat{A}_{ij} define the influx rate from $n = j$ to $n = i$, and the diagonal elements are the net flux at each stage. The survival probability is given by the probability of being in any of the non-lethal damage compartments:

$$\mathcal{S}(t) = \sum_{n=0}^{\infty} P_n(t). \quad (2)$$

In Jung's original model, the applied thermal dose is proportional to the treatment time for a fixed heat intensity (determined by the temperature) $D = \dot{D}(T)t$. When cellular damage is inflicted, biological responses are triggered and may take seconds to days to complete^{37,38}. In HT treatments with conventional heat sources, the dose rate is the pace of heat deposition and is related to temperature. The treatment temperature is usually set in HT experiments, i.e., the exposure time determines the applied total thermal dose. In the case of RT in preclinical, experimental settings, the dose rate is usually pre-determined by the power of the irradiation device; the desired total dose is then administered by adjusting the exposure time. Thus, time refers to treatment duration, while damage advancement and fixation rates depend on the dose rate \dot{D} . For the dose rates typically used in external-beam radiotherapy, the exposure times (duration of single RT treatment or fraction) are relatively short, and the concomitant rapid induction of DNA damage is generally counteracted by repair processes taking place on a different time scale³⁹. Hence, cell recovery or (reproductive) death do not occur during the short treatment interval of RT; the survival outcome thus depends, in most cases, on the applied irradiation dose but not the dose rate.

Regression rate in Jung's model

Jung's model does not include the possibility of regressing in the chain of SLD. We incorporate this feature to describe possible tissue adaptation or recovery. We consider two possibilities for the regression rate q , dependent either on the stage of damage n or the treatment time t , to ensure we cover all potential scenarios. When an n -dependent regression rate q_n is included in Jung's model, the net advance rate $r_n = r - q_n$ changes with the level of SLD. The general solution of $P_n(t)$ is presented in Section SI.2 of the supplementary information (Eq. (SI.2)), and the survival probability is given by $\mathcal{S}(t) = \sum_{n=0}^{n_{max}} P_n(t)$, where we have assumed that a finite number n_{max} of SLD stages are populated. We tried different stage-dependent functions for q_n (cf. Eqs. (SI.4)-(SI.6)), but the results yielded no improvement over the original Jung's model.

After ruling out a stage-dependent regression, we examine a dose-dependent regression function, i.e., treatment time t for a fixed \dot{D} . Including a time-dependent function $q(t)$ also makes the transition matrix $\hat{A} \rightarrow \hat{A}_t$ time-dependent. In this particular case, the detailed balance equation reads

$$\frac{dP_n(t)}{dt} = -r(t)P_n(t) - ncP_n(t) + r(t)P_{n-1}(t), \quad (3)$$

The net advance rate in the SLD chain in Eq. (3) is then given by

$$r(t) = r - q(t). \quad (4)$$

The solution is approximated at first order in the Magnus expansion as

$$\vec{P}(t) = e^{\hat{A}_t} \vec{P}(t=0), \quad (5)$$

with integrated transition matrix $\hat{A}_t = \int_0^t dt' \hat{A}(t')$ equal to

$$\hat{A}_t = \begin{pmatrix} -\int_0^t dt' r(t') & 0 & \dots & 0 \\ \int_0^t dt' r(t') & -\int_0^t dt' (r(t') + c) & \ddots & \vdots \\ 0 & \int_0^t dt' r(t') & \ddots & 0 \\ \vdots & \ddots & \ddots & \vdots \\ 0 & \dots & 0 & -\int_0^t dt' (r(t') + (n_{max} - 2)c) \\ & & & \int_0^t dt' r(t') & 0 \\ & & & & -\int_0^t dt' (r(t') + (n_{max} - 1)c) \end{pmatrix}. \quad (6)$$

Since it is impossible to calculate all the contributions from an infinite series, we assess the error as the contribution of the first order, assuming that each next order contributes less and less for a repair function that is saturating to a constant value. Moreover, if the parameter k is small relative to treatment time, the time-dependent regression rate saturates fast to a constant value, and the error does not increase with treatment time. Therefore, we calculate the error of $\vec{P}(t)$ as the difference between the probabilities at first and second order. This results in small error values when the parameters are almost constant throughout treatment. As an example, using the Umodel's parameters obtained for UT-SCC-14 cells under 44.5 °C HT, the error values ranged below 10^{-4} at $t = 1$ min and below 10^{-46} at $t = 60$ min (more details shown in SI section SI.3, Eqs. (SI.7)-(SI.9)).

As radiation- and heat-induced damage is detected and restored by enzymatic mechanisms, we propose to model the regression process (in time) by means of an "effective" enzymatic reaction representing the average kinetics of the restored molecules in the cell population. Detailed mathematical models have been proposed for some of the intracellular processes involved in DNA repair and protein refolding, introducing and numerically solving large sets of coupled differential/integral equations^{30,40-46}. These frameworks lead to the desired regression rates but require numerous adjustable parameters, makingv those approaches unsuitable for practical survival models. Therefore, we introduce a source (damage) term into the Michaelis-Menten (MM) kinetics, an approach adapted to cover all cellular restoration processes based on common enzymatic reactions with a single average function. The underlying MM model consists of four differential equations describing the following enzymatic chemical reaction:



Here, $[E]$, $[S]$, and $[P]$, denote the concentrations of the enzyme, the substrate (damaged molecule), and the product (restored molecule), respectively. $[E \cdot S]$ refers to the concentration of enzyme-substrate intermediate complex. In this equation, the enzyme E is associated to a substrate molecule S . This step occurs at rate k_f but can also be reversed at rate k_r . After the interaction, the enzyme dissociates unchanged, and the substrate turns into a product molecule P . This part of the process occurs with a rate of catalysis k_{cat} ⁴⁷. After including the source of damage r into the substrate and product equations, the time-evolution of the concentrations is given by:

$$\begin{aligned} \frac{d[E]}{dt} &= -k_f[E][S] + (k_r + k_{cat})[E \cdot S] \\ \frac{d[S]}{dt} &= -k_f[E][S] + k_r[E \cdot S] + r \\ \frac{d[E \cdot S]}{dt} &= k_f[E][S] - (k_r + k_{cat})[E \cdot S] \\ \frac{d[P]}{dt} &= k_{cat}[E \cdot S] - r[P]. \end{aligned} \quad (8)$$

Since the source term r in the substrate kinetics is the rate of SLD production, it connects the enzymatic process with Jung's model. Under a quasi-steady state approximation, the enzyme-substrate complex is assumed to be constant $\frac{d[E \cdot S]}{dt} = 0$. Accordingly, after upregulation, the total enzyme concentration remains constant ($\frac{d[E]}{dt} = 0$ and equal to the initial value

$[E] + [E \cdot S] = [E]_0$). The net rate of molecular mending $\frac{d[P]}{dt}$ is obtained by subtracting the damage rate from the damage regression rate $\frac{d[P]}{dt} = q(t) - r[P]$. This means that the regression rate can be modeled as:

$$q(t) = k_{cat}[E \cdot S] = \frac{q_{max}[S]}{k' + [S]}, \quad (9)$$

where $q_{max} = k_{cat}[E]_0$, and $k' = \frac{k_r + k_{cat}}{k_f}$. The solution of Eq. (8) for the concentration of impaired molecules (substrate) reads

$$[S] = \frac{k'}{q_{max} - r} \left[r + q_{max} W_0 \left(\frac{-e^y}{k q_{max}} \right) \right]. \quad (10)$$

Here W_0 is the principal branch of the Lambert function, with $y = \frac{(q_{max} - r)^2 t - k r}{k q_{max}}$. Since $[S]$ is a monotonically increasing function of time, we keep it to first order in the Taylor expansion $[S] \sim [S]_0 + r t$ to simplify the model. This approximation is valid in the regime of slow advance rates. Assuming also $[S]_0 = 0$ at the beginning of the treatment, Eq. (9) gets

$$q(t) = \frac{d[P]}{dt} = \frac{q_{max} t}{k + t}, \quad (11)$$

with $k = k'/r$ being the average time to achieve the half of the maximum cellular capacity of mending impaired molecules, yielding a sigmoid rise of the repaired molecules over time. This is in line with the functional forms documented in^{30,41}, but with the advantage of only requiring two adjustable parameters. The temperature dependence of the repair parameters adhering to the MM kinetics is explained as follows: the maximum/saturation value of the repair function $q_{max} = E_0 k_{cat}$, depends on the initial amount of repair enzymes E_0 , which is influenced by the treatment stimuli, such as heat. The turnover number k_{cat} reflecting enzyme efficiency and the time to achieve the half response $k = (k_r + k_{cat})/(k_f r)$ are also conditional on temperature, with each (average) chemical rate following an Arrhenius-type behavior. In this way, the parameters in the regression rate $q(t, T)$ can be linked to average temperature-dependent biochemical responses.

By inserting Eq. (11) into Eq. (4), the survival probability reads:

$$S(t) = \exp \left\{ \frac{\int_0^t r(t') dt'}{ct} [1 - ct - e^{-ct}] \right\}, \quad (12)$$

with $\int_0^t r(t') dt' = r t - q_{max} \left[t + k \ln \left(\frac{k}{k + t} \right) \right]$. Notably, the treatment time can be exchanged by the total dose ($t \rightarrow D$) in Eq. (12), given that the dose rate is constant throughout the treatment. This variable substitution only changes the units of the adjustable parameters r, c, q_{max} , and k .

At first glance, our model with a regression rate closely resembles the Multi-Hit-Repair (MHR) model of Scheidegger et al.³³, which describes the effects of RT and HT-induced radiosensitization (notably, the MHR model is not designed to reflect HT mono-treatment). However, the mathematical concepts defining doses and rates differ critically. In the MHR model, RT and HT doses are represented by state variables Γ and Λ , proportional to dose rate (R) and repair protein damage (k_1), counteracted by dose-dependent repair rates (γ and k_2), respectively. The SLD accumulation rate is proportional to R , with a constant damage fixation rate. In contrast, our model specifies a constant SLD advance rate r and a fixation rate c proportional to the SLD accumulation stage n . Furthermore, in the MHR approach, the probability of repair from RT and TRT damage decreases exponentially with dose. On the contrary, in our model, repair is upregulated by treatment intensity, saturating at a maximum value. This unique feature of our model, among others, sets it apart from the MHR model, providing a comprehensive and distinct approach to describing the clonogenic survival curve flattening at higher doses.

Multiparametric optimizations

We utilize the versatile non-linear least-square minimization of the python package `lmfit`⁴⁸ to fit the necessary parameters of each model, i.e., the radiosensitivities (α, β) of the LQ-model, the advance and damage fixation rates (r and c) of Jung's model, and the parameters (r, c, q_{max} , and k) of the Umodel (see Eq. (12)). All values are adjusted using the Levenberg-Marquardt algorithm^{49,50} to fit the corresponding biological effect ($-\ln(S)$), experimentally obtained from the survival assays. The parameters are determined by minimizing the residuum ϵ of the biological effect

$$\epsilon = \sum_i [\ln S_i - \ln f_S(x_i, \{\gamma\})]^2. \quad (13)$$

Here, i is a label for each survival probability S_i in the experimental data set, $\{\gamma\}$ is the set of adjustable parameters, and $f_S(x_i, \{\gamma\})$ is the corresponding prediction of the survival probability from the applied model. We set reasonable boundaries for the parameters, i.e., typically $r[\text{min}^{-1}] \in [0, 50]$, $c[\text{min}^{-1}] \in [0, 1]$, $Q_{\max}[\text{min}^{-1}] \in (0, 50]$, $k[\text{min}] \in (0, 1]$, $\alpha[\text{Gy}^{-1}] \in [0, 1]$ and $\beta[\text{Gy}^{-2}] \in [0, 1]$. Note that, while any fit for r and c in Jung's model is in principle also valid for the Umodel with $q_{\max} = 0$, we explicitly restrict the minimization to different parameter values ($q_{\max}, k > 0$). The parameters' standard error (estimated 1σ error-bar) is also obtained from the optimization, and reported (Tables [SI.9](#), [SI.10](#)).

We must emphasize that the existence of several local minima for the error function hinders the search for a global solution. Thus, different values of adjustable parameters may produce similar values of $R^2 \sim 1$. This disadvantage is called "lack of identifiability", a significant problem in mathematical models of biological systems⁵¹⁻⁵³. It is important to note that lack of identifiability is not the same as *overfitting*. Overfitting occurs when a model is too complex and includes parameters that are unnecessary to represent the data accurately. For instance, the parameters α and β of the LQ model are very identifiable, while Jung's model lacks identifiability despite the same number of adjustable parameters. In our model, the lack of identifiability is inherited from Jung's original model. To help overcome this problem, we restrict the solution space to parameters that satisfy the thermodynamic prediction described in²⁹. This condition improves the identifiability of the parameters in HT but does not fully solve it. As highlighted in the results section, the thermodynamic condition states that the SLD rate should grow exponentially with treatment temperature. Hence, for the Umodel in HT, r is also restricted to depend exponentially on temperature. Moreover, we presume that the maximum repair rate q_{\max} follows the trend of the inflicted damage. Accordingly, to reduce the ambiguity of the fitted parameters, we similarly imposed the exponential condition on q_{\max} , for which the model reproduces the experimental data equally well. To account for these restrictions, the parameters at all temperatures T are optimized simultaneously for each cell line, and the deviation of the functions $r(T)$, $q_{\max}(T)$ from linear fits $\log[r(T)] = b(T - T_g)$, $\log[q_{\max}(T)] = b^*(T - T_g^*)$, is added to the residuum. This way, the parameters r and q_{\max} do not have to exhibit perfect exponential dependencies, which would be the case if they are directly replaced by exponential functions with the parameters b , T_g , b^* , and T_g^* in the optimization. Instead, matching the fitted r , q_{\max} with exponential functions in terms of the corresponding coefficient of determination R^2 serves as an additional quality control of the model assumptions (see Table [SI.8](#) and Figs. [SI.2](#), [SI.7](#), and [SI.8](#)).

In all the cases, the resulting goodness-of-fit is reported by the coefficient of determination R^2 concerning the logarithm of the survival fraction. In addition, the corresponding Akaike information criterion AIC is reported to account for the impact of the degrees of freedom. (see Tables [SI.9](#), [SI.10](#)). Note that due to the exponential dependencies of r and q_{\max} , the model has effectively fewer degrees of freedom when fitting survival fractions at several different temperatures. For instance, when fitting data at N_T temperatures, there are effectively $4 + 2N_T$, instead of $4N_T$, fit parameters. Like other multiparametric optimization methods, the Levenberg-Marquardt algorithm is an iterative procedure that depends on the initial estimate of the parameter set $\{\gamma\}_0$ and only converges to the global minimum if the initial estimate is already close to the solution.

Experimental methods

Cell culturing

Eight human HPV-negative HNSCC cell lines were applied in this study: SAS and HSC4 (HSRRB/JCRB, Osaka, Japan), UT-SCC-5, UT-SCC-14, and UT-SCC-60A (University of Turku, Finland), Cal33 (DSMZ, Germany), XF354 (DKFZ, Germany), and a subline of the FaDu-ATCC HTB-43 model (Dresden, Germany)⁵⁴. Before use, the cell lines' genetic profile was verified via microsatellite analyses at the Institute of Legal Medicine (TU Dresden, Germany). They were also routinely tested free of mycoplasmas using a PCR Mycoplasma Kit (AppliChem, Darmstadt, Germany), as detailed earlier⁵⁵. The cell cultures were grown from validated frozen stocks for >2 to 620 passages (<120 cumulative population doublings) and cultured in standard Dulbecco's Modified Eagle Medium (DMEM) with L-glutamine, D-glucose (1 g/L) and 25 mM HEPES supplemented with 10% heat-inactivated fetal calf serum (FCS) and 1% penicillin/streptomycin (10,000 U/mL/ 10 mg/mL). Cells were kept in a humidified air atmosphere with 8% CO₂ at 37 °C. All culture media, supplements, solutions, and buffers were purchased from PAN- Biotech (Aidenbach, Germany).

Colony formation assay (CFA)

Exponentially growing cultures were enzymatically dissociated using 0.05% trypsin/0.02% EDTA in phosphate-buffered saline (PBS) to obtain single-cell suspensions. A CASY® TTC analyzer (Roche Innovatis, Reutlingen, Germany) was used to monitor cell culture quality and assess cell numbers and volumes in the single-cell suspensions for further use. Cells were then

diluted appropriately and seeded in 6-well plates in cell line- and treatment-dependent concentrations using 1 ml of supplemented DMEM per well. Cells were incubated at 37 °C for 20-24 h (less than one culture doubling for all of the cell lines) to allow adherence and overcome a potential proliferative lag phase due to the dissociation procedure. Plates were then exposed to HT and/or RT. After completion of treatment, 1 ml of supplemented DMEM medium was added to each well for extended culturing at standard conditions. The culture period for colon formation ranged between 7 and 14 days, according to ≥ 5 cell line-specific culture doublings. The colonies were then washed with PBS, fixed for 10 min with 80% ethanol followed by staining with a Coomassie blue solution. Colonies with ≥ 50 cells were manually counted at low magnification to determine plating efficiencies and calculate survival fractions (S) of the treated samples relative to untreated controls. The choice of CFA setup is briefly discussed in Section [SI.4](#). All data used in the present study derive from $N \geq 3$ independent experiments with $n = 3$ biological repeats.

Implementation of treatment: Hyperthermia and irradiation

All hyperthermia treatments were performed using a pre-heated temperature-controlled PST-60HL-4 Plate Thermo-Shaker (BioSan, Latvia). The 6-well plates were transferred into the pre-heated shaker for defined times at temperatures of 40.5°C to 46.5°C, comprising the entire treatment period - from placing the plates in the device to removing them. As a prerequisite, heating profiles in selected wells were recorded for different temperature settings via a TC-08 8-channel thermocouple data logger (Pico Technology, UK) combined with type T thermocouples (RS Components, UK) before using the system for standardized HT treatment, according to⁵⁶ to confirm that the target temperature in the 2-D culture setting is reached within a few minutes and the cooling period is negligible. Control plates were incubated in parallel at 37°C in the standard incubator. In the HT+RT treatment regimes, cells were irradiated at room temperature with 0 - 6 Gy single dose X-rays (200 kV; 0.5-mm Cu filter, approx. 1.32 Gy/min; Yxlon Y.TU 320 (Yxlon.international, Germany)) applied directly after completion of exposure to HT. The RT mono-treatment data used for modeling were acquired similarly but have been published previously⁵⁵.

Inclusion criteria for experimental data sets from the literature

Cell survival curves as a function of the applied dose were included only if they presented at least five experimental data points per curve. For RT, we exclusively extracted survival curves displaying dose-dependent flattening from the referenced literature. In these data sets, the dose needed to be given in Gy and the irradiation power reported in the original articles. For HT, the dose had to be expressed as treatment time for at least three different temperatures. Experimental points and error bars (when reported) from each data set were extracted using *WebPlotDigitizer*[®]. The names of the cell models follow the Cellosaurus nomenclature. Details of all data from the literature used in this study are given in [Table 1](#).

Results and Discussion

In this work, we have developed a mathematical model to best describe clonogenic survival upon both radiation and hyperthermia mono-treatments and their combination. Our research shows that Jung's approach, initially designed to model cell survival after heat exposure, is also suitable for reproducing clonogenic survival curves after single-dose irradiation. This finding suggests that Jung's model could be a versatile tool for predicting both therapies' outcomes based on the accumulation of sublethal damage regardless of the energy type and a specific underlying cell death mechanism. However, Jung's basic model does not comprise a component of cellular recovery, which is essential to delineate the impact of heat on proteins of the DNA damage repair machinery. Therefore, as detailed in the Methods section, we propose a modified Jung's model (termed Umodel) that mathematically incorporates a regression rate. We applied the Umodel to clonogenic dose-response survival curves recorded in our laboratory for several HNSCC cell lines exposed to RT and HT treatments. Overall, the U-model demonstrates an improved performance, particularly in reflecting and predicting the survival of cell populations that display changes in cellular recovery with increasing dose manifested as straightening or flattening of the clonogenic cell survival curves. To emphasize this feature further, we fitted the Umodel to additional data reported in the literature (cf. [Table 1](#)). The subsequent subsections present the results of multiparametric optimizations, demonstrating at least one set of parameters that lead to good performance in each case. The goodness-of-fit of the proposed Umodel is compared with the original Jung's models as well as the LQ and the LQC model. For the latter two the sign of the quadratic and cubic term is explicitly not restricted, such that these models are capable to reflect the straightening of survival curves³⁴. More examples of the Umodel applied to HT or RT treatments can be found in [Sections SI.5 and SI.6](#) respectively.

Rationale and performance of the Umodel in HT and RT mono-treatment modeling

In experimental radiotherapy, the LQ model stands as a stalwart, providing a robust approach to predicting the survival fraction as a function of the irradiation dose¹⁸. However, in the widely accepted mechanistic explanation by Chadwick and Leenhouts¹⁹, the LQ-model parameters (α and β) represent the appearance and accumulation of DNA double-strand breaks, which are not directly inflicted upon HT exposure. Despite the LQ model's simplicity and good performance, this discrepancy hinders its

Table 1. Data set details including cell type, treatment strategy and literature source

Used data sets of RT or HT individually applied						
Source	Cell line	Entity (cell type)	Treatment	HT temperatures [°C]	Displays flattening	
					RT	HT
Own experiments	Cal33	human HNSCC	HT,RT	42.5, 44.5, 46.5	no	no
	HSC4	human HNSCC	HT,RT	42.5, 44.5, 46.5	no	no
	SAS	human HNSCC	HT,RT	42.5, 44.5, 46.5	no	no
	FaDu	human HNSCC	HT,RT	42.5, 44.5, 46.5	no	no
	XF354	human HNSCC	HT,RT	42.5, 44.5, 46.5	no	no
	UT-SCC-5	human HNSCC	HT,RT	42.5, 44.5, 46.5	no	no
	UT-SCC-14	human HNSCC	HT,RT	42.5, 44.5, 46.5	no	at 44.5 °C
	UT-SCC-60A	human HNSCC	HT,RT	42.5, 44.5, 46.5	no	no
25	CHO	chinese hamster ovary	HT	40, 41, 41.5, 42, 42.5, 43.5, 44, 44.5	-	no
57	Hela	human cervical carcinoma	HT	41, 42, 43, 44, 45	-	at 41, 42, 43 °C
58	CFU-MG	murine bone marrow granulocyte–macrophage progenitor	HT	41.8, 42, 42.3, 42.5, 43, 44	-	at 42, 42.3 °C
59	CCD-18Lu	normal human lung fibroblasts	HT	41, 43, 45	-	at 41, 43, 45 °C
59	WiDr	human colon carcinoma	HT	41, 43, 45	-	at 41, 43 °C
59	A549	human lung carcinoma	HT	41, 43, 45	-	at 41, 43, 45 °C
59	U87MG	human glioblastoma-astrocytoma	HT	41, 43, 48	-	at 43 °C
28	CHO	Chinese hamster ovary	HT	41.5, 42, 42.5, 43, 43.5, 44, 44.5	-	at 41.5, 42, 42.5 °C
60	CHO	Chinese hamster ovary	HT	42.2, 42.3, 42.4, 42.5	-	all
61	C3H/10T1/2	mouse embryonic spontaneously immortalized cell line	RT (Xray)	-	no	-
62	HepG2	human hepatoblastoma	RT (¹² C)	-	yes	-
62	HepG2	human hepatoblastoma	RT (¹⁶ O)	-	yes	-
62	HUH7	hepatocellular carcinoma	RT (¹² C)	-	yes	-
62	PLC	hepatocellular carcinoma	RT (¹² C)	-	yes	-
63	SW1353	human chondrosarcoma	RT (¹² C)	-	yes	-
63	HDF	normal human dermal fibroblasts	RT (¹² C)	-	yes	-
64	CHO-xrs-5	X-ray hypersensitive mutant of CHO	RT (¹² C)	-	yes	-
31	HCT116	human colon cancer	RT (Xray), HT	45, 46, 47	no	no
65	CHO	chinese hamster ovary	RT (Xray), HT	42.5, 43	no	no

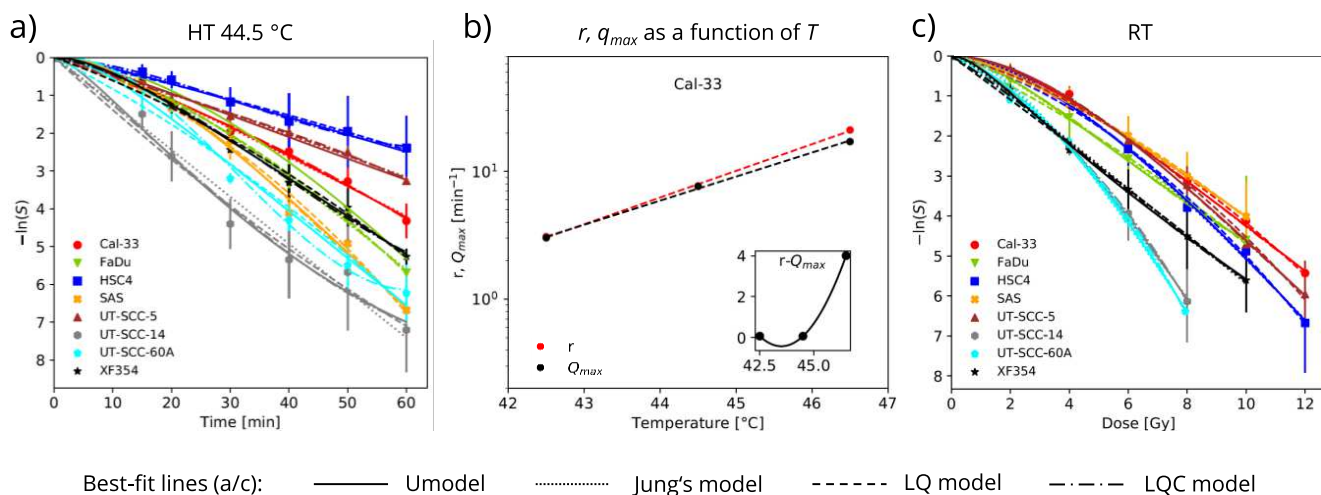


Figure 2. The Umodel shows comparable performance to the Jung's, LQ, and LQC models to resemble clonogenic survival in HNSCC cells upon HT and RT mono-treatment. Symbols represent cell survival fractions ($-\ln(S)$) of eight human HNSCC cell lines exposed to a) HT at 44.5°C or c) 0-12 Gy single dose Xray⁵⁵. The experimental, clonogenic survival curves for 42.5°C and 46.5°C are reported in Figure SI.1. Data show means (\pm SD) from $N = 3$ independent experiments with the models' best-fit lines. The coefficients of determination R^2 , AIC values and parameters' uncertainties are listed in Tables SI.2 and SI.3. The advance rate in the SLD chain r and the maximum repair rate q_{max} determined from a) are documented as function of temperature in supplementary Figure SI.2 and exemplified for Cal-33 cells in b) with exponential fits (dashed lines); the inset displays the difference between the two parameters on a linear scale.

translation to the cellular survival processes under HT. In contrast, considering an underlying mechanism of SLD accumulation, Jung's model promises to describe the damage induced by any treatment in a more general way. This untapped potential of Jung's model is an encouraging avenue for further exploration.

For the hyperthermia treatment, we experimentally determined the clonogenic survival curves in eight HNSCC cell lines as a function of HT exposure time at three different temperatures: 42.5 °C, 44.5 °C, and 46.5 °C (Figure 2a, Figure SI.1). In principle, all four models - Jung's, LQ, LQC, and Umodel - perform similarly well, except for the UT-SCC-14 cell line at 44.5 °C (see Table SI.2, for R^2 , AIC and parameters' uncertainties). UT-SCC-14 cells present a significantly different behavior at this temperature than the other cell models, as the survival curve critically flattens with longer HT exposure times (Figure 2a). In this case, the Umodel achieves better results. These observations indicate that the dose-dependent regression rate is not essential for curves with typical shoulders, and a constant SLD rate suffices. However, it is crucial for populations that show reduced cytotoxic effects as doses rise.

Since different sets of parameters in the Umodel lead to good fitting, we used a thermodynamic condition that restricts the rates r and q_{max} to grow exponentially with increasing temperature²⁹. As described in the Methods section, this condition aids the fitting and offers insight into some underlying phenomena and correlations without increasing the number of adjustable parameters of the model. For most HNSCC cell types, the difference between the damage and regression rates increases with temperature, and the curves start deviating as exemplified for the Cal-33 cell in Figure 2b (other cell line data are shown in Figure SI.2; the q_{max} values are listed in Table SI.2).

Figure 2c presents the clonogenic survival with all fittings (LQ, LQC, Jung's and Umodel) for our previously published data sets obtained from the same eight HNSCC cell types treated with 200 kV X-rays instead of HT⁵⁵. In these cases, the Umodel again gives coefficients of determination comparable to the other models (see detailed results, R^2 , AIC and parameters' uncertainties in Table SI.3). Since repair speed and saturation might be encoded in the slope of the survival curves, we also tested the Umodel for the experimental data from Wells and Bedford⁶¹, who recorded RT survival curves for C3H/10T1/2 cells using three different radiation dose rates (0.49 Gy/h, 2.4 Gy/h, 55.8 Gy/h). The Umodel again demonstrated excellent fit results comparable to the benchmark models. To adjust the Umodel, we made assumptions based on the numbers of damaged target molecules and repair/response-associated mechanisms. Here, it is important to note that the common variances in the dose rates documented in preclinical therapy experiments and in clinical routine procedures when delivering individual fractions (1

- 5 Gy/min) do not affect the biological kinetics of DNA damage induction and repair³⁹. This differs from the application and study of real low-dose-rate irradiations³⁹ and ultra-high-dose rate FLASH radiotherapy⁶⁶, which is beyond the scope of the present study but might be subject to future mathematical modelings.

Based on these assumptions, we considered the dose rate as the sequential application of two small fractions within a finite interval, with T as the target molecules (e.g., DNA) and M as the repair/response molecules. The first fraction then damages the portion T^* of T and repairs M^* of M . During the interval, the remaining $(M - M^*)$ molecules initiate the damage response of T^* . With the second fraction, this process iterates. If no interval exists, both fractions concurrently damage $2A^*$ and $2M^*$ molecules, leaving fewer $(M - 2M^*)$ molecules to respond to more damaged targets $2T^*$. This simplified approach suggests that sublethal damage (r) accumulates similarly in both treatment scenarios, and the maximum repair capacity (q_{max}) is equally affected. However, the activation time for the repair mechanisms (k) and the conversion rate from sublethal to lethal damage (c) increase due to frequent injury. Thus, we fixed the rates r and q_{max} in the Umodel and observed a monotonic increase in rates c and k , achieving a goodness-of-fit coefficient of $R^2 \geq 0.98$. Figure SI.3 visualizes the results; all values, including R^2 and AIC uncertainty parameters, are detailed in Table SI.4.

Our model nicely reflects the flattening of the survival curve, as the sigmoidal regression function given by Eq. (11) is upregulated and saturates to q_{max} with increasing doses or treatment times. This behavior is not mimicked by models where the treatment doses reduce repair. The feature is particularly relevant for predicting treatment outcomes. Indeed, while all models quite well resemble any existing data points, some of them critically fail in prediction. The lack of predictive power becomes evident in extrapolated fittings, such as those shown for HT in Figure 3a-c. Notably, the non-mechanistic LQC model, which in most cases seems to perform best in data fitting (see Tables SI.2 to SI.3), is exceptionally poor in prediction beyond the existing data points (see for example curve fittings for UT-SCC-60 cells at 44.5 °C and 46.5 °C HT, SAS and FaDu cells at 46.5 °C, or HSC4 and UT-SCC-5 cells at 42.5 °C). In this context, we observed plausible results with the Umodel when applied to saturating (flattening) and non-saturating HT cell survival curves. In contrast, reasonably extrapolated fittings are achieved with all four models for the HNSCC clonogenic survival data upon RT; notably, none of the latter RT survival curves exhibit flattening (Figure 3d). Because of the Umodel's overall favorable performance, we emphasize its predictive power for future applications.

Emphasis on the peculiarity of survival curve flattening

Our observation prompted us to test the Umodel further using more HT and RT survival data from the literature displaying the specific behavior of treatment response adaptation and clonogenic survival curve flattening. In principle, Jung's model fails to reproduce this type of data. The regression function introduced in the Umodel (Eq. (11)) critically improves the capability of the model to describe the referred behavior of the cellular population, such that the Umodel performs better than the LQ, the LQC, and Jung's model in those cases, see Table 2. Again, most prominently, the Umodel shows more realistic predictions beyond the reported experimental data. The results highlighted hereafter document all fittings and their extrapolated predictions side-by-side.

Hyperthermia and thermal-adaptation. When cell cultures under HT become more resistant to increasing thermal doses, the logarithmic clonogenic survival curves start flattening⁶⁷. We call this behavior adaptation to treatment. It is cell line-dependent and especially frequent for cells exposed to mild HT. We experienced such behavior in some of our HNSCC models, and similar observations come from several independent literature data sets documenting clonogenic survival upon HT treatment^{25,28,57-60}. In these cases, Jung's model reaches the limit of a straight line since it does not include possible cell recovery and mitigation of thermal damage. This is where our proposed modified model, the Umodel, comes in. It predicts clonogenic survival under these circumstances more precisely, as visualized in Figure 4 and Figures SI.4 to SI.6; Tables SI.5 to SI.6 document the respective fit data. The corresponding increase in the rates r and q_{max} with temperature is reported in Figures SI.7 to SI.8.

We hypothesize that cell cultures exposed to moderate HT, particularly around $\approx 43^\circ\text{C}$, adapt to stressful conditions by up-regulating survival mechanisms and enhancing recovery. Consequently, the decline in the survival rate slows down as the exposure time increases, and the expected shoulder of the survival curve ($-\ln(S)$) no longer takes place. Several studies have shown that the response to HT is triggered by protein denaturation, where heat shock proteins (HSPs) are activated, and heat shock factors (HSFs) are upregulated in a nonlinear manner⁴²⁻⁴⁶. Our work comprises, and mathematically simplifies, those regulatory mechanisms through a modified Michaelis-Menten model, capable of describing the nonlinear rise of the refolded proteins during the exposure time, as dictated by Eq. (9). Introducing a mending rate (Eq. (11)) into Jung's model (Eq. (12)) thus mathematically defines the adaptation to treatment.

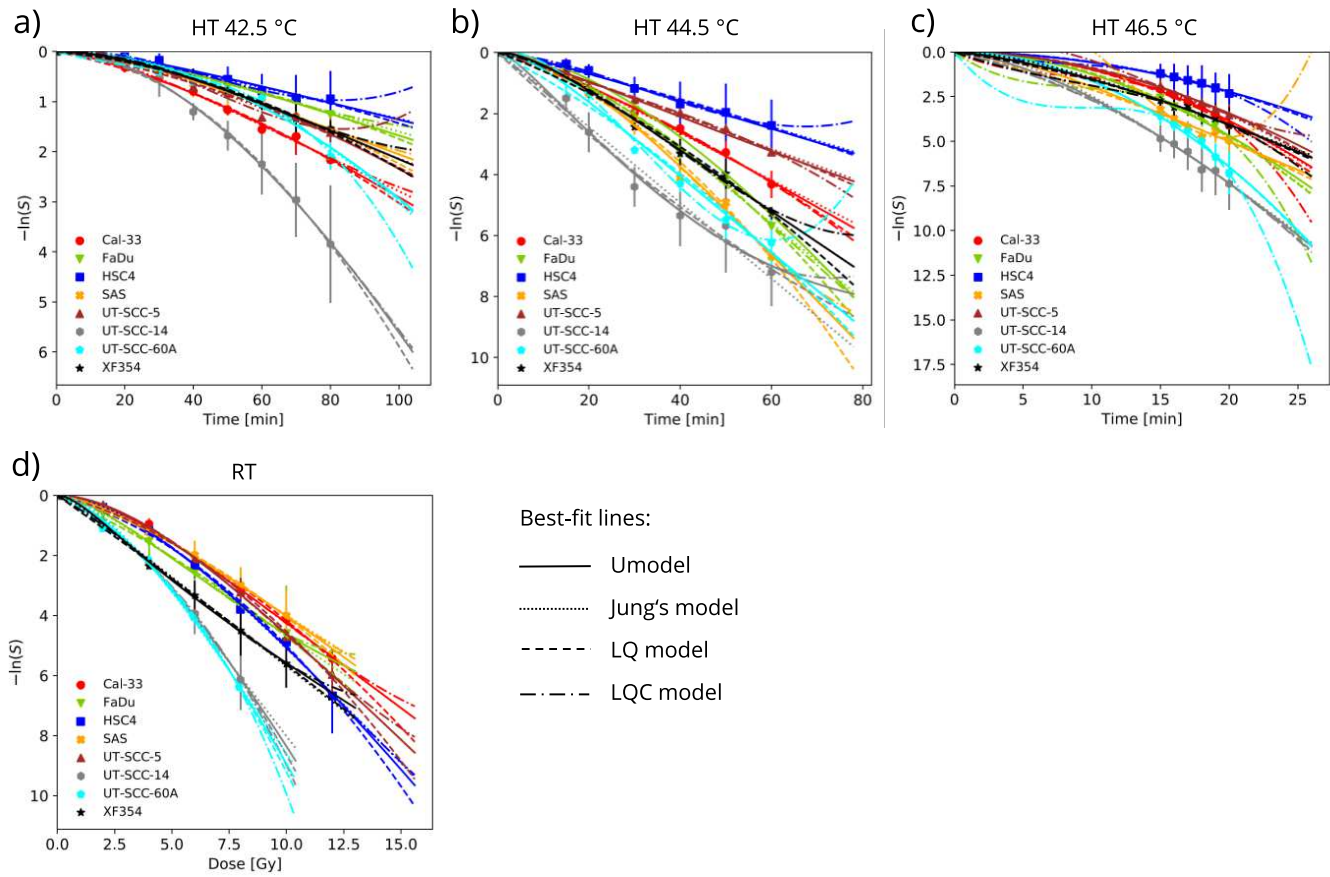


Figure 3. Extrapolations indicate plausible HT and RT survival outcome predictions with the Umodel but not the LQC model. All model fittings from Figures 2a),c) and SI.1 describing a-c) HT and d) RT responses in HNSCC cells are extrapolated up to 130% of the total thermal/radiation dose.

Irradiation and the high-dose radioresistance phenomenon. A meta-study from 2021⁶⁸ compared the outcomes of ion beam irradiation with reference photon irradiation (X-ray), surveying *in vitro* clonogenic cell survival data across the literature. The authors identified several experimental series showing signs of cell resistance with higher radiation doses, i.e., the linear-quadratic behavior at lower doses transitioning into a purely logarithmic or flattening (saturating) dose-response relationship at higher doses. The flattening in the survival curve is expressed as negative β -values in the LQ model fittings. This may lead to even concave line of best fit and also contradicts the mechanistic interpretation of the radiobiological parameters in the LQ model¹⁹. The LQC model addresses this discrepancy by employing an additional cubic term in the exponent of the LQ model. We, therefore, next tested the LQ and the LQC models versus the Umodel in three of such data sets extracted from published literature, ensuring a thorough and meticulous process. Again, we discover the Umodel's superior performance in prediction. The results, documented in Figure 5 are a testament to the robustness of our approach. Table SI.7 provide a comprehensive summary of all parameters and R^2 values.

An early mechanistic interpretation of the high-dose radioresistance phenomenon in single-dose irradiation experiments suggests that cell subpopulations with different sensitivities co-exist. Here, the resistant subpopulations dominate clonogenic survival at higher doses, manifesting a "resistant tail" of the survival curve⁶⁹. The regression rate of the Umodel reflects such scenarios to some extent by encompassing an average upregulation in the DNA repair capacity. A more recent alternative hypothesis by Friedrich et al.²² proposes a model based on the spatial distribution of the DSBs within a discrete organized chromatin region on a megabase pair scale - a giant loop. In this case, the deviation from the survival curve at higher radiation doses predicted via the LQ model is attributed to the formation of clustered DNA damage, defined as the mutual effect of DSBs over more considerable genomic distances. The model assumes the highest radiation efficiency if precisely two DSBs are induced within one loop. More than two DSBs on average per loop do not linearly enhance the radiation response. As a consequence, the relative contribution to lethality per DSB decreases, and a saturation effect occurs²³. This phenomenon may

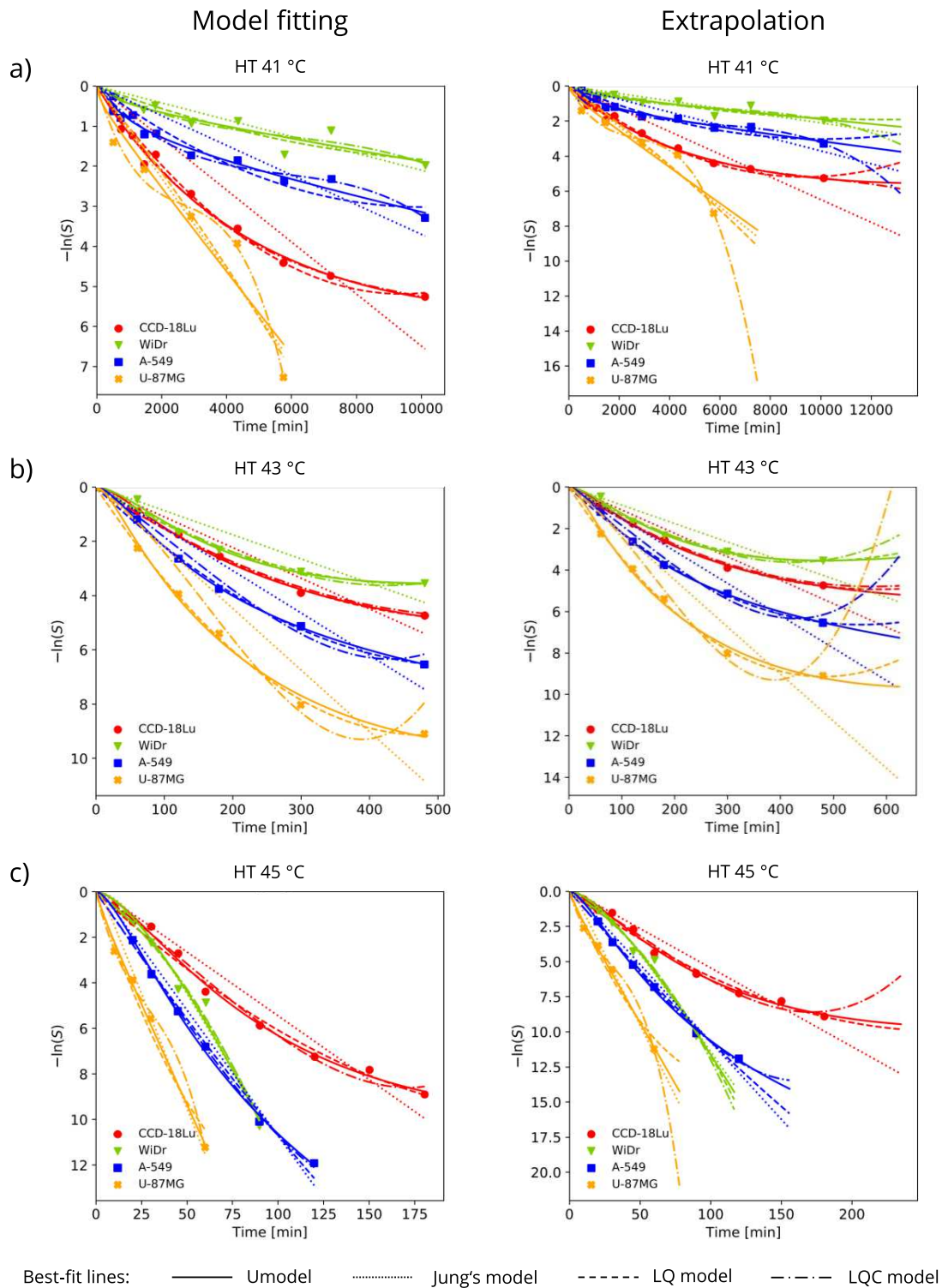


Figure 4. The Umodel shows better performance than the Jung's, LQ, and LQC models in fitting and predicting flattening clonogenic survival curves upon HT. Symbols represent cell survival fractions ($-\ln(S)$) obtained from clonogenic assay data extracted from the literature; selected data from different human cell types - normal human fibroblasts CCD-18Lu, lung carcinoma A-549, glioblastoma-astrocytoma U-87MG, and colon carcinoma WiDr- exposed to HT at a) 41°C, b) 43°C, and c) 45°C⁵⁹ are shown. The data are fitted with the Umodel, Jung's, and the LQ and LQC models (left panel) and the resulting curves extrapolated up to 130% of the maximal treatment time (right panel). The coefficients of determination R^2 , AIC values and parameters' uncertainties are listed in Tables SI.6 and SI.9. Additional supporting data are documented in Figure SI.8.

Table 2. Comparison of R^2 values for all cases displaying flattening in the clonogenic survival curves.

Cell line	Treatment	LQ model R^2	LQC model R^2	Jung's model R^2	Umodel R^2
CCD-18Lu ⁵⁹	HT 41 °C	0.989	0.992	0.846	0.993
A-549 ⁵⁹	HT 41 °C	0.932	0.983	0.824	0.978
WiDr ⁵⁹	HT 41 °C	0.878	0.903	0.827	0.898
CCD-18Lu ⁵⁹	HT 43 °C	0.998	0.997	0.939	0.998
WiDr ⁵⁹	HT 43 °C	0.986	0.988	0.872	0.995
A-549 ⁵⁹	HT 43 °C	0.998	0.987	0.928	1.000
U87MG ⁵⁹	HT 43 °C	0.999	0.958	0.885	0.997
A-549 ⁵⁹	HT 45 °C	0.995	0.999	0.984	0.999
CCD-18Lu ⁵⁹	HT 45 °C	0.991	0.992	0.961	0.995
CFU-GM ⁵⁸	HT 42 °C	0.994	0.994	0.984	0.994
CFU-GM ⁵⁸	HT 42.3 °C	0.978	0.982	0.980	0.987
CHO ²⁵	HT 41 °C	0.991	0.993	0.992	0.992
CHO ²⁸	HT 41.5 °C	0.769	0.770	0.684	0.801
CHO ²⁸	HT 42 °C	0.961	0.968	0.659	0.973
CHO ²⁸	HT 42.5 °C	0.956	0.967	0.884	0.987
CHO ⁶⁰	HT 42.2 °C	0.983	0.989	0.886	0.995
CHO ⁶⁰	HT 42.3 °C	0.985	0.985	0.861	0.988
CHO ⁶⁰	HT 42.4 °C	0.988	0.988	0.922	0.991
CHO ⁶⁰	HT 42.5 °C	0.989	0.989	0.804	0.991
Average		0.966	0.969	0.880	0.976

Cell line	Treatment	LQ model R^2	LQC model R^2	Jung's model R^2	Umodel R^2
SW1353 ⁶³	RT	0.999	0.995	0.987	1.000
HDF ⁶³	RT	0.996	0.990	0.996	1.000
XRS5 ⁶⁴	RT	0.977	0.977	0.953	0.982
Average		0.991	0.987	0.979	0.994

explain the lower effectiveness of higher doses as reflected by straight or flattening tails of the survival curves. Such a mechanism is expected to be more critical for high LET/particle irradiation, i.e., the probability of inducing cluster DNA damage is higher than for conventional X-rays²³. Variation in the LQ model β values with LET have already been demonstrated^{68,70}. This particular mechanistic link has not yet been considered in our model. However, the reduced lethality at higher doses can still be modeled as a decreased advance rate r , equivalent to the more effective repair in the Umodel.

While not our primary focus, we shall emphasize that the radiation response curve flattening phenomenon is also observed in lymphocytes. Indeed, clonogenic survival assessment in peripheral blood lymphocytes has been a gold standard *in vitro* assay for determining individual radiosensitivities in humans. However, response rates may also derive from distinct analytical endpoints and may not unequivocally overlap with clonogenic survival outcomes. A 2023 comprehensive review of *in vitro* and *in vivo* studies in this field revealed that lymphocyte response curves based on different analytical endpoints show more shallow slopes and saturation at higher doses in most cases³⁵. Pham *et al.* recently presented a mathematical saturation model assuming a Poisson distribution of cell survival over DNA damage to better reflect the radiation response of lymphocytes³⁶. This model performed better than the LQ model when surviving fractions were estimated from apoptosis (rate) detection. While this seems reasonable in lymphocyte response assessment, it is known that the survival of cancer cells upon radiation is not related to apoptosis induction. Therefore, our model development focuses on clonogenic survival curve flattening only, thereby avoiding the exclusion of any specific mechanism leading to permanent loss of reproductive capacity referring to radiotherapeutic “cell kill” as highlighted earlier (see Introduction: key biological terms).

Survival curve flattening in the context of RT and metabolic targeting. The Umodel allows for mathematical simulation of different damage sources. Hence, it can also be considered for modeling the outcomes of simultaneous combination therapies. For demonstration, we next applied the Umodel to selected clonogenic cell survival data of a previously published study from our laboratory, where we identified cases of survival curve flattening when combining RT with a metabolic targeting strategy⁵⁵. Here, a panel of HNSCC cell lines was deprived during clonogenic survival assessment of the proteinogenic amino acid argi-

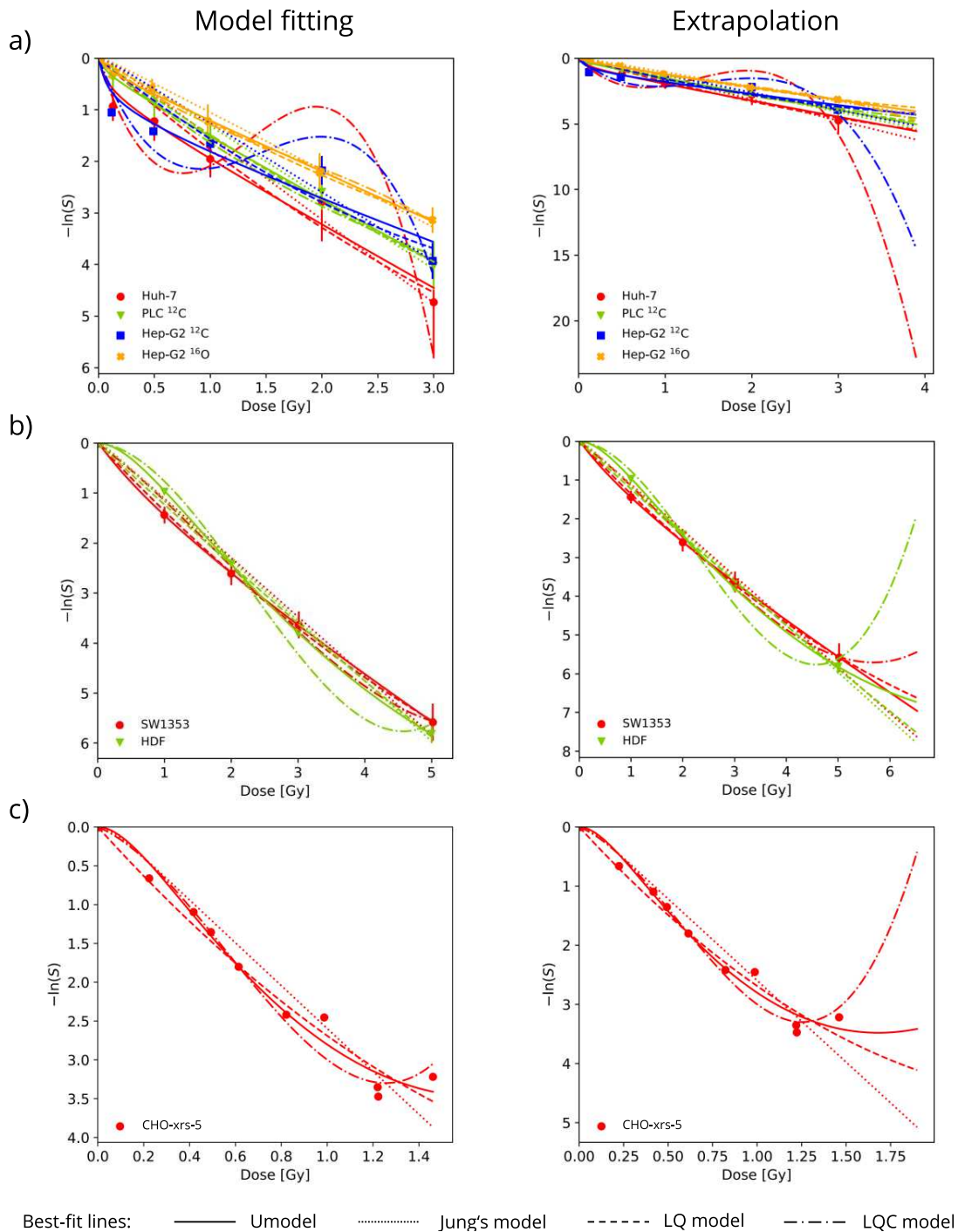


Figure 5. The Umodel shows better performance than the Jung's, LQ, and LQC models in fitting and predicting flattening clonogenic survival curves upon particle RT. Symbols represent cell survival fractions ($-\ln(S)$) obtained from clonogenic assay data extracted from the literature; a) human hepatocellular carcinomas Huh-7 and PLC and hepatoblastoma HepG2 exposed to carbon ions ¹²C and hepatoblastoma HepG2 exposed to oxygen ions ¹⁶O⁶² b) chondrosarcoma SW1353 and normal human dermal fibroblasts HDF exposed to carbon ions ¹²C⁶³, c) radiosensitive mutant of Chinese hamster ovary cells CHO-xrs-5 exposed to carbon ions ¹²C⁶⁴. The data are fitted with the Umodel, Jung's, and the LQ and LQC models (left panel) and the resulting curves extrapolated up to 130% of the maximal treatment time (right panel). The coefficients of determination R^2 , AIC values and parameters' uncertainties are listed in Tables SI.7 and SI.9.

nine for 24 hours before and throughout irradiation and compared to RT alone. Jung's model and the Umodel fit most of the selected data series very well. However, those survival curves that display a flattening course at higher radiation doses are again reproduced more precisely by the Umodel and the LQC approach as opposed to Jung's initial and the LQ model (Figure 6, Table SI.10). Mechanistically, the decrease in the slope of the treatment outcome ($-\ln(S)$) for this simultaneous combinatorial treatment could be explained by the potential existence of subpopulations with different sensitivities and responsiveness to proteogenic and ER stress resulting from the extended lack of arginine. According to the RT and HT mono-treatments, the model appears better suited for predicting the response to combinatorial therapy beyond the existing data points than the LQC model. In summary, our fittings to these data sets thus further demonstrate the versatility of the Umodel for generalized predictions that do not rely on a single or selective underlying biological mechanism. Accordingly, we expect the Umodel also to predict the outcomes of simultaneous TRT. However, TRT is most frequently provided consecutively without or with a treatment gap between the individual modalities. Accordingly, more complex interrelations must be considered, requiring advanced mathematical combination treatment modeling, as will be briefly highlighted in the next chapter.

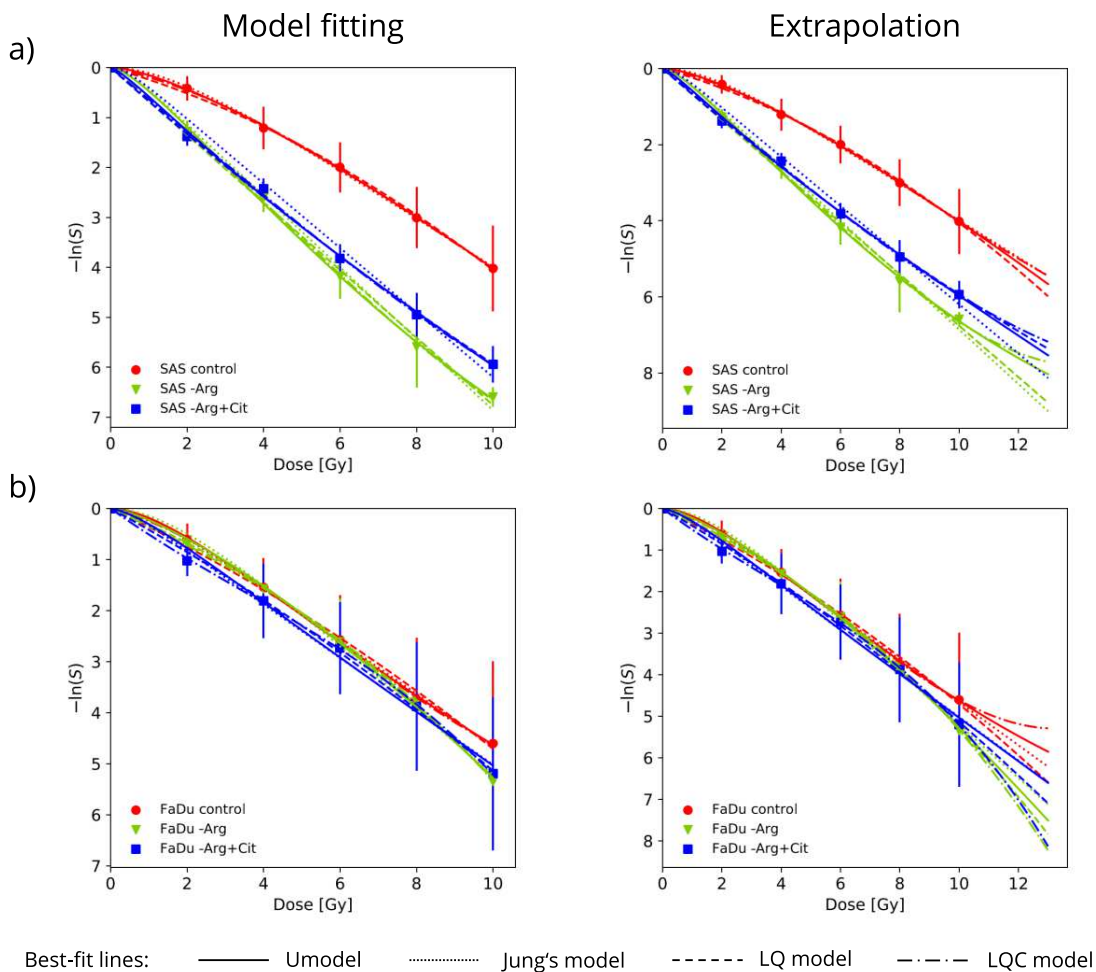


Figure 6. The Umodel performs well in resembling and predicting clonogenic survival upon simultaneous combinatorial RT employing different damage sources: an example of metabolic targeting therapy simultaneously applied with RT in two HNSCC cell lines. Symbols represent cell survival fractions ($-\ln(S)$) obtained from clonogenic assays using a) SAS and b) FaDu HNSCC cell lines exposed to metabolic stress conditions, i.e., arginine deprived without (-Arg) or with citrulline enrichment (-Arg+Cit), combined with 0-10 Gy of single dose X-ray irradiation⁵⁵. Data show means (\pm SD) from $N = 3$ independent experiments and the best-fit lines of all mathematical models of interest (left panel). The fittings are also extrapolated up to 130% of the maximal radiation dose (right panel). The coefficients of determination R^2 , AIC values and parameters' uncertainties are listed in Table SI.10.

Taken together, survival curves that do not conform to the standard LQ model can appear upon HT and irradiation mono-

treatments and simultaneous combinatorial RT. The pressing need for more generalizable mathematical models is underscored by the fact that the underlying phenomena also have profound relevance for treatment planning and prognosis in the clinical setting. The limitations of the current models in capturing the full complexity of these survival curves further emphasize the necessity of our proposed Umodel, which includes a regression function between consecutive stages of SLD accumulation, making it versatile and applicable for atypical clonogenic survival curves.

Considerations, challenges and perspectives in modeling TRT with the Umodel

As a starting point for the sustained added value of our unique approach, we here demonstrate the first application of the Umodel to survival data of two HNSCC cell lines treated consecutively with HT and RT. Notably, these data sets do not show any flattening. Anyways, our mathematical approach, describing therapy outcome via SLD accumulation, has been adapted to encompass various biological aspects affecting the state of the cells and cell populations within the compartments for the TRT setting. The radiosensitizing efficacy of HT has been widely proven in different *in vitro* and *in vivo* models of various normal and cancer cell types^{4,56,71–74}. One of the most plausible mechanisms proven to explain, at least partially, the thermal enhancement of ionizing radiation is the impairment of the DNA-repair machinery that fix the radiation-induced damage. This additional synergistic effect might be the result of thermal denaturation of DNA-repair enzymes, particularly affecting the base excision repair (BER) and homologous recombination (HR) pathways, as observed in various mouse and human cell types^{5,75–77}.

In the adapted Umodel, the parameters of the mono-treatments, i.e., RT and HT at different temperatures, are calibrated independently as before. Since the combined treatment in our data sets starts with hyperthermia, outcome is computed by integrating the set of ordinary differential equations of the Umodel Eq. (1) with the parameters of hyperthermia mono-treatment. The proposed HT-RT synergistic effect mainly depends on the impact of HT on repair and is functionally implemented by the enhancement of sublethal damage of RT. From thermodynamic principles, linear and exponential relations of SLD augmentation with HT treatment time and temperature, respectively, are considered. Mathematically this is achieved by adjusting, i.e., reducing, the maximal RT repair rate q_{\max} , affecting the probabilities of cells within successive compartments and the overall progress towards the death compartment, see Section SI.7. In principle, the Umodel will allow to model the outcomes for different treatment orders and is also considered to mimic the impact of treatment gaps which shall be the focus of future work.

According to the highlighted scheme, the Umodel is fitted to experimental clonogenic survival data of FaDu and SAS HNSCC cells which were first exposed to three different HT treatments (40.5 °C, 42.5 °C, and 44.5 °C for 15-30 minutes) and then immediately thereafter irradiated with 0–6 Gy single dose X-ray. Notably, the gap between applications in the combined treatment has effectively been null in all of these experiments. Averaged clonogenic survival curves from $N = 3$ independent experiments and the respective Umodel fittings are documented in Figure SI.9, showing the expected excellent performance; the fitting parameters are summarized in Table SI.11. With rising temperatures, the model predicts an increase in the SLD rate as expected, but counterintuitively shows a decrease in the damage fixation rate of radiation (see Figure SI.10 (e-f), and c values in Table SI.11). This observation is difficult to interpret but clearly leads to new mechanistic hypotheses to be addressed in future studies by specifically designed experiments.

The main limitation of the proposed Umodel is the lack of identifiability of its parameters inherited from Jung's model. Lack of identifiability is quite a common problem in mathematical models and is receiving increasing attention in the applied mathematics community^{51–53}. It follows from the fact that some parameters correlate with each other, and therefore, different sets of parameter values lead to very similar goodness-of-fit within the uncertainty of the experimental data. This flaw in the model hinders the interpretation of the specific parameter values and their association with the sensitivity of different cell types to treatment. Consequently, in this paper, we can describe trends of the parameters as a function of thermal or radiation dose but not yet the biological meaning of the specific parameter values. Nevertheless, the parameter trends can provide more insights into the underlying phenomena because they come from simultaneous fitting to several independent data sets. One way to improve the identifiability is to restrict the multiparametric space, as we have done by introducing thermodynamic conditions for the dependence of the model parameters on HT exposure time and temperature. However, the problem still needs to be fully solved; more specific experimental data describing DNA damage and repair would be helpful to validate our current predictions and define a reasonable physiological range for the parameters, improving their identifiability. For instance, extensive experimental quantification of enzyme activities relevant to DNA repair or protein refolding upon treatment would help to refine the proposed model regarding its biological relevance and robust interpretability.

Conclusions and Outlook

In this work, we extended Jung's model, which initially described clonogenic cell survival after HT, to also predict radiation treatment outcomes and incorporate adaptation to therapy. Due to its compartmental structure, the developed unified model (Umodel) allows the accumulation of SLD without assuming or excluding any particular mechanism of injury. This feature and its mathematical formulation make the model suitable for describing/predicting the therapeutic outcome of the individual treatments (RT, HT) and their synergistic combination based on the same general principles. The thermodynamic condition for the HT dependence of the Umodel's parameters helps the fitting, supporting protein denaturation as a plausible explanation for radiosensitization. Our consistent approach opens a range of options for further model developments and strategic therapy outcome predictions, e.g., to account for differences in sequential treatments with intervals between them, which could not yet be implemented.

Since the Umodel model rests on the accumulation of non-lethal damage, it also naturally allows the inclusion of pro-survival mechanisms, modeled as effective enzymatic reactions. This characteristic is highly relevant to describe tumor cells that can adapt to treatment, e.g., some cell subpopulations under selected radiation treatments or mild hyperthermia. Our model of enzymatic restoration of damaged molecules contains several simplifications encompassing different processes such as DNA repair, protein refolding, or the redistribution of subpopulations due to heterogeneity and plasticity. Through an effective overall enzymatic reaction, the Umodel is able with only two adjustable parameters to reproduce and predict even atypical average outcomes of the entire cell populations. The high predictive power of the Umodel is stressed especially in cases presenting adaptation to treatment and flattening of survival curves, where other models may fail.

The Umodel describes effects as damage accumulation and death in cell cultures as a function of the heat or radiation dose, assessed by treatment time at fixed dose rates. Future extensions of the model could incorporate chronological time. For calibration, this requires additional analytical endpoints of cell damage and death after treatment that can be monitored over time, such as DNA damage and repair or factors reflecting regulated and non-regulated cell death processes. Moreover, our unique model possesses two crucial attributes that broaden its potential applications, which we plan to explore in future work. Firstly, treatment is represented mathematically as an operator that modifies the initial state of the cell population. Secondly, it provides a closed expression for cell survival. We envision that these features will facilitate outcome prediction of sequential treatments applied in different orders and varying recovery intervals between them. Fractionated treatment scenarios may also be explored. We further propose its direct incorporation into more complex mathematical models of multicellular dynamics, such as tumor spheroids, to predict *in vivo*-like, more clinically translational outcomes⁷⁸.

Authors contributions

A.M.D.M. conceived the presented idea and developed the theory. S.M. and L.A.K-S designed and supervised the experiments. S.M. and L.E. performed the experiments. A.M.D.M., P.S.C, S.L., and A.G.M. performed the numerical calculations and analyses. All authors contributed to the interpretation of the results. A.M.D.M., S.M., S.L, and L.A.K-S designed and wrote the manuscript. L.A.K-S. supervised the project

Acknowledgments

This work was supported by the German Federal Ministry of Education and Research (BMBF; 03Z1N512; 16dkwn001). We thank Ms. Marit Wondrak for technical support of the biological experiments and Dr. Damian D. McLeod and Dr. Oleg Chen for helpful discussion.

References

1. Chandra, R. A., Keane, F. K., Voncken, F. E. M. & Thomas, C. R. Contemporary radiotherapy present and future. *The Lancet* **398**, DOI: [10.1016/S0140-6736\(21\)00233-6](https://doi.org/10.1016/S0140-6736(21)00233-6) (2021).
2. Begg, A. C., Stewart, F. A. & Vens, C. Strategies to improve radiotherapy with targeted drugs. *Nat. Rev. Cancer* **11**, 239–253, DOI: [10.1038/nrc3007](https://doi.org/10.1038/nrc3007) (2011).
3. Overgaard, J. The heat is (still) on: The past and future of hyperthermic radiation oncology. *Radiother. Oncol.* **109**, 185–187, DOI: [10.1016/j.radonc.2013.11.004](https://doi.org/10.1016/j.radonc.2013.11.004) (2013).
4. Overgaard, J. Simultaneous and sequential hyperthermia and radiation treatment of an experimental tumor and its surrounding normal tissue in vivo. *Int. J. Radiat. Oncol.* **6**, 1507–1517, DOI: [10.1016/0360-3016\(80\)90008-5](https://doi.org/10.1016/0360-3016(80)90008-5) (1980).
5. Mei, X. *et al.* Radiosensitization by hyperthermia: The effects of temperature, sequence, and time interval in cervical cell lines. *Cancers* **12**, DOI: [10.3390/cancers12030582](https://doi.org/10.3390/cancers12030582) (2020).

6. Elming, P. B. *et al.* Hyperthermia: The optimal treatment to overcome radiation resistant hypoxia. *Cancers* **11**, DOI: [10.3390/cancers11010060](https://doi.org/10.3390/cancers11010060) (2019).
7. Clinicaltrials. <http://ClinicalTrials.gov>. 55 clinical trials reported active or completed for cancer treatment with hyperthermia and radiation. Accessed: Jul-30-2024.
8. Kok, H. P. *et al.* Heating technology for malignant tumors a review. *Int. J. Hyperth.* **37**, 711–741, DOI: [10.1080/02656736.2020.1779357](https://doi.org/10.1080/02656736.2020.1779357) (2020).
9. Georgios P. Skandalakis, C. D. R. A. B. J. G. J. R. D. B., Daniel R. Rivera & Hadjipanayis, C. G. Hyperthermia treatment advances for brain tumors. *Int. J. Hyperth.* **37**, 3–19, DOI: [10.1080/02656736.2020.1772512](https://doi.org/10.1080/02656736.2020.1772512) (2020).
10. Schupper, A. J., Chanenchuk, T., Racanelli, A., Price, G. & Hadjipanayis, C. G. Laser hyperthermia: Past, present, and future. *Neuro-Oncology* **24**, S42–S51, DOI: [10.1093/neuonc/noac208](https://doi.org/10.1093/neuonc/noac208) (2022).
11. lian, Y. *et al.* Recent advances on the magnetic nanoparticle–based nanocomposites for magnetic induction hyperthermia of tumor: a short review. *Adv. Compos. Hybrid Mater.* **4**, 925–937, DOI: [10.1007/s42114-021-00373-3](https://doi.org/10.1007/s42114-021-00373-3) (2021).
12. Cheng, Y. *et al.* The role of hyperthermia in the multidisciplinary treatment of malignant tumors. *Integr. cancer therapies* **18**, 1–11, DOI: [10.1177/1534735419876345](https://doi.org/10.1177/1534735419876345) (2019).
13. Paulides, M. M., Verduijn, G. M. & Van Holthe, N. Status quo and directions in deep head and neck hyperthermia. *Radiat. Oncol.* **11**, 1–14, DOI: [10.1186/s13014-016-0588-8](https://doi.org/10.1186/s13014-016-0588-8) (2016).
14. Kang, J. K. *et al.* Principles and applications of nanomaterial-based hyperthermia in cancer therapy. *Arch. Pharmacol Res.* **43**, 46–57, DOI: [10.1007/s12272-020-01206-5](https://doi.org/10.1007/s12272-020-01206-5) (2020).
15. Hillen, T., de Vries, G., Gong, J. & Finlay, C. From cell population models to tumor control probability: Including cell cycle effects. *Acta Oncol.* **49**, 1315–1323, DOI: [10.3109/02841861003631487](https://doi.org/10.3109/02841861003631487) (2010).
16. Naqa, I. E. *et al.* Datamining approaches for modeling tumor control probability. *Acta Oncol.* **49**, 1363–1373, DOI: [10.3109/02841861003649224](https://doi.org/10.3109/02841861003649224) (2010).
17. Borkenstein, K., Levegrün, S. & Peschke, P. Modeling and computer simulations of tumor growth and tumor response to radiotherapy. *Radiat. Res.* **162**, 71–83, DOI: [10.1667/RR3193](https://doi.org/10.1667/RR3193) (2004).
18. Brenner, H. J. & Yerushalmi, A. Combined local hyperthermia and x-irradiation in the treatment of metastatic tumours. *Br. J. Cancer* **33**, 91–95, DOI: [10.1038/bjc.1976.9](https://doi.org/10.1038/bjc.1976.9) (1975).
19. Chadwick, K. H. & Leenhouts, H. P. A molecular theory of cell survival. *Phys. Medicine Biol.* **18**, 78–87, DOI: [10.1088/0031-9155/18/1/007](https://doi.org/10.1088/0031-9155/18/1/007) (1973).
20. Lepock, J. R. Role of nuclear protein denaturation and aggregation in thermal radiosensitization. *Int. J. Hyperth.* **20**, 115–130, DOI: [10.1080/02656730310001637334](https://doi.org/10.1080/02656730310001637334) (2004).
21. Tobias, C. A. The repair-misrepair model in radiobiology: comparison to other models. *Radiat. Res.* **104**, 77–95, DOI: [10.2307/3576635](https://doi.org/10.2307/3576635) (1985).
22. Friedrich, S. U. D. M., Thomas & Scholz, M. Calculation of the biological effects of ion beams based on the microscopic spatial damage distribution pattern. *Int. J. Radiat. Biol.* **88**, 103–107, DOI: [10.3109/09553002.2011.611213](https://doi.org/10.3109/09553002.2011.611213) (2012).
23. Friedrich, T., Durante, M. & Scholz, M. Modeling cell survival after photon irradiation based on double-strand break clustering in megabase pair chromatin loops. *Radiat. Res.* **178**, 385–394, DOI: [10.1667/RR2964.1](https://doi.org/10.1667/RR2964.1) (2012).
24. Pearce, J. A. Comparative analysis of mathematical models of cell death and thermal damage processes. *Int. J. Hyperth.* **29**, 262–280, DOI: [10.3109/02656736.2013.786140](https://doi.org/10.3109/02656736.2013.786140) (2013).
25. Jung, H. A generalized concept for cell killing by heat: Effect of chronically induced thermotolerance. *Radiat. Res.* **127**, 235–242, DOI: [10.2307/3577936](https://doi.org/10.2307/3577936) (1991).
26. Roti, J. L. R. Cellular responses to hyperthermia (40–46°C): Cell killing and molecular events. *Int. J. Hyperth.* **24**, 3–15, DOI: [10.1080/02656730701769841](https://doi.org/10.1080/02656730701769841) (2008).
27. Uchida, N., Kato, H. & Ishida, T. A model for cell killing by continuous heating. *Med. Hypotheses* **41**, 548–553, DOI: [https://doi.org/10.1016/0306-9877\(93\)90112-4](https://doi.org/10.1016/0306-9877(93)90112-4) (1993).
28. Mackey, M. A. & Roti-Roti, J. L. A model of heat-induced clonogenic cell death. *J. Theor. Biol.* **156**, 133–146, DOI: [https://doi.org/10.1016/S0022-5193\(05\)80669-1](https://doi.org/10.1016/S0022-5193(05)80669-1) (1992).
29. De Mendoza, A. M. *et al.* Mathematical model for the thermal enhancement of radiation response: thermodynamic approach. *Sci. Reports* **11**, 1 – 14, DOI: [10.1038/s41598-021-84620-z](https://doi.org/10.1038/s41598-021-84620-z) (2021).

30. McMahon, S. J., Schuemann, J., Paganetti, H. & Prise, K. M. Mechanistic modelling of dna repair and cellular survival following radiation-induced dna damage. *Sci. Reports* **6**:33290, 1 – 14, DOI: <https://doi.org/10.1038/srep33290> (2016).
31. Brüningk, S. C. *et al.* A comprehensive model for heat-induced radio-sensitisation. *Int. J. Hyperth.* **34**, 392–402, DOI: [10.1080/02656736.2017.1341059](https://doi.org/10.1080/02656736.2017.1341059) (2018). PMID: 28641499.
32. Park, C., Papiez, L., Zhang, S., Story, M. & Timmerman, R. D. Universal survival curve and single fraction equivalent dose: useful tools in understanding potency of ablative radiotherapy. *Int. journal radiation oncology, biology, physics* **71**, 847–852, DOI: [10.1016/j.ijrobp.2007.10.059](https://doi.org/10.1016/j.ijrobp.2007.10.059) (2008).
33. Scheidegger, S., Fuchs, H. U., Zaugg, K., Bodis, S. & Füchslin, R. M. Using State Variables to Model the Response of Tumour Cells to Radiation and Heat: A Novel Multi-Hit-Repair Approach. *Comput. Math. Methods Medicine* **2013**, 1–15, DOI: <https://doi.org/10.1155/2013/587543> (2013).
34. Bodgi, L. *et al.* Mathematical models of radiation action on living cells: From the target theory to the modern approaches. a historical and critical review. *J. Theor. Biol.* **394**, 93–101, DOI: <https://doi.org/10.1016/j.jtbi.2016.01.018> (2016).
35. Paganetti, H. A review on lymphocyte radiosensitivity and its impact on radiotherapy. *Front. Oncol.* **13**, DOI: [10.3389/fonc.2023.1201500](https://doi.org/10.3389/fonc.2023.1201500) (2023).
36. Pham, T.-N., Coupey, J., Thariat, J. & Valable, S. Lymphocyte radiosensitivity: An extension to the linear-quadratic model? *Radiother. Oncol.* **198**, 110406, DOI: [10.1016/j.radonc.2024.110406](https://doi.org/10.1016/j.radonc.2024.110406) (2024).
37. Frankenberg-Schwager, M. Review of repair kinetics for dna damage induced in eukaryotic cells in vitro by ionizing radiation. *Radiother. Oncol.* **14**, 307–320, DOI: [10.1016/0167-8140\(89\)90143-6](https://doi.org/10.1016/0167-8140(89)90143-6) (1989).
38. Alberts, B. *et al.* *Molecular Biology of the Cell* (Garland, 2002), 4th edn.
39. Joiner, C., Michael & van der Kogel, A. J. *Basic Clinical Radiobiology* (CRC Press, 2009), 4 edn.
40. Hall, E. J. & Giaccia, A. J. *Radiobiology for the radiologist* (Lippincott Williams and Wilkins, 2012), 7 edn.
41. Crooke, P. S. & Parl, F. F. A mathematical model for dna damage and repair. *J. Nucleic Acids* **Special issue: DNA Damage, Mutagenesis, and DNA Repair**, 1 – 7, DOI: [10.4061/2010/352603](https://doi.org/10.4061/2010/352603) (2010).
42. Zheng, X. *et al.* Dynamic control of hsf1 during heat shock by a chaperone switch and phosphorylation. *eLife* **5**, e18638, DOI: [10.7554/eLife.18638](https://doi.org/10.7554/eLife.18638) (2016).
43. Ladjimi, M. T. *et al.* Dynamical thermal dose models and dose time-profile effects. *Int. J. Hyperth.* **36**, 720–728, DOI: [10.1080/02656736.2019.1633478](https://doi.org/10.1080/02656736.2019.1633478) (2019). PMID: 31353987.
44. Sivéry, A., Courtade, E. & Thommen, Q. A minimal titration model of the mammalian dynamical heat shock response. *Phys. Biol.* **13**, 066008, DOI: [10.1088/1478-3975/13/6/066008](https://doi.org/10.1088/1478-3975/13/6/066008) (2016).
45. Scheff, J. D., Stallings, J. D., Reifman, J. & Rakesh, V. Mathematical modeling of the heat-shock response in hela cells. *Biophys. J.* **109**, 182 – 193, DOI: [10.1016/j.bpj.2015.06.027](https://doi.org/10.1016/j.bpj.2015.06.027) (2015).
46. Peper, A., Grimbergen, C. A., Spaan, J. A. E., Souren, J. E. M. & Van Wijk, R. A mathematical model of the hsp70 regulation in the cell. *Int. J. Hyperth.* **14**, 97–124, DOI: [10.3109/02656739809018218](https://doi.org/10.3109/02656739809018218) (1998). PMID: 9483450.
47. Roskoski, R. Michaelis-menten kinetics. In *Reference Module in Biomedical Sciences*, DOI: <https://doi.org/10.1016/B978-0-12-801238-3.05143-6> (Elsevier, 2015).
48. Newville, M., Stensitzki, T., Allen, D. B. & Ingargiola, A. Lmfit: Non-linear least-square minimization and curve-fitting for python, DOI: [10.5281/zenodo.11813](https://doi.org/10.5281/zenodo.11813) (2014).
49. Levenberg, K. A method for the solution of certain non-linear problems in least squares. *Q. Appl. Math.* **2**, 164–168, DOI: [10.1090/qam/10666](https://doi.org/10.1090/qam/10666) (1944).
50. Marquardt, D. W. An algorithm for least-squares estimation of nonlinear parameters. *J. Soc. for Ind. Appl. Math.* **11**, 431–441, DOI: [10.1137/0111030](https://doi.org/10.1137/0111030) (1963).
51. Wu, Z., Phan, T., Baez, J., Kuang, Y. & Kostelich, E. J. Predictability and identifiability assessment of models for prostate cancer under androgen suppression therapy. *Math. Biosci. Eng.* **16**, 3512–3536, DOI: [10.3934/mbe.2019176](https://doi.org/10.3934/mbe.2019176) (2019).
52. Muñoz Tamayo, R. *et al.* Review: To be or not to be an identifiable model. is this a relevant question in animal science modelling? *animal* **12**, 701–712, DOI: [10.1017/S1751731117002774](https://doi.org/10.1017/S1751731117002774) (2018).
53. Alahmadi, A. *et al.* Influencing public health policy with data-informed mathematical models of infectious diseases: Recent developments and new challenges. *Epidemics* **32**, 100393, DOI: [10.1016/j.epidem.2020.100393](https://doi.org/10.1016/j.epidem.2020.100393) (2020).

54. Eicheler, W., Zips, D., Dörfler, A., Grénman, R. & Baumann, M. Splicing mutations in tp53 in human squamous cell carcinoma lines influence immunohistochemical detection. *J. Histochem. Cytochem.* **50**, 197–204, DOI: [10.1177/002215540205000207](https://doi.org/10.1177/002215540205000207) (2002).
55. Chen, O. *et al.* Dual role of er stress in response to metabolic co-targeting and radiosensitivity in head and neck cancer cells. *Cell. Mol. Life Sci.* **78**, 3021–3044, DOI: <https://doi.org/10.1007/s00018-020-03704-7> (2021).
56. Chen, O. *et al.* Efficient heat shock response affects hyperthermia-induced radiosensitization in a tumor spheroid control probability assay. *Cancers* **13**, DOI: [10.3390/cancers13133168](https://doi.org/10.3390/cancers13133168) (2021).
57. Gerner, E. W. Thermal dose and time-temperature factors for biological responses to heat shock. *Int. J. Hyperth.* **3**, 319–327, DOI: [10.3109/02656738709140402](https://doi.org/10.3109/02656738709140402) (1987).
58. O'hara, M. D., Xiong, Q. B., Boyer, J. W. & Leeper, D. B. Intrinsic thermal response, thermotolerance development and stepdown heating in murine bone marrow progenitor cells. *Int. J. Hyperth.* **8**, 451–461, DOI: [10.3109/02656739209037983](https://doi.org/10.3109/02656739209037983) (1992).
59. Armour, E. P., McEachern, D., Wang, Z., Corry, P. M. & Martinez, A. Sensitivity of Human Cells to Mild Hyperthermia. *Cancer Res.* **53**, 2740–2744 (1993).
60. Sapareto, S. A., Hopwood, L. E. & Dewey, W. C. Combined effects of x irradiation and hyperthermia on cho cells for various temperatures and orders of application. *Radiat. Res.* **73**, 221–233 (1978).
61. Wells, R. L. & Bedford, J. S. Dose-Rate Effects in Mammalian Cells: IV. Repairable and Nonrepairable Damage in Noncycling C3H 10T 1/2 Cells. *Radiat. Res.* **94**, 105–134, DOI: [10.2307/3575868](https://doi.org/10.2307/3575868) (1983).
62. Habermehl, D. *et al.* The relative biological effectiveness for carbon and oxygen ion beams using the raster-scanning technique in hepatocellular carcinoma cell lines. *PLOS ONE* **9**, 1–10, DOI: [10.1371/journal.pone.0113591](https://doi.org/10.1371/journal.pone.0113591) (2014).
63. Yagi, M. *et al.* A consistent protocol reveals a large heterogeneity in the biological effectiveness of proton and carbon-ion beams for various sarcoma and normal-tissue-derived cell lines. *Cancers* **14**, 1–12, DOI: [10.3390/cancers14082009](https://doi.org/10.3390/cancers14082009) (2009).
64. Weyrather, W. K., Ritter, S., Scholz, M. & Kraft, G. Rbe for carbon track-segment irradiation in cell lines of differing repair capacity. *Int. J. Radiat. Biol.* **75**, 1357–1364, DOI: [10.1080/095530099139232](https://doi.org/10.1080/095530099139232) (1999).
65. Dikomey, E. & Jung, H. W. Thermal radiosensitization in cho cells by prior heating at 41-46 degrees c. *Int. journal radiation biology* **59**, 815–25, DOI: [10.1080/09553009114550711](https://doi.org/10.1080/09553009114550711) (1991).
66. Nikitaki, Z. *et al.* Key biological mechanisms involved in high-let radiation therapies with a focus on dna damage and repair. *Expert. Rev. Mol. Medicine* **24**, e15, DOI: [10.1017/erm.2022.6](https://doi.org/10.1017/erm.2022.6) (2022).
67. Dewey, W. C. Interaction of heat with radiation and chemotherapy. *Cancer Res.* **44**, 4714s–4720s (1984).
68. Friedrich, T., Pfuhl, T. & Scholz, M. Update of the particle irradiation data ensemble (pide) for cell survival. *J. Radiat. Res.* **62**, 645–655, DOI: [10.1093/jrr/rrab034](https://doi.org/10.1093/jrr/rrab034) (2021).
69. Denekamp, J., Whitmore, G. & Jeggo, P. Biphasic survival curves for xrs radiosensitive cells: subpopulations or transient expression of repair competence? *Int. journal radiation biology* **55**, 605–617, DOI: [10.1080/09553008914550651](https://doi.org/10.1080/09553008914550651) (1989).
70. Friedrich, T., Scholz, U., Elsässer, T., Durante, M. & Scholz, M. Systematic analysis of rbe and related quantities using a database of cell survival experiments with ion beam irradiation. *J. Radiat. Res.* **54**, 494–514, DOI: [10.1093/jrr/rrs114](https://doi.org/10.1093/jrr/rrs114) (2012). <https://academic.oup.com/jrr/article-pdf/54/3/494/2960831/rrs114.pdf>.
71. Vujaskovic, Z. & Song, C. W. Physiological mechanisms underlying heat-induced radiosensitization. *Int. J. Hyperth.* **20**, 163–174, DOI: [10.1080/02656730310001619514](https://doi.org/10.1080/02656730310001619514) (2004).
72. Konings, A. W. T. *Interaction of Heat and Radiation In Vitro and In Vivo*, 89–102 (Springer Berlin Heidelberg, 1995).
73. Oei, A. *et al.* Molecular and biological rationale of hyperthermia as radio- and chemosensitizer. *Adv. Drug Deliv. Rev.* **163-164**, 163–174, DOI: [10.1016/j.addr.2020.01.003](https://doi.org/10.1016/j.addr.2020.01.003) (2020).
74. Brüningk, S. C., Ziegenhein, P., Rivens, I., Oelfke, U. & Haar, G. t. A cellular automaton model for spheroid response to radiation and hyperthermia treatments. *Sci. Reports* **9**, DOI: [10.1038/s41598-019-54117-x](https://doi.org/10.1038/s41598-019-54117-x) (2019).
75. Oei, A. L., Vriend, L. E. M., Crezee, J., Franken, N. A. P. & Krawczyk, P. M. Effects of hyperthermia on DNA repair pathways: one treatment to inhibit them all. *Radiat. Oncol.* **165**, DOI: [10.1186/s13014-015-0462-0](https://doi.org/10.1186/s13014-015-0462-0) (2015).
76. Kampinga, H. H. & D, E. D. Hyperthermic radiosensitization: mode of action and clinical relevance. *Int. J. Radiat. Biol.* **77**, 399–408, DOI: [10.1080/09553000010024687](https://doi.org/10.1080/09553000010024687) (2001).

77. Kampinga, H. H., Dynlacht, J. R. & Dikomey, E. Mechanism of radiosensitization by hyperthermia (43°C) as derived from studies with dna repair defective mutant cell lines. *Int. J. Hyperth.* **20**, 131–139, DOI: [10.1080/02656730310001627713](https://doi.org/10.1080/02656730310001627713) (2004).
78. Franke, F. *et al.* Efficient radial-shell model for 3d tumor spheroid dynamics with radiotherapy. *Cancers* **15**, DOI: [10.3390/cancers15235645](https://doi.org/10.3390/cancers15235645) (2023).
79. Guerrero, M. & Li, X. Extending the linear-quadratic model for large fraction doses pertinent to stereotactic radiotherapy. *Phys. medicine biology* **49**, 4825–35, DOI: [10.1088/0031-9155/49/20/012](https://doi.org/10.1088/0031-9155/49/20/012) (2004).
80. Carlone, M., Wilkins, D. & Raaphorst, P. The modified linear-quadratic model of guerrero and li can be derived from a mechanistic basis and exhibits linear-quadratic-linear behaviour. *Phys. Medicine & Biol.* **50**, L9, DOI: [10.1088/0031-9155/50/10/L01](https://doi.org/10.1088/0031-9155/50/10/L01) (2005).
81. Scheidegger, S., Lutters, G. & Bodis, S. A lq-based kinetic model formulation for exploring dynamics of treatment response of tumours in patients. *Zeitschrift für Medizinische Physik* **21**, 164–173, DOI: <https://doi.org/10.1016/j.zemedi.2010.11.001> (2011).
82. Feng, Y., Tinsley Oden, J. & Rylander, M. N. A Two-State Cell Damage Model Under Hyperthermic Conditions: Theory and In Vitro Experiments. *J. Biomech. Eng.* **130**, 041016 (2008).
83. Rybiński, M., Szymańska, Z., Lasota, S. & Gambin, A. Modelling the efficacy of hyperthermia treatment. *J. The Royal Soc. Interface* **10**, 1–10 (2013).
84. Tzeghai, G. E. & Jain, R. K. A semi-empirical model for cell kill kinetics during hyperthermia. *J. Therm. Biol.* **4**, 257–258, DOI: [https://doi.org/10.1016/0306-4565\(79\)90011-1](https://doi.org/10.1016/0306-4565(79)90011-1) (1979).
85. Brüningk, S. *et al.* Combining radiation with hyperthermia: a multiscale model informed by in vitro experiments. *J. The Royal Soc. Interface* **15**, 20170681, DOI: [10.1098/rsif.2017.0681](https://doi.org/10.1098/rsif.2017.0681) (2018).
86. Sapareto, S. A., Hopwood, L. E., Dewey, W. C., Raju, M. R. & Gray, J. W. Effects of hyperthermia on survival and progression of chinese hamster ovary cells1. *Cancer Res.* **38**, 393–400 (1978).
87. Kok, H. P. *et al.* Quantifying the combined effect of radiation therapy and hyperthermia in terms of equivalent dose distributions. *Int. J. Radiat. Oncol. Biol. Phys.* **88**, 739–745, DOI: <https://doi.org/10.1016/j.ijrobp.2013.11.212> (2014).
88. van Leeuwen, C. M. *et al.* The effect of time interval between radiotherapy and hyperthermia on planned equivalent radiation dose. *Int. J. Hyperth.* **34**, 901–909, DOI: [10.1080/02656736.2018.1468930](https://doi.org/10.1080/02656736.2018.1468930) (2018).
89. Loshek, D. D., Orr, J. S. & Solomonidis, E. Interaction of hyperthermia and radiation: the survival surface. *Br. J. Radiol.* **50**, 893–901, DOI: [10.1259/0007-1285-50-600-893](https://doi.org/10.1259/0007-1285-50-600-893) (2014).
90. Magnus, W. On the exponential solution of differential equations for a linear operator. *Commun. on Pure Appl. Math.* **7**, 649–673, DOI: <https://doi.org/10.1002/cpa.3160070404> (1954).

Supplemental Information

SI.1 Mathematical models of cell survival

As part of the present study, a review has been made as complete as possible of mathematical cell survival models developed to predict the clonogenic survival fraction of cultures subjected to ionizing radiation, hyperthermia treatment and the combination of both. The results are summarized and presented in tabular form in Tables [SI.1a-c](#).

SI.2 Repair rate dependent on n

When an n -dependent repair rate q_n is incorporated into the model, the net advance rate $r_n = p - q_n$ changes with the level of SLD. The probability that the cell is in the n -th compartment is given by the solution of the modified balance equation

$$\frac{dP_n(t)}{dt} = -r_n P_n(t) - nc P_n(t) + r_{n-1} P_{n-1}(t), \quad (\text{SI.1})$$

Since the rates r and c are not time-dependent, the evolution of the state vector can be written as $\frac{d\vec{P}(t)}{dt} = \hat{A}\vec{P}(t)$. The elements of the transition matrix \hat{A}_{ij} define the influx rate from $n = j$ to $n = i$, and the diagonal elements \hat{A}_{ii} are the net flux at each stage. The general solution of Eq. [SI.1](#) is $\vec{P}(t) = e^{\hat{A}t}\vec{P}(t=0)$, which are expressed for the n -th element as

$$P_n(t) = \left(\prod_{i=0}^{n-1} r_i \right) \sum_{i=0}^n \frac{(-1)^i e^{-Y_i t}}{\prod_{j=0}^{i-1} F_{j,i} \prod_{j=i+1}^n F_{i,j}} \quad (\text{SI.2})$$

with $Y_n = nc + r_n$, and $F_{k,l} = \begin{cases} 1 & \text{if } k \geq l \\ Y_l - Y_k & \text{otherwise.} \end{cases}$

The survival probability is equal to the likelihood of being at any of the non-lethal damage compartments $S(t) = \sum_{n=0}^{\infty} P(n, t)$. In the case without repair ($q_n = 0$ and $r_n \rightarrow r$), the original Jung's model is recovered, and the survival probability reads $S(t) = \exp\left\{\frac{r}{c}[1 - ct - e^{-ct}]\right\}$. When repair is included in Jung's model (Eq. [\(SI.2\)](#)), it is not possible to obtain a closed exponential for the survival probability. Instead, we assume that the cell goes through a maximum number of possible nonlethal lesions n_{max} and calculate numerically:

$$S(t) = \sum_{n=0}^{n_{max}} P(n, t) \quad (\text{SI.3})$$

We proposed and tried three different functional forms for the repair function:

$$q_n = r \left(\frac{n - n_{max}}{n_{max}} \right), \quad (\text{SI.4})$$

$$q_n = q/n, \quad (\text{SI.5})$$

$$q_n = \frac{qn}{k+n}. \quad (\text{SI.6})$$

Equation [\(SI.4\)](#) describes a linear increase of the repair as a function of the damage stage n . Equation [\(SI.5\)](#) represents a non-linear decay with an additional adjustable parameter q . Equation [\(SI.6\)](#) implies a possible sigmoidal up-regulation of repair when the sublethal damage (SLD) increases. The results (not shown) exhibited no improvement over the original Jung's model.

Table SI.1. b) Review of mathematical models for the description/prediction of clonogenic cell survival of cultures subjected to HT.

Model's name/author	Reference	Main equations	Parameters definitions	Category	Subcategory	Number of adjustable parameters
Jung's model (1986)	25	$\frac{dP(n)}{dt} = p \cdot P(n-1) - p \cdot P(n) - n \cdot c \cdot P(n)$ $P(n) = \exp(-pt) \frac{\left(\frac{p}{c} [1 - \exp(-ct)]\right)^n}{n!}$ $S(t) = \sum_{n=0}^{\infty} P(n)$ $S(t) = \exp\left(\frac{p}{c} [1 - ct - \exp(-ct)]\right)$ $f(\epsilon) = \frac{1}{\sqrt{2\pi}} e^{-\frac{(\epsilon - \epsilon_m)^2}{2}}$	<p>p: rate of sublethal damage accumulation. c: rate of dame fixation</p>	Mechanistic	Single differential equation	2
Stochastic model for clonogenicity loss (Mackey and Roti)	26,28	$\frac{d\epsilon_m}{dt} = -k(\epsilon_m - \epsilon_{m,f})$ $\epsilon_m = \epsilon_{m,f} + C e^{-kt}$ $S(t) = \frac{1}{\sqrt{2\pi}} \int_{\epsilon_{min}}^{\infty} d\epsilon \exp\left[-\frac{(\epsilon - \epsilon_{m,f}(1 - e^{-kt}))^2}{2}\right]$	<p>ϵ: relative clonogenicity of a single cell (normally disributed). ϵ_m, f: steady state average value</p>	Statistical/Semiempirical	Single differential equation	2
Two-state cell damage model (Feng et al. 2008)	24,82	$\bar{\epsilon} = \epsilon_0 p_0(t, T) + \epsilon_1 p_1(t, T) \quad \lambda(t, T) = -\frac{[a - btT - cT]}{k_B T}$ $p_0 = \frac{e^{\lambda \epsilon_0}}{e^{\lambda \epsilon_0} + e^{\lambda \epsilon_1}} \quad p_1 = \frac{e^{\lambda \epsilon_1}}{e^{\lambda \epsilon_0} + e^{\lambda \epsilon_1}}$ $S(t, T) = p_1 = \frac{\exp\left[-\frac{[a - btT - cT]}{k_B T}\right]}{1 + \exp\left[-\frac{[a - btT - cT]}{k_B T}\right]}$ $\frac{dA}{dt} = -k_f A + k_b V = -k_f A + k_b(1 - A - D)$	<p>ϵ_1 is alive state=1 ϵ_0: dead state=0. Adjustable parameters a, b, c</p>	Mechanistic/statistical 1 is an empirical term	Statistical model-closed expression	3
Three-state model	24	$\frac{dD}{dt} = k_f V = k_f(1 - A - D)$	<p>k_{f0} is a scaling constant T_k sets the rate of the exponential increase of k_f with temperature T. k_b is the rate of vulnerability regression</p>	Mechanistic	System of coupled differential equations	
Single rate	26	$k_f = k_{f0} e^{T/T_k(1-A)}$ $S = e^{kt} \ln(k) = \ln(A) - \frac{E_a}{RT}$	<p>k: death rate. A, E_a: Frequency and activation energy (Arrhenius parameters)</p>	Empirical	Single differential equation	2
Rybinski's et al model	83	<p>HSP:HSP+S\rightleftharpoonsHSP:S+HSP, 3:HSP\rightarrowHSP₃, HSP₃+HSE\rightleftharpoonsHSE:HSP₃, HSE:HSP₃\rightarrowHSE:HSP₃+mRNA, HSP+HSP₃\rightarrowHSP:HSP+2:HSP, HSP+S\rightleftharpoonsHSP:S, HSP+HSP\rightleftharpoonsHSP:HSP, HSP\rightarrow0, HSP:S\rightarrowHSP+P, P\rightarrowS, mRNA\rightarrowmRNA+HSP, mRNA\rightarrow0.</p> $S(T, t + \Delta t, t_{rc}, r) \cdot S(T, t, t_{rc}, r) = \frac{\sum_{m_1=0}^r \sum_{m_2=0}^r W(T, t - t_{rc}, t, m_1) \cdot W(T, t, t + \Delta t, m_2)}{\sum_{m_1=0}^r W(T, t - t_{rc}, t, m_1)}$	<p>16 rates, one for each forward or reverse reactions</p>	Mechanistic	System of coupled differential equations	16
Uchida's model (1996)	27	$W(T, t - t_{rc}, t, m_1) = \frac{1}{m_1!} \int_{t-t_{rc}}^t \exp(-E_a/RT + \beta) dt_1^{m_1} \cdot \exp\left[-\int_{t-t_{rc}}^t \exp(-E_a/RT + \beta) dt\right]$ $t_{rc} = t_0 + \int_0^t \sin(T - T_0) \cdot a \cdot t^{-b} \cdot T - T_0 ^c \cdot dt \quad t_{rc} = t_{min}$ $\frac{dN}{dt} = -K_1 N^v \quad t = \tau \quad N = N_0$	<p>Assuming that the cell survives when it receives damage up to r times. t_0: damage repair time before heating. T_0: critical temperature. a, b and c are additional coefficients. E_a and b are Arrhenius parameters. t_{min} is a minimum value of the damage repair time</p>	Mechanistic/statistical trc is an empirical term	Statistical model-closed expression	9
Tzeghai's model	84	$f = [1 - (1 - \nu)K(t - \tau)]^{1/(1-\nu)}$ $f = \exp[-K(t - \tau)] \quad \nu = 1$ $K = K_1 N_0^{1-\nu}$	<p>τ: delay time before cell killing starts. k_1: the reaction rate constant ν is the reaction order.</p>	Semiempirical		3
Inherited from radiation						
AlphaR	31	$Y = -\ln(S)$ $\frac{dY}{dD} = \alpha_0 - F_R(D) \quad F_R(D) = \begin{cases} \alpha_R - 2\beta D \leq D_T = \frac{\alpha_R}{2\beta} \\ 0 \quad D > D_T \end{cases}$	<p>α_0 and β from LQ model. α_R: rate of damage compensation. D_T: limiting dose up to which repair mechanisms are active</p>	Semiempirical	LQ Modified	4
Multitarget	34,67	$S(D) = 1 - (1 - e^{-\frac{D}{D_0}})^n$	<p>D_0: mean lethal dose for which the mean number of lethal events per cell is equal to 1. n: number of targets to hit in order to kill the cell.</p>	Mechanistic	Poissonian	4
LQ	26,34	$1/\bar{D}_0 = K' \text{sec}^{-1} = 2.05(10)^{10} T e^{\Delta S/2} e^{-\Delta H/2T}$ $S(D) = e^{-\alpha D - \beta D^2}$	<p>ΔS: entropy of inactivation ΔH: inactivation energy of the critical rate limiting molecules that cause cell lethality α, β: sensitivity parameters with no mechanistic meaning</p>	Empirical	Poissonian	2

Table SI.1. a) Review of mathematical models for the description/prediction of clonogenic cell survival of cultures subjected to RT. For other treatment modalities see b) HT and c) TRT on the following pages.

Model's name/author	Reference	Main equations	Parameters definitions	Category	Subcategory	Number of adjustable parameters
Multitarget	34	$S(D) = 1 - (1 - e^{-D/D_0})^n$	D_0 : mean lethal dose for which the mean number of lethal events per cell is equal to 1. n : number of targets to hit in order to kill the cell	Mechanistic	System of differential equation	2
LQ	34	$S(D) = e^{-\alpha D - \beta D^2}$	α : Average number of DSBs produced by 1-Hit. β : Average number of DSBs produced by 2-Hits	Empirical @Mechanistic	Poissonian	2
LQC	34	$S(D) = e^{-\alpha D - \beta D^2 + \gamma D^3}$ $S(D) = e^{-(\alpha D - \beta G(AT) D^2)}$	α and β : remain. γ : high-doses correction	Semiempirical	LQ-Modified	3
LQ-L	79,80	$G(AT) = 2(AT + e^{-AT} - 1)/(AT)^2$ $G(AT) \rightarrow G(AT + \delta D)$ $Y = -\ln(S)$	α and β : remain. l : repair rate, d : increased repair	Empirical @Mechanistic	LQ-Modified	3
Alpha-R	31	$\frac{dY}{dD} = \alpha_0 - F_R(D)$ $F_R(D) = \begin{cases} \alpha_R - 2\beta D \leq D_T = \frac{\alpha_R}{2\beta} \\ 0 & D > D_T \end{cases}$	α_0 and β from LQ model. α_R : rate of damage compensation. D_T : limiting dose up to which repair mechanisms are active	Semiempirical	LQ-Modified	4
Repair-Misrepair model	21,34	$\frac{dU}{dt} = -\lambda U(t) - K(t)$	$U(t)$: the mean number of lesions before any repair activation λ : the linear self-repair coefficient k : the coefficient for cooperative repair φ : the probability that self-repair steps	Empirical @Mechanistic	LQ-Modified	3
Lethal-potentially lethal model	34	$S_\varphi = e^{-U_0} \left[1 + \frac{U_0(1 - e^{-AT})}{\epsilon} \right]^{\varphi \epsilon}$ $\frac{dn_{PL}}{dt} = -\epsilon_{PL} n_{PL}(t) - \epsilon_{2PL} n_{PL}(t)^2$ $\frac{dn_L}{dt} = \epsilon_{2PL} n_{PL}(t)^2$ $S = e^{-n_{tot}(T + t_r)}$	n_L : Rate of production per unit absorbed dose of lethal lesions n_{PL} : Rate of production per unit absorbed dose of potentially lethal lesions ϵ_{PL} : Average rate constant per unit time ϵ_{2PL} : Interaction with each other with rate constant	Mechanistic	LQ-Modified	4
Saturable repair model	34	$\frac{dn}{dt} = -kcn$ $n_T = \frac{n_0 - c_0}{1 - \frac{c_0}{n_0} e^{kT(c_0 - n_0)}}$ $S(D) = e^{-\frac{n_0 - c_0}{1 - \frac{c_0}{n_0} e^{kT(c_0 - n_0)}}$	$n(t)$ is the number of unrepaired lesions $c(t)$ the number of repair molecules or enzymes k is a proportionality coefficient T is the time available for repair	Mechanistic	LQ-Modified	3
Universal survival curve	32	$\ln S = \begin{cases} -(\alpha \cdot d + \beta \cdot d^2) & D \leq D_T \\ -\frac{1}{D_0} d + \frac{D_0}{D_T} & D \geq D_T \end{cases}$ $D_T = \frac{2 \cdot D_0}{1 - \alpha \cdot D_0}$ $\ln S = \begin{cases} -n \cdot (\alpha \cdot d + \beta \cdot d^2) & D \leq D_T \\ -n \cdot (\frac{1}{D_0} d + \frac{D_0}{D_T}) & D \geq D_T \end{cases}$ $S(D) = e^{-N_{lethal}(D)} = e^{-\epsilon_1 D}$ $S = e^{-(n_1 \epsilon_1 + n_2 \epsilon_2)}$	d_1 and D_0 : parameters that determine the initial (first log kill) and final "slopes" of the survival curve D_T : single transition dose α, β, D_0, D_T	Empirical	LQ-Modified	4
Friedrich's et al model	68	$S = \sum_{k_1} \sum_{k_2} g(k_1, k_2) (1 - \epsilon_1)^{k_1} (1 - \epsilon_2)^{k_2}$ $\frac{dL_k}{dt} = \alpha R N_{k-1} - (\alpha R + c_r e^{-(\mu_T T + \mu_A \Lambda)} + C_e) \cdot L_k + c_r e^{-(\mu_T T + \mu_A \Lambda)} + L_{k+1}$ $\frac{d\Gamma}{dt} = R - \gamma \Gamma$ $P = P_T P_\Lambda = e^{-(\mu_T T + \mu_A \Lambda)}$	ϵ_1 and ϵ_2 : average quantities allows the treatment of all iDSBs and cDSBs in the same way k_i : the probability for a cell to not be killed by of these.	Mechanistic	Single differential equations, Poissonian	4
Multi-Hit-Repair model (2013)	33	$\frac{dL_k}{dt} = \alpha R N_{k-1} - (\alpha R + c_r e^{-(\mu_T T + \mu_A \Lambda)} + C_e) \cdot L_k + c_r e^{-(\mu_T T + \mu_A \Lambda)} + L_{k+1}$ $\frac{d\Gamma}{dt} = R - \gamma \Gamma$ $P = P_T P_\Lambda = e^{-(\mu_T T + \mu_A \Lambda)}$ $f(\Gamma) = \gamma \Gamma$ $\lim_{T \rightarrow \infty} \left[\int_0^T f(\Gamma(\tau)) d\tau \right] = \lim_{T \rightarrow \infty} [D(T)] = D_{tot}$	Γ : Effective dose, reduced by the kinetics of repair of sublethal lesions. R : Dose rate. μ_T and μ_A : decreasing rates of repair rate of radiation and heat damages. γ : rate of decay per unit dose equivalent.	Semiempirical (effective dose)	System of differential equations-numerical solution	5
Γ -LQ model	81	$\frac{dN}{dt} = -(\alpha + 2\beta \Gamma) \cdot R \cdot N$ $\frac{d\Gamma}{dt} = R - f(\Gamma) \leftarrow f(\Gamma) = \gamma \Gamma$ $f(\Gamma) = \gamma \cdot \Gamma_1^2$	Γ : Effective dose, reduced by the kinetics of repair of sublethal lesions. p : the yield per unit dose of sublethal lesions R is the dose rate β is given by $\beta = p2\epsilon$.	Semiempirical (effective dose)	LQ Modified	3

Table SI.1. c) Review of mathematical models for the description/prediction of clonogenic cell survival of cultures subjected to TRT.

Model's name/author	Reference	Main equations	Parameters definitions	Category	Subcategory	Number of adjustable parameters
		$Y = -\ln(S)$				
AlphaR	31	$\frac{dY}{dD} = \alpha_0 - F_R(D)$ $F_R(D) = \begin{cases} \alpha_R - 2\beta D \leq D_T = \frac{\alpha_R}{2\beta} \\ 0 & D > D_T \end{cases}$ $\alpha_0(T) = a_1 \cdot e^{a_2(T-43^\circ C)}$ $\beta(T) = b_1 \cdot e^{b_2(T-43^\circ C)}$ $Y = -\ln(S)$	α_0 and β from LQ model. α_R : rate of damage compensation. D_T : limiting dose up to which repair mechanisms are active a_1, a_2, b_1, b_2 : parameters for the exponential empirical fit of α_0 and β	Semiempirical	LQ Modified	5
AlphaR - multiscale	85	$Y_{RT+HT} = Y_{HT}(t_{43}) + Y_{RT}(D) + Y_{int}$ $Y_{int} = at_{43}d$	α_0 and β from LQ model. Y_{HT} and Y_{RT} Biological effect of HT and RT respectively, obtained with the AlphaR model. t_{43} : thermal dose in equivalent minutes at 43°C ³⁶ . D : Radiation dose in Gy. Y_{int} : Synergistic effect of HT and RT, proportional to thermal dose t_{43} .	Semiempirical	LQ Modified	9
Kok's et al. model	87	$\alpha_{int}(T) = \alpha_{in}(T) \quad T \leq 42.5^\circ C$ $\alpha_{int}(T) = \alpha_{in}(42.5) + \frac{\alpha_{exp}(45) - \alpha_{in}(42.5)}{45 - 42.5} (T - 42.5) \quad T > 42.5^\circ C$ $S F_{HT}(T, t) = \exp[-k(T) \cdot t] \quad k(T) = 2.05 \cdot 10^{10} \cdot (T + 273.15) \cdot \exp\left[\frac{\Delta S}{2} - \frac{\Delta H}{2 \cdot (T + 273.15)}\right]$ $S F_{RT}(D, T, t_{in}) = \exp[-\alpha(T, t_{in}) \cdot D - \beta(T, t_{in}) \cdot D^2]$	$T_0 = \frac{16}{\ln \frac{\alpha_{in}(41)}{\alpha_{37}}}$	Empirical	LQ Modified	2
Van Leuwen's et al. model	88	$\alpha(T, t_{in}) = \alpha_{37} \cdot \exp\left[\frac{T-37}{41-37} \ln\left[\frac{\alpha_{41}}{\alpha_{37}}\right] \cdot \exp[-\mu \cdot t_{in}]\right]$ $\beta(T, t_{in}) = \beta_{37} \cdot \exp\left[\frac{T-37}{41-37} \ln\left[\frac{\beta_{41}}{\beta_{37}}\right] \cdot \exp[-\mu \cdot t_{in}]\right]$	ΔS : entropy of inactivation ΔH : inactivation energy of the critical rate-limiting molecules that cause cell lethality. $\alpha_{37}, \beta_{37}, \alpha_{41}, \beta_{41}$ μ : rate at which the radiosensitising effect of hypertherm	Empirical	LQ Modified	7=2 HT + 5 RT
Thermodynamic approach	29	$-\ln(S) = \alpha T E R D_{R+H} + \beta (T E R)^2 D_{R+H}^2$ $T E R = 1 + k(T) t \quad k(T) \approx e^{k(T-T_g)}$ $\frac{dL_k}{dt} = \alpha R L_{k-1} - (\alpha R + c_r e^{-(\mu_r T + \mu_r \Lambda)} + C_r) \cdot L_k + c_r e^{-(\mu_r T + \mu_r \Lambda)} + L_{k+1}$	α and β from LQ model. T_g : average melting temperature. b : slope of the heat capacity around T_g	Mechanistic	4	4
Multi-Hit-Repair model (2013)	33	$\frac{d\Gamma}{dt} = R - f(t) \quad \lim_{t \rightarrow \infty} \left[\int_{-\infty}^t f(\Gamma(\tau)) d\tau \right] = \lim_{t \rightarrow \infty} [D(t)] = D_{tot}$ $f(\Gamma) = \gamma \Gamma$ $\frac{d\Upsilon}{dt} = -k_1 \Upsilon + k_2 \Lambda \quad \frac{d\Lambda}{dt} = k_1 \Upsilon + k_2 \Lambda \leftarrow k_1 = k \cdot e^{-\frac{E_a}{RT}}$	Γ : Effective dose, reduced by the kinetics of repair of sublethal lesions. R : Dose rate. μ_r and μ_Λ : decreasing rates of repair rate of radiation and heat damages. γ : rate of decay per unit dose equivalent.	Mechanistic	System of coupled differential equations	8=5 RT + 3 synergy with HT
Multitarget - Dewey et al	67	$S(D) = 1 - (1 - e^{-\frac{D}{D_0}})^n$ $1/D_0 = K' s e c^{-1} = 2.05(10)^{10} T e^{\Delta S/2} e^{-\Delta H/2T}$	D_0 : mean lethal dose for which the mean number of lethal events per cell is equal to 1. n : number of targets to hit in order to kill the cell. ΔS : entropy of inactivation ΔH : inactivation energy of the critical rate-limiting molecules that cause cell lethality	Mechanistic	Poissonian	4
Survival surface	89	$\frac{\partial \ln S}{\partial D} = f(t) \quad \frac{\partial \ln S}{\partial t} = f(D)$ $-\ln S = C_1 D + C_2 t + C_3 D t + C_4$		Semiempirical	Single differential equation	4

SI.3 Approximation in the Magnus series

When the sublethal damage accumulation rate r is time-dependent, the transition matrix \hat{A} also becomes time-dependent; then, we aim to solve

$$\frac{d\vec{P}(t)}{dt} = \hat{A}(t)\vec{P} \quad (\text{SI.7})$$

for the initial condition $\vec{P}(0) = (1, 0, 0, \dots, 0)^T$, where the superscript T denotes the transpose of a matrix. This initial condition indicates that at the onset of the treatment, the entire cell population is in the $n = 0$ compartment, meaning that no damage has been inflicted yet. However, the solution $\vec{P}(t) = e^{\int_0^t \hat{A}(t) dt} \vec{P}(0)$ does not hold anymore, and one needs to be careful because the transition matrix \hat{A} becomes a function of time. This implies that the matrix does not commute when it is evaluated at different times $[\hat{A}(t_i), \hat{A}(t_j)] = \hat{A}(t_i) \cdot \hat{A}(t_j) - \hat{A}(t_j) \cdot \hat{A}(t_i) \neq 0$.

The solution to this initial-value problem was introduced by Magnus⁹⁰, expressing the solution through the exponential of a certain $n \times n$ matrix $\hat{\Omega}(t)$:

$$\vec{P}(t) = e^{\hat{\Omega}(t)} \vec{P}(0), \quad (\text{SI.8})$$

where $\hat{\Omega}(t)$ is subsequently constructed as a series expansion $\hat{\Omega}(t) = \sum_{k=1}^{\infty} \hat{\Omega}_k(t)$, with

$$\begin{aligned} \hat{\Omega}_1(t) &= \int_0^t A(t_1) dt_1, \\ \hat{\Omega}_2(t) &= \frac{1}{2} \int_0^t dt_1 \int_0^{t_1} dt_2 [A(t_1), A(t_2)], \\ \hat{\Omega}_3(t) &= \frac{1}{6} \int_0^t dt_1 \int_0^{t_1} dt_2 \int_0^{t_2} dt_3 ([A(t_1), [A(t_2), A(t_3)]] + [A(t_3), [A(t_2), A(t_1)]]), \\ \hat{\Omega}_4(t) &= \frac{1}{12} \int_0^t dt_1 \int_0^{t_1} dt_2 \int_0^{t_2} dt_3 \int_0^{t_3} dt_4 ([[A_1, A_2], A_3], A_4) \\ &\quad + [A_1, [[A_2, A_3], A_4]] + [A_1, [A_2, [A_3, A_4]]] + [A_2, [A_3, [A_4, A_1]]]), \\ &\quad \vdots \end{aligned}$$

Keeping $\hat{\Omega}(t)$ to first order in the expansion is a valid approximation when the parameters are approximately constant for most of the treatment time. Then, the approximated solution of Eq. (SI.7) would again read as

$$\vec{P}(t) \approx e^{\int_0^t \hat{A}(t) dt} \vec{P}(0).$$

Since higher-order terms become smaller, we estimate the error as the difference between the second and the first-order contributions:

$$\epsilon = e^{\hat{\Omega}_1(t) + \hat{\Omega}_2(t)} \vec{P}(0) - e^{\hat{\Omega}_1(t)} \vec{P}(0). \quad (\text{SI.9})$$

As an example, we calculate the error for the parameters obtained for the UT-SCC-14 cell line under 45°C HT, because it is the only case in our experiments displaying adaptation to treatment and, therefore, showing a time-dependent rate of SLD accumulation. At $t = 1\text{min}$, this error ranges below 10^{-4} and below 10^{-46} at $t = 60\text{min}$. The parameters used for these results are reported in Table SI.2.

SI.4 Rationales for experimental CFA setup

Despite all their limitations, two-dimensional (2-D) colony formation assays (CFA) are still standard in radiation research and treatment. Accordingly, 2-D clonogenic survival curves as a function of the applied dose reflecting the tumor cells' intrinsic radioresponsiveness remain the backbone for most mathematical modeling concepts in the field. We chose a robust CFA

designed for combinatorial RT testing in our HNSCC cells, where 6-well plates for all treatment arms in one experimental series are prepared from the same single-cell solution before the treatment. This strategy reduces preparatory artifacts and variations frequently seen in experiments requiring individual post-treatment processing of differently treated samples, i.e., when dissociation, cell counting, diluting, and seeding are carried out independently for each treatment arm. Thereby, we also avoid misleading results due to distinct adverse effects, e.g., on the adherence of the cells, when the dissociation procedure follows different treatment modalities. Notably, the period for the HNSCC cell lines to sufficiently adhere as single cells to the 6-well plate surface to allow further processing and plate manipulation ranges between 4 h and 8 h. The cell-line dependent culture doubling time under the standard conditions highlighted in “cell culturing” is > 26 h to < 56 h, not considering the time for adherence and a putative growth lag phase. The uniform 20-24 h incubation period before HT treatment guaranteed stable adherence and complete recovery of the cells. Notably, a subpopulation of the seeded and adhered single cells may already have divided at the onset of treatment, leading to enhanced clonogenic survival rates. However, in light of the aforementioned aspects, most HNSCC cell lines experience limited cell division within 24 hours after the sparse single-cell seeding. Its impact on the readout is thus considered acceptable as the disadvantage of this systematic measurement error is offset by the advantages of reproducibly good adherence and recovery of the inoculated cells required for standardized monitoring of RT, HT, and TRT outcomes with the same setup.

SI.5 Hyperthermia treatment results

We present the optimization results for cells treated with HT administered by different conventional heating techniques, i.e., various thermal baths or ovens. The Umodel parameters (r, c, q_{max} , and k) are reported in Table SI.2 for the HNSCC cell lines from experiments performed in our laboratory and Tables SI.5 and SI.6 for different HT-treated cell types documented in the literature; the respective goodness-of-fit R^2 values of competitor models are listed for comparison. Figures SI.1, 4, SI.6 show the respective survival curves. In our experiments (Table SI.2, Figure SI.1), UT-SCC-14 cells at 45 °C primarily present adaptation to treatment. In the second set of data (Table SI.5), some cell types at certain “mild” temperatures also display flattening in the logarithmic survival curves (examples are shown in Figure SI.4). In the third data set (Table SI.6), most curves reflect such behavior, as seen in Figures 4 to SI.6 (cf. Table 1 in the Main text).

Again, on average and in most cases, the Umodel performs better or similarly, providing insights into the cellular population recovery. As it can be observed, the Umodel provides a great advantage to describe logarithmic survival curves exhibiting adaptation to the treatment.

The temperature dependence of the sublethal damage rate displays the exponential behavior $r = e^{b(T-T_g)}$ predicted and explained in reference²⁹. Here, b represents the slope of the temperature-dependent heat capacity function of the cell, and T_g is the average melting point of cellular proteins undergoing denaturation under the effect of heat. Table SI.8 lists the adjusted values for b and T_g . The exponential behavior of r is also set for q_{max} to describe the upregulation of the repair mechanisms as a consequence of the damaging stimulus (as explained in the Methods section). The results are graphically documented in Figure SI.2 for our experiments and Figures SI.7 and SI.8 for data sets from the literature.

SI.6 Radiation treatment results

The Umodel parameters (r, c, q_{max} and k) are presented in Table SI.3 for the head and neck squamous cell carcinoma (HNSCC) cell lines from our experiments, with the respective goodness of the fit (R^2) of the LQ model and Jung’s model for comparison. In most cases, the Umodel performs better or similarly because the logarithmic survival curves ($-\ln(S)$) do not display adaptation to treatment (see Fig. 2a) in the Main text). When cellular populations reduce their sensitivity in a dose-dependent manner, neither the LQ nor Jung’s model can describe survival. Then, the regression rate of the Umodel (with two extra parameters) is required to delineate the cell population response, providing insight into the recovery mechanisms. Such curves were found for six cell types (Xrs5, HepG2, HUH7, PLC, SW153 and HDF) reported in reference⁶². These results are displayed in Fig. 5 of the main text, and the coefficients and R^2 values are reported in Table SI.7.

Dose-rate effect: We fit the experimental results provided by the work of Wells and Bedford⁶¹, who performed clonogenic survival assays with C3H/10T1/2 cells at three different RT dose-rates (0.49 Gy/h, 2.4 Gy/h, and 55.8 Gy/h). The results are presented in Fig. SI.3 and Table SI.4. The Umodel rates r and q_{max} are kept constant while c and k are adjusted, displaying a linear dependency with the dose rate (not shown). The results are explained in more detail in the main text.

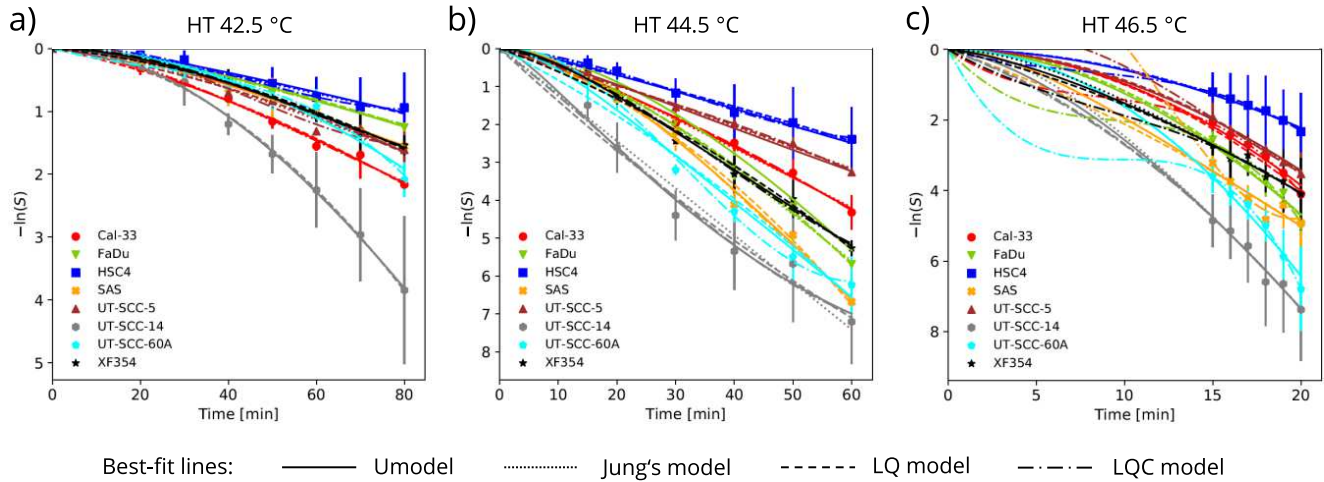


Figure SI.1. The Umodel shows comparable performance to the Jung's, LQ, and LQC models to resemble clonogenic survival in HNSCC cells upon HT mono-treatment. Symbols represent cell survival fractions ($-\ln(S)$) of eight human HNSCC cell lines exposed to HT at a) 42.5 °C, b) 44.5 °C, and c) 46.5 °C. Data show means (\pm SD) from $N = 3$ independent experiments with the models' best-fit lines. The coefficients of determination R^2 , AIC values and parameters' uncertainties are listed in Tables SI.2 and SI.9.

SI.7 Combined treatment: Thermoradiotherapy

The radiosensitizing efficacy of HT has been widely proven in different *in vitro* and *in vivo* models of various normal and cancer cell types^{4,56,71-74}. As an outlook, we demonstrate a possible application of the Umodel to combination treatment (TRT) for four cell lines exposed consecutively to hyperthermia and radiation without a gap between treatments. Firstly, the parameters of the mono-treatments, RT and HT at different temperatures, are independently calibrated as described before. Then, if the combined treatment starts with hyperthermia, the state vector \vec{P} after such a treatment is computed by integrating the set of ordinary differential equations of the Umodel Eq. (1) with the parameters of hyperthermia mono-treatment. The state vector after the first treatment is then used as the initial state vector at the beginning of the following treatment (i.e., the Umodel with parameters of the radiotherapy mono-treatment is applied to this state vector). From the state vector after this second treatment, the survival probability S is extracted according to Eq. (2). To account for radiosensitization of the cells due to the hyperthermia treatment, only the parameters r_{RTold} , c_{RTold} of the radiotherapy treatment are then updated to r_{RTnew} , c_{RTnew} based on the survival data from the experiments with combined treatment. The enhancement of the sublethal damage is assessed through the ratio between the HT-modified SLD rate, and the same rate for the RT-only treatment $ER = \frac{r_{RTnew}}{r_{RTold}}$. Based on thermodynamic considerations²⁹ we assume the enhancement ratio to follow $ER = 1 + te^{b(t-T_g)}$.

Following the above scheme, the Umodel was fitted to experimental clonogenic survival data recorded upon combined TRT. Two HNSCC cell lines (SAS and FaDu) were first exposed to three different HT doses (40.5°C, 42.5°C, and 44.5°C for 15-30 minutes) and then immediately exposed to 0 - 6 Gy of X-ray irradiation. Averaged clonogenic survival curves from three independent experiments and the respective model fittings are documented in Figure SI.9a-f, showing good performance. Notably, the gap between applications in the combined treatment has effectively been null in all experiments. The thermal enhancement ratios (TER) were calculated as a fold change of the advance rate of RT combined with HT r_{RTnew} in comparison to the advance rate of RT alone r_{RTold} . TERs are plotted as a function of exposure time and temperature in Fig. SI.10; a,c for FaDu, b,d for SAS. When the TERs are linear functions of the HT treatment time, the slopes display exponential dependencies with HT temperature, as previously found and predicted^{4,29}. All fitting parameters and TER calculations are summarized in Table SI.11.

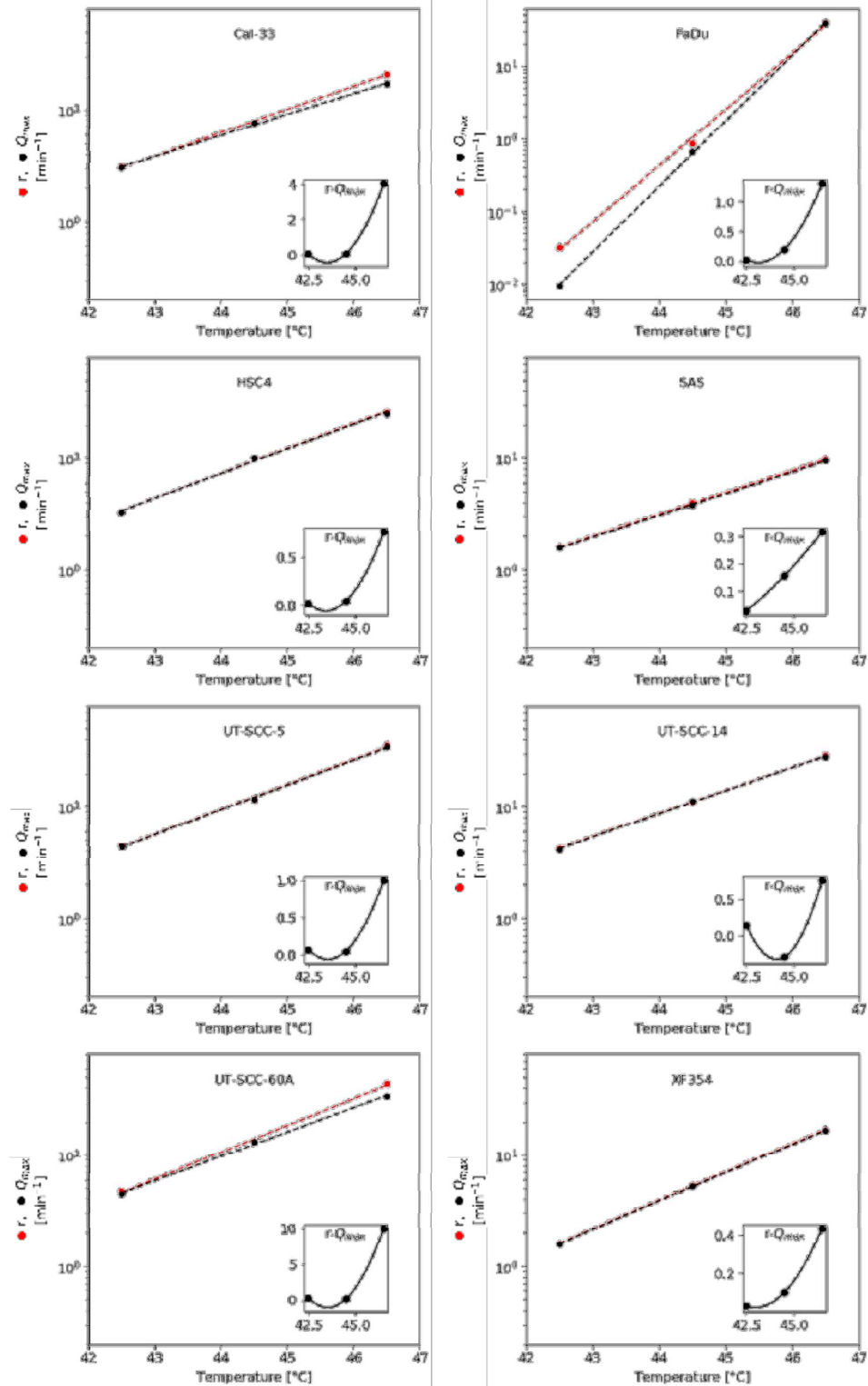


Figure SI.2. The difference between the Umodel parameters of damage and regression rate increases with temperature. The advance rate in the SLD chain r and the maximum repair rate q_{\max} corresponding to the fits in Figure SI.1 are reported as function of temperature; dashed lines correspond to exponential fits, see Table SI.8. The insets display the difference between the two parameters on a linear scale.

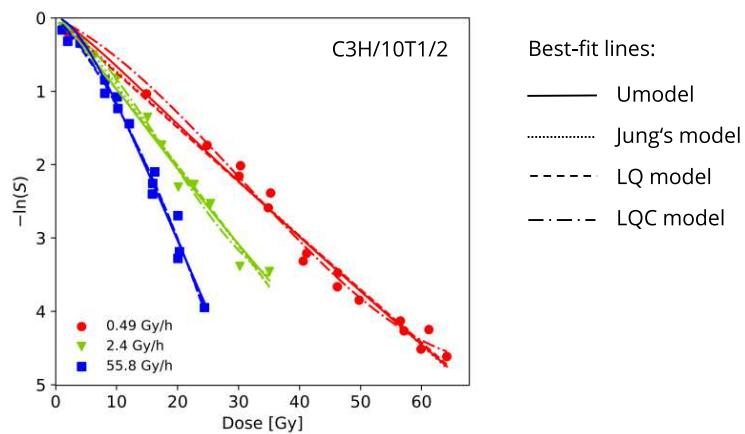


Figure SI.3. Umodel shows consistent performance when applied clonogenic survival curves upon RT of varying dose rates. Symbols represent cell survival fractions ($-\ln(S)$) obtained from clonogenic assays using C3H/10T1/2 exposed to varying dose-rates of RT⁶¹. The data was fitted with the Umodel, Jung's, and the LQ and LQC models. The coefficients of determination R^2 , AIC values and parameters' uncertainties are listed in Table SI.4.

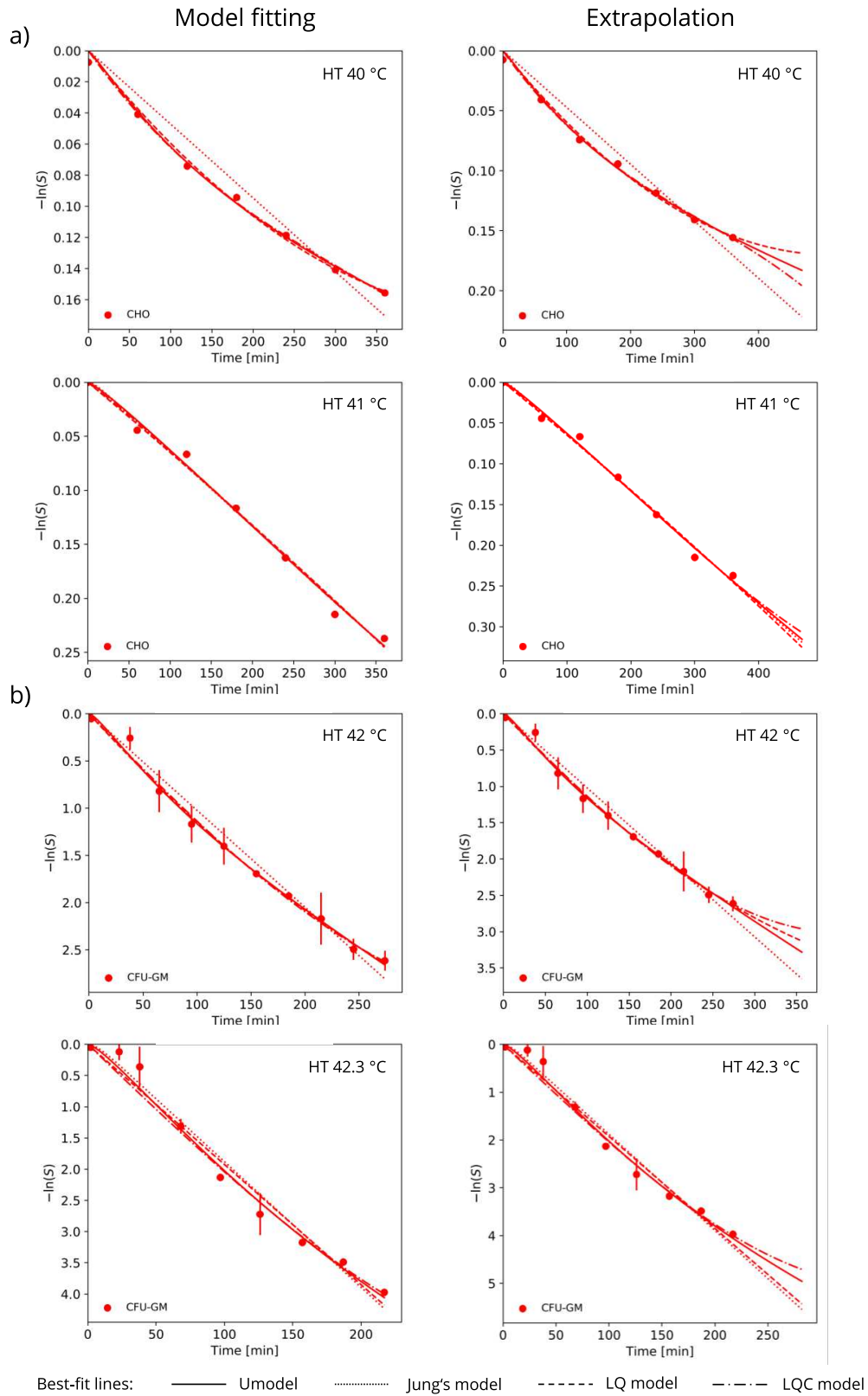


Figure SI.4. Umodel shows improved performance in comparison to the Jung's, LQ, and LQC models, when applied to flattening clonogenic survival curves upon HT extracted from literature. Symbols represent cell survival fractions ($-\ln(S)$) obtained from clonogenic assays using a) CHO²⁵ and b) CFU-GM⁵⁸ cell models exposed to HT different temperatures. The data was fitted (best-fit lines) with the Umodel, Jung's, and the LQ and LQC models (left panel) and extrapolated up to 130 % of the total thermal dose (right panel). The coefficients of determination R^2 are listed in Table SI.5, AIC and parameters' uncertainties in Table SI.9.

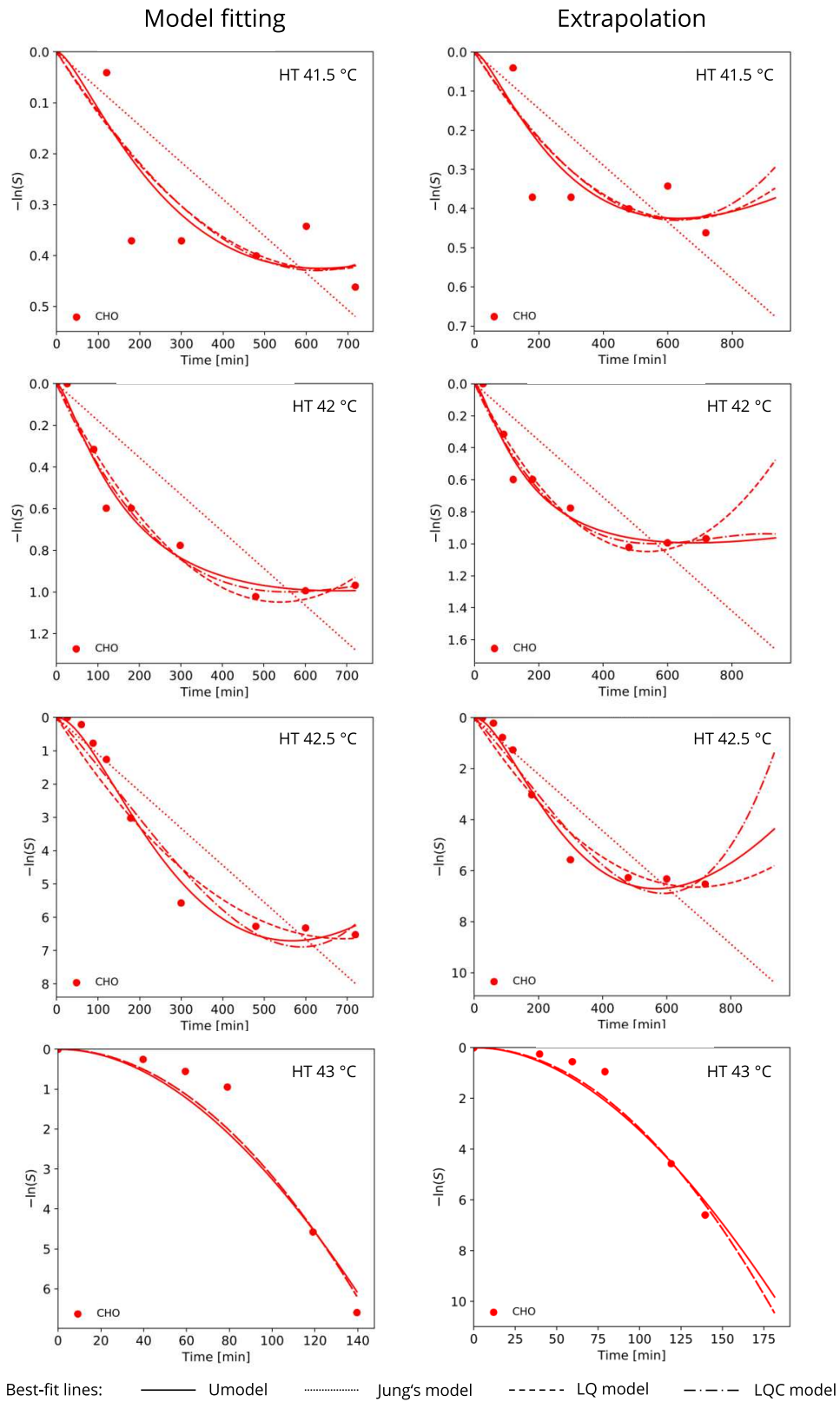
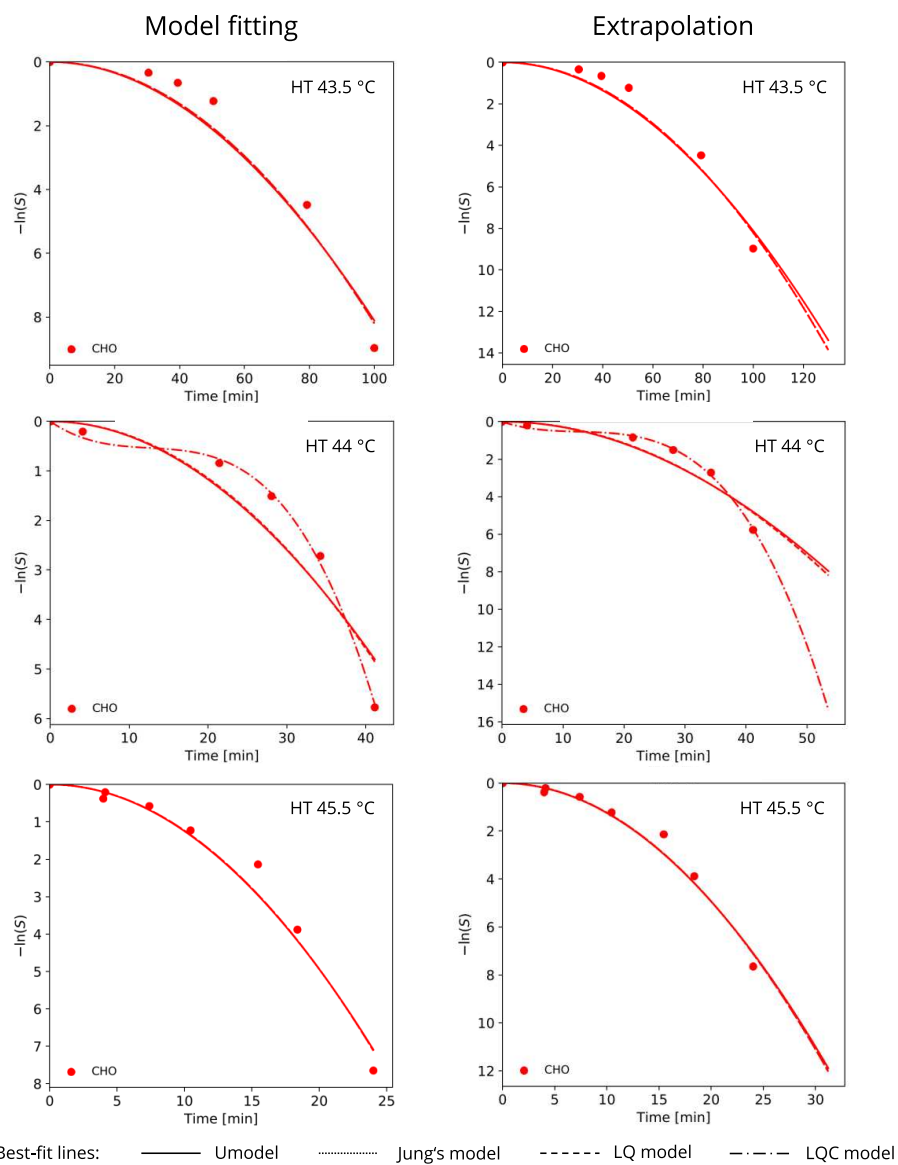


Figure SI.5. Umodel shows improved performance in comparison to the Jung's, LQ, and LQC models, when applied to flattening clonogenic survival curves upon HT extracted from literature. Symbols represent cell survival fractions ($-\ln(S)$) obtained from clonogenic assays using CHO cell line exposed to HT different temperatures²⁸. The data was fitted (best-fit lines) with the Umodel, Jung's, and the LQ and LQC models (left panel) and extrapolated up to 130 % of the total thermal dose (right panel). The coefficients of determination R^2 are listed in Table SI.6, AIC and parameters' uncertainties in Table SI.9. The Figure continues on the next page.

Continuation of Fig. SI.5



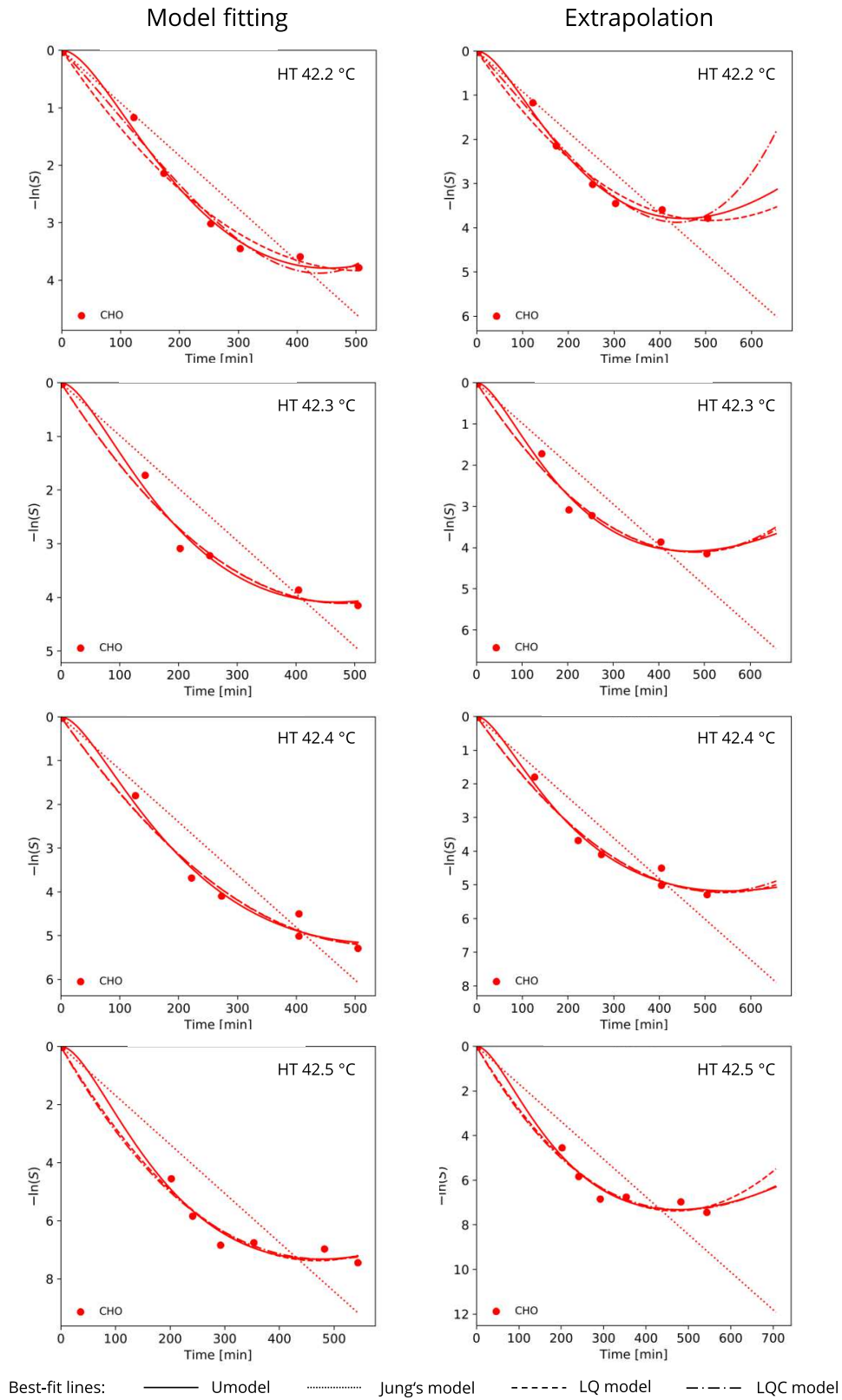


Figure SI.6. Umodel shows improved performance in comparison to the Jung's, LQ, and LQC models, when applied to flattening clonogenic survival curves upon HT extracted from literature. Symbols represent cell survival fractions ($-\ln(S)$) obtained from clonogenic assays using CHO cell line exposed to HT different temperatures⁶⁰. The data was fitted (best-fit lines) with the Umodel, Jung's, and the LQ and LQC models (left panel) and extrapolated up to 130% of the total thermal dose (right panel). The coefficients of determination R^2 are listed in Table SI.6, AIC and parameters' uncertainties in Table SI.9.

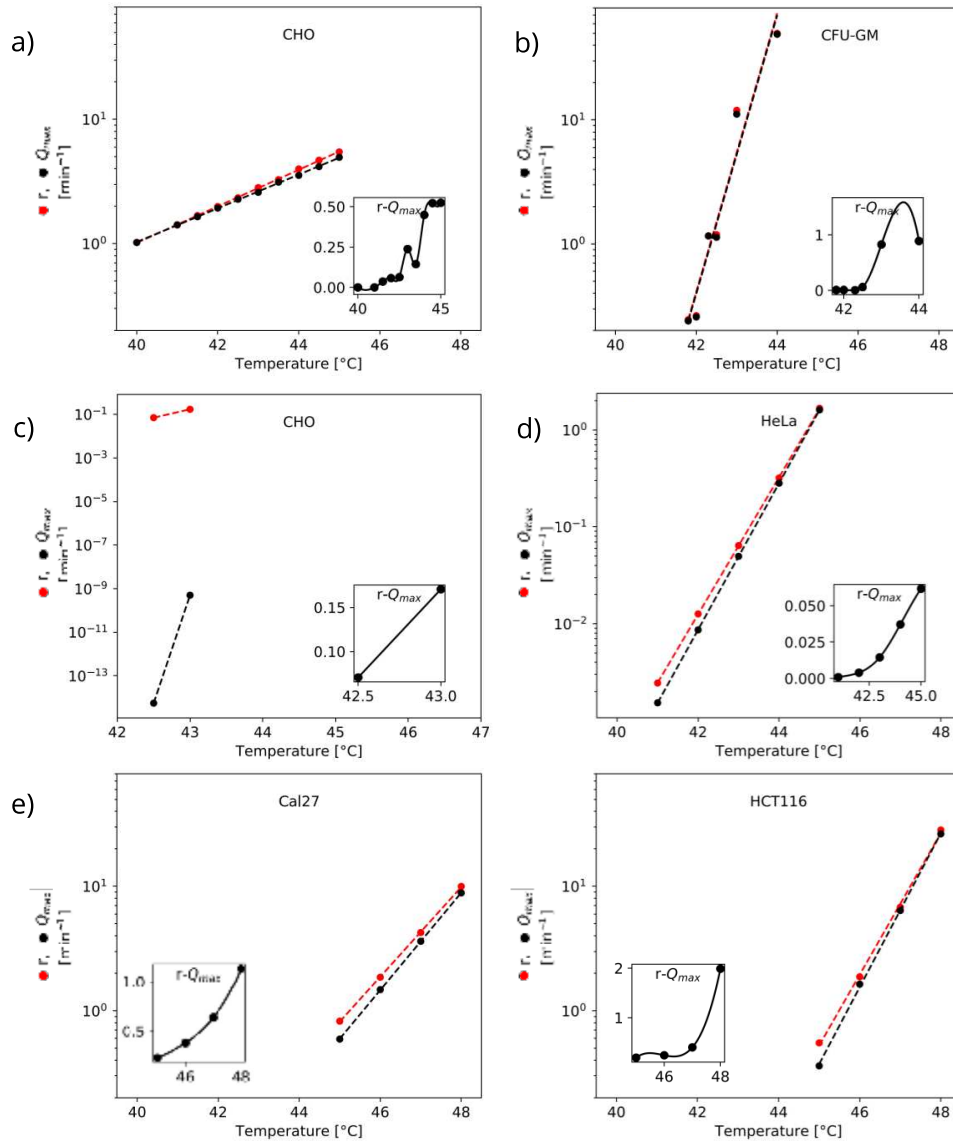


Figure S1.7. The difference between the Umodel parameters of damage and regression rate increases with temperature. The advance rate in the SLD chain r and the maximum repair rate q_{max} a)²⁵ and b)⁵⁸ corresponding to the fits in Figure SI.4 and c)⁶⁵, d)⁵⁷, and e)³¹ corresponding to the fits in Table SI.5, are reported as function of temperature; dashed lines correspond to exponential fits, see Table SI.8. The insets display the difference between the two parameters on a linear scale.

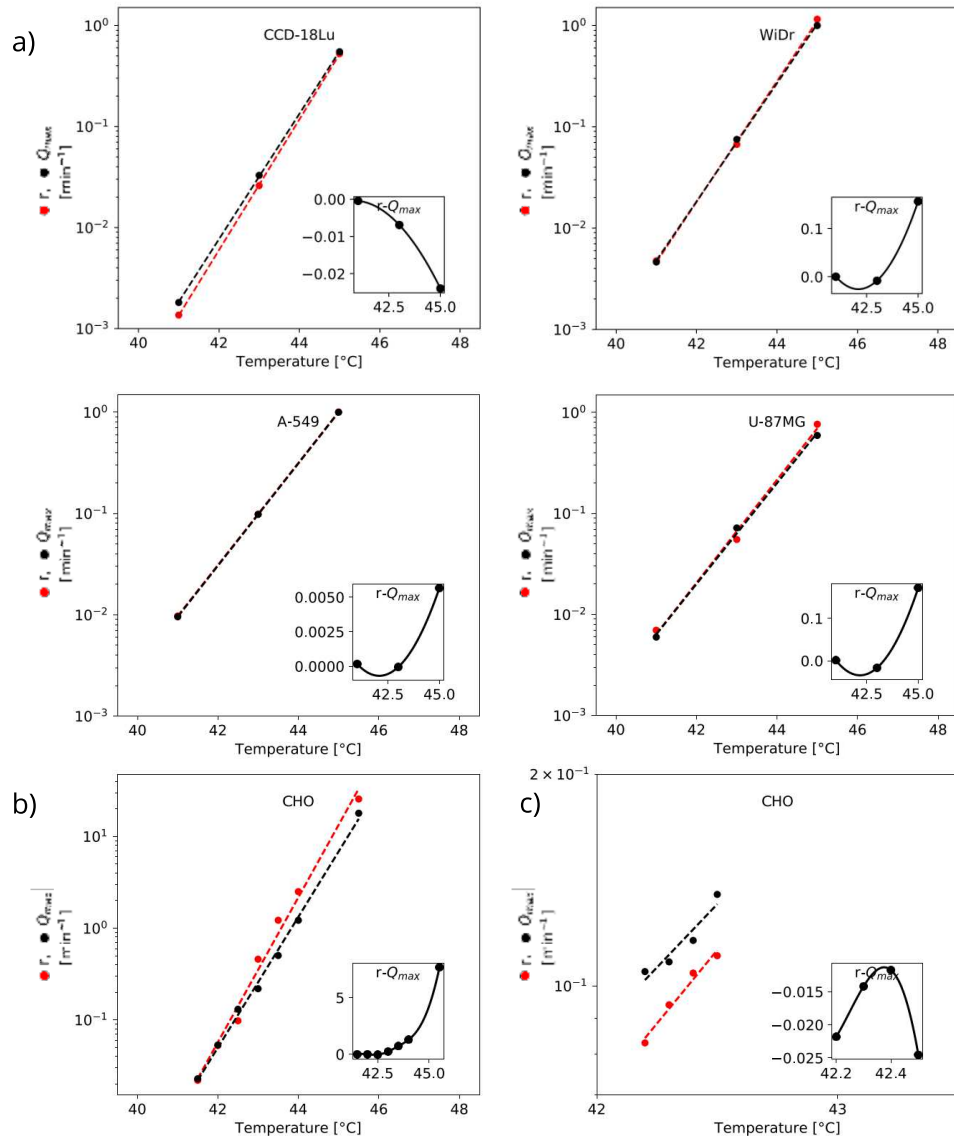


Figure S1.8. The difference between the Umodel parameters of damage and regression rate increases with temperature. The advance rate in the SLD chain r and the maximum repair rate q_{max} a)⁵⁹ corresponding to the fits in Figure 4, b)²⁸ corresponding to Figure SI.5, and c)⁶⁰ corresponding to Figure SI.6 (see also Table SI.6) are reported as function of temperature; dashed lines correspond to exponential fits, see Table SI.8. The insets display the difference between the two parameters on a linear scale.

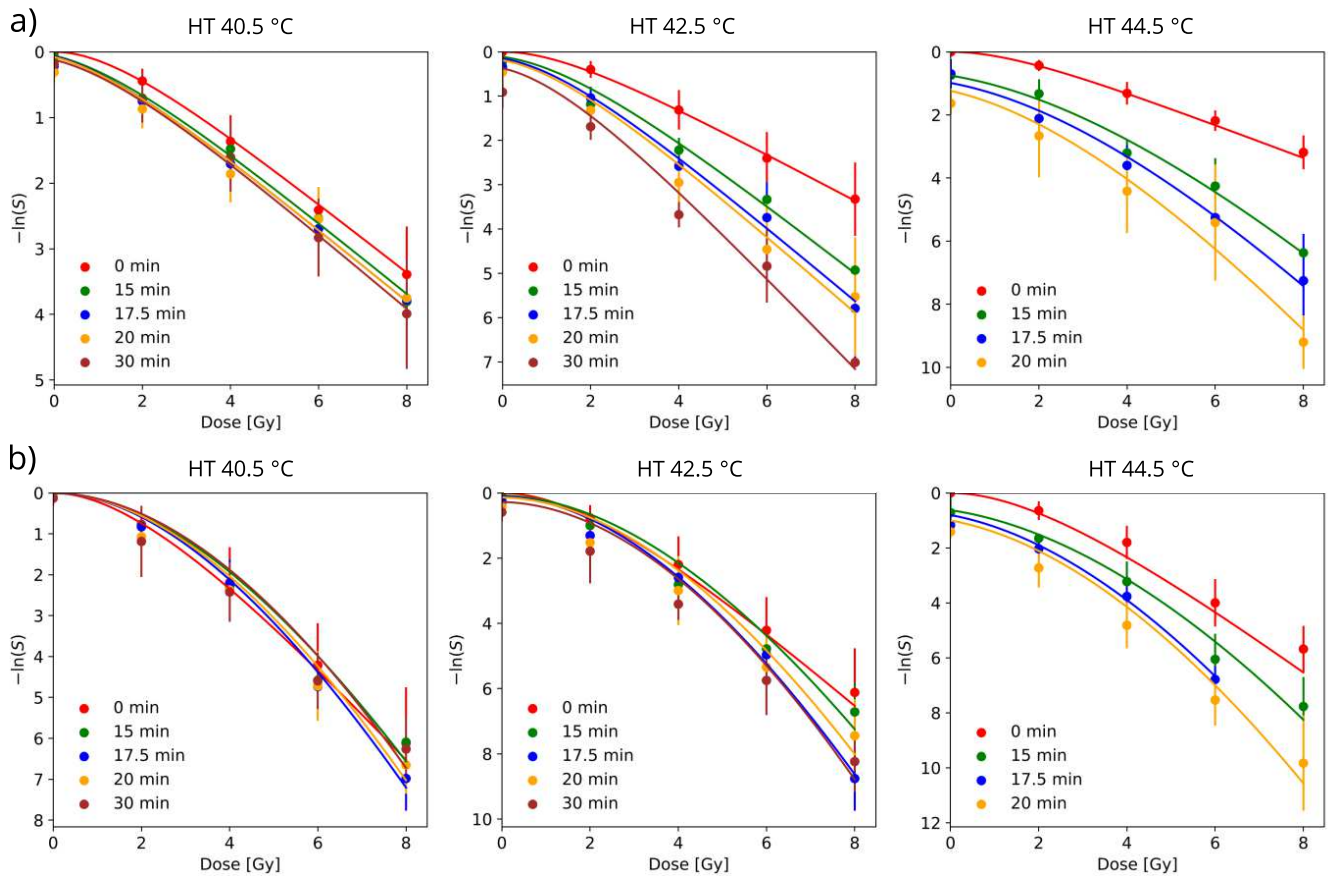


Figure SI.9. Umodel can be fitted to clonogenic survival experiments of HNSCC cell lines exposed to combined TRT. Symbols represent cell survival fractions ($-\ln(S)$) obtained from clonogenic assays using human HNSCC cell lines a) SAS and b) FaDu exposed to combined TRT with interval between the treatments effectively null. The best-fit lines represent the theoretical prediction of the Umodel. The parameters and coefficients of determination R^2 are listed in Table SI.11.

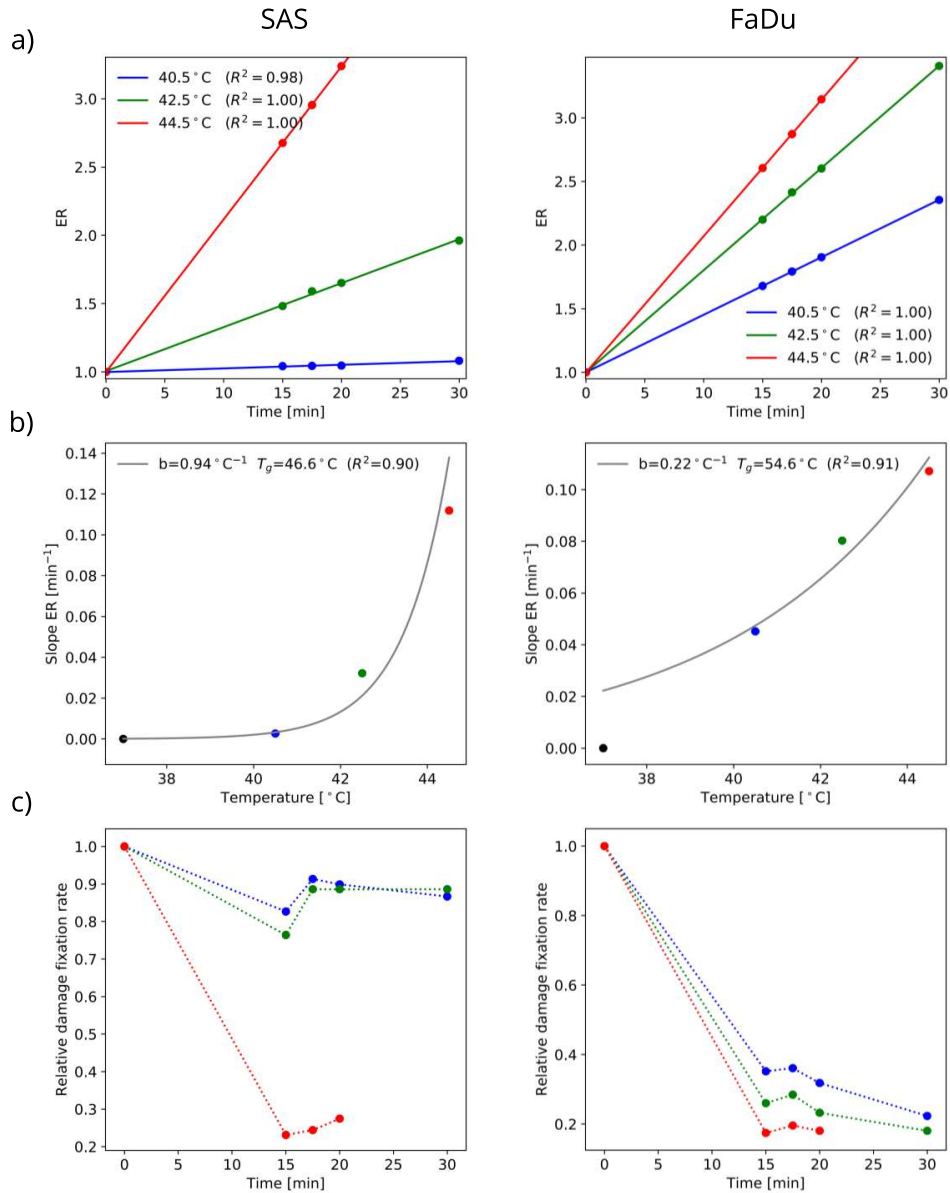


Figure SI.10. Enhancement of radiation response by HT as a function of exposure time and temperature. Calculations corresponding to data from Figure SI.9 in SAS (left panel) and FaDu (right panel) cell lines. a) Linear dependency of the enhancement ratios (ER) with HT exposure time. b) Slopes from a) as a function of HT temperature. c) Relative damage fixation rate C_{RTnew}/C_{RTold} as function of the HT exposure time.

Table SI.2. Best fitting parameters of Jung's and Umodel to clonogenic survival data from eight HNSCC cell lines exposed to HT. For the corresponding parameters' uncertainties and Aikake information criterion values see Table SI.9.

T[°C]	Cell line	LQ-model			LQC-model				Jungs model			Unified model				
		α [min ⁻¹]	β [min ⁻²]	R ²	α [min ⁻¹]	β [min ⁻²]	γ [min ⁻³]	R ²	r[min ⁻¹]	c[min ⁻¹]	R ²	r[min ⁻¹]	c[min ⁻¹]	Q _{max} [min ⁻¹]	k[min]	R ²
42.5	Cal-33	1.438E-02	1.585E-04	0.993	8.288E-03	3.933E-04	-2.056E-06	0.994	3.318E-02	6.229E-02	0.994	3.085E+00	3.157E-03	3.020E+00	9.992E-01	0.994
	FaDu	7.478E-03	9.967E-05	0.981	2.250E-03	3.010E-04	-1.763E-06	0.984	1.946E-02	5.566E-02	0.986	3.147E-02	4.013E-02	9.290E-03	1.000E-12	0.984
	HSC4	7.719E-03	6.589E-05	0.955	-4.626E-03	5.384E-04	-4.119E-06	0.988	1.566E-02	6.957E-02	0.969	3.287E+00	4.943E-02	3.270E+00	1.000E-12	0.964
	SAS	9.002E-03	1.339E-04	0.993	4.010E-03	3.262E-04	-1.684E-06	0.995	2.558E-02	5.024E-02	0.996	1.590E+00	5.022E-02	1.564E+00	1.000E-12	0.996
	UT-SCC-5	1.094E-02	1.221E-04	0.963	-7.663E-03	8.448E-04	-6.364E-06	0.978	2.554E-02	6.132E-02	0.974	4.479E+00	5.500E-03	4.408E+00	1.000E-01	0.957
	UT-SCC-14	5.499E-03	5.335E-04	0.996	2.726E-14	7.549E-04	-1.991E-06	0.997	1.461E-01	1.062E-02	0.997	4.276E+00	1.069E-02	4.131E+00	4.222E-07	0.997
	UT-SCC-60A	1.405E-03	2.819E-04	0.968	1.828E-02	-3.681E-04	5.691E-06	0.983	4.406E+01	1.374E-05	0.967	4.715E+00	2.050E-03	4.419E+00	2.623E-02	0.967
	XF354	6.890E-03	1.649E-04	0.993	-1.248E-03	4.772E-04	-2.727E-06	0.999	2.990E-02	3.438E-02	0.997	1.598E+00	3.440E-02	1.568E+00	1.728E-06	0.997
Average R ²			0.980				0.990			0.985					0.982	
44.5	Cal-33	4.984E-02	3.536E-04	0.990	5.227E-02	2.251E-04	1.518E-06	0.990	7.727E-02	1.709E-01	0.990	7.704E+00	1.208E-02	7.640E+00	2.599E-01	0.990
	FaDu	4.050E-02	9.086E-04	0.994	2.811E-02	1.565E-03	-7.750E-06	0.995	1.267E-01	6.174E-02	0.994	8.644E-01	1.629E-02	6.649E-01	1.000E+00	0.972
	HSC4	3.293E-02	1.306E-04	0.986	1.179E-02	1.250E-02	-1.322E-05	0.995	4.466E-02	1.897E-01	0.992	1.012E+01	5.224E-02	1.008E+01	1.415E-02	0.989
	SAS	4.412E-02	1.141E-03	0.989	8.430E-03	3.031E-03	-2.232E-05	0.992	1.548E-01	5.639E-02	0.992	3.960E+00	5.639E-02	3.805E+00	4.054E-10	0.992
	UT-SCC-5	4.511E-02	1.360E-04	0.993	5.298E-02	-2.804E-04	4.918E-06	0.994	5.512E-02	3.703E-01	0.992	1.168E+01	6.923E-02	1.163E+01	1.260E-02	0.990
	UT-SCC-14	1.429E-01	-4.093E-04	0.979	1.177E-01	9.282E-04	-1.580E-05	0.980	1.242E-01	3.000E+00	0.972	1.102E+01	9.845E-03	1.131E+01	9.871E-01	0.983
	UT-SCC-60A	7.825E-02	5.217E-04	0.973	-1.667E-02	5.561E-03	-5.961E-05	0.995	1.248E-01	1.334E-01	0.984	1.332E+01	1.334E-01	1.319E+01	4.459E-09	0.984
	XF354	5.579E-02	5.374E-04	0.984	2.472E-02	2.183E-03	-1.943E-05	0.988	1.008E-01	1.198E-01	0.990	5.360E+00	1.198E-01	5.259E+00	1.000E-12	0.990
Average R ²			0.986				0.991			0.988					0.986	
46.5	Cal-33	0.000E+00	1.002E-02	0.984	3.470E-01	-3.362E-02	1.322E-03	0.999	5.000E+01	3.872E-04	0.991	2.114E+01	4.964E-03	1.713E+01	5.021E-06	0.990
	FaDu	0.000E+00	1.180E-02	0.989	5.458E-01	-5.335E-02	1.915E-03	0.995	5.000E+01	4.704E-04	0.989	3.939E+01	2.037E-02	3.808E+01	1.000E-12	0.985
	HSC4	0.000E+00	5.622E-03	0.994	1.429E-01	1.235E-02	5.491E-04	0.999	5.000E+01	2.226E-04	0.995	2.588E+01	1.601E-02	2.511E+01	1.000E-12	0.991
	SAS	1.726E-01	3.899E-03	0.978	-1.082E+00	1.477E-01	-4.079E-03	0.988	3.185E-01	2.315E-01	0.979	9.711E+00	2.298E-01	9.392E+00	4.348E-08	0.979
	UT-SCC-5	5.551E-16	8.708E-03	0.996	-2.273E-01	3.487E-02	-7.381E-04	0.998	1.660E+01	1.073E-03	0.998	3.559E+01	1.945E-02	3.459E+01	1.000E-12	0.995
	UT-SCC-14	1.672E-01	1.004E-02	0.995	1.835E-01	8.178E-03	5.278E-05	0.995	5.962E-01	1.178E-01	0.995	2.891E+01	4.630E-02	2.814E+01	3.221E-02	0.995
	UT-SCC-60A	2.497E-11	1.609E-02	0.991	9.556E-01	-9.791E-02	3.356E-03	0.999	5.000E+01	6.460E-04	0.991	4.394E+01	3.291E-03	3.397E+01	1.000E-12	0.990
	XF354	1.113E-01	4.622E-03	0.992	2.807E-01	-1.478E-02	5.505E-04	0.992	2.926E-01	1.566E-01	0.992	1.697E+01	2.731E-02	1.653E+01	1.036E-01	0.992
Average R ²			0.990				0.996			0.991					0.990	

Table SI.3. Best fitting parameters of the LQ, Jung's and Umodel to clonogenic survival data from eight HNSCC cell lines exposed to RT. For the corresponding parameters' uncertainties and Aikake information criterion values see Table SI.9.

Cell line	LQ-model			LQC-model				Jungs model			Unified model				
	α [Gy ⁻¹]	β [Gy ⁻²]	R ²	α [Gy ⁻¹]	β [Gy ⁻²]	γ [Gy ⁻³]	R ²	r[Gy ⁻¹]	c[Gy ⁻¹]	R ²	r[Gy ⁻¹]	c[Gy ⁻¹]	Q _{max} [Gy ⁻¹]	k[Gy]	R ²
Cal-33	2.223E-01	1.948E-02	0.994	1.056E-01	4.995E-02	-1.785E-03	0.996	5.726E-01	3.782E-01	0.997	6.711E-01	3.781E-01	9.845E-02	1.274E-04	0.997
FaDu	3.499E-01	1.209E-02	0.996	1.886E-01	6.222E-02	-3.494E-03	1.000	5.167E-01	1.026E+00	0.999	3.624E+01	1.473E-02	4.026E+01	1.168E+00	0.999
HSC4	2.077E-01	2.922E-02	0.997	1.055E-01	5.590E-02	-1.564E-03	0.998	8.000E-01	2.530E-01	0.998	5.076E+00	6.005E-02	4.180E+00	1.242E+00	0.998
SAS	2.223E-01	1.832E-02	0.999	1.559E-01	3.895E-02	-1.438E-03	1.000	4.885E-01	5.433E-01	0.999	4.025E+01	1.582E-02	3.965E+01	3.553E-01	1.000
UT-SCC-5	1.802E-01	2.729E-02	0.997	4.188E-02	6.340E-02	-2.116E-03	1.000	7.439E-01	2.392E-01	0.999	7.439E-01	2.392E-01	3.006E-08	1.185E+00	0.999
UT-SCC-14	3.640E-01	5.003E-02	1.000	4.376E-01	2.173E-02	2.436E-03	1.000	9.989E-01	5.036E-01	0.996	4.026E+01	7.197E-02	3.869E+01	6.992E-02	0.999
UT-SCC-60A	3.389E-01	5.827E-02	0.998	4.879E-01	5.485E-04	5.010E-03	0.999	1.142E+00	3.971E-01	0.992	4.026E+01	6.563E-02	3.824E+01	7.037E-02	0.996
XF354	5.423E-01	2.161E-03	0.996	4.479E-01	3.146E-02	-2.042E-03	0.997	5.933E-01	2.415E+00	0.997	1.267E+00	8.052E-01	8.680E-01	1.242E+00	0.998
Average R ²			0.997				0.999			0.997					0.998

Table SI.4. Best fitting parameters of LQ, Jung's and Umodel to clonogenic survival data obtained at different dose rates. Data from reference⁶¹

Cell line	LQ-model			Jungs model			Unified model				
	α [Gy ⁻¹]	β [Gy ⁻²]	R ²	r[Gy ⁻¹]	c[Gy ⁻¹]	R ²	r[Gy ⁻¹]	c[Gy ⁻¹]	Q _{max} [Gy ⁻¹]	k[Gy]	R ²
0.49 Gy/h	7.430E-02	0.000E+00	0.984	7.460E-02	5.344E+00	0.984	1.535E+02	1.190E-01	1.534E+02	6.097E-04	0.985
2.4 Gy/h	9.534E-02	2.600E-04	0.979	1.101E-01	5.876E-01	0.982	3.133E+01	2.529E-02	3.132E+01	4.928E-02	0.982
55.8 Gy/h	8.893E-02	3.068E-03	0.984	1.937E-01	2.276E-01	0.981	1.348E+00	3.670E-02	1.347E+00	4.609E+00	0.981
Average R ²			0.982			0.982					0.983

Table SI.5. Best fitting parameters of Jung's and Umodel to clonogenic survival data from cells exposed to HT, extracted from literature^{25,57} (sorted by temperature). For the corresponding parameters' uncertainties and Aikake information criterion values see Table SI.9..

T[°C]	Cell line	LQ-model			LQC-model				Jungs model			Unified model				
		α [min ⁻¹]	β [min ⁻²]	R^2	α [min ⁻¹]	β [min ⁻²]	γ [min ⁻³]	R^2	r [min ⁻¹]	c [min ⁻¹]	R^2	r [min ⁻¹]	c [min ⁻¹]	Q_{max} [min ⁻¹]	k [min]	R^2
40	CHO	6.589E-04	-6.383E-07	0.997	7.480E-04	-1.413E-06	1.514E-09	0.999	4.739E-04	3.000E+00	0.957	1.021E+00	1.461E-02	1.021E+00	1.224E-02	0.998
41	CHO	6.373E-04	1.231E-07	0.991	5.777E-04	6.424E-07	-1.014E-09	0.993	6.926E-04	1.372E-01	0.992	1.415E+00	1.231E-03	1.415E+00	1.101E-01	0.992
	HeLa	1.577E-03	-2.579E-06	0.827	1.880E-03	-5.716E-06	7.289E-09	0.849	9.449E-04	3.000E+00	0.724	2.450E-03	9.992E-01	1.531E-03	1.000E+00	0.738
	Average R^2			0.909				0.921			0.858					0.865
41.5	CHO	3.095E-04	1.862E-05	0.998	-1.075E-04	2.579E-05	-2.776E-08	0.998	1.417E-02	3.476E-03	0.998	1.682E+00	1.124E-03	1.646E+00	3.150E-02	0.998
41.8	CFU-GM	3.701E-03	8.534E-06	0.949	2.616E-03	2.073E-05	-3.116E-08	0.950	6.956E-03	2.459E-02	0.952	2.453E-01	3.850E-02	2.390E-01	1.161E-02	0.948
42	CFU-GM	1.249E-02	-1.042E-05	0.994	1.183E-02	-2.741E-06	-2.008E-08	0.994	1.026E-02	3.000E+00	0.984	2.641E-01	3.397E-02	2.574E-01	7.651E-01	0.994
	CHO	3.477E-03	4.002E-05	0.991	6.353E-03	-1.002E-05	1.955E-07	0.993	1.754E-02	1.251E-02	0.985	1.988E+00	1.462E-03	1.931E+00	5.000E-01	0.990
	HeLa	4.167E-03	5.351E-08	0.965	8.009E-03	-3.972E-05	9.240E-08	0.993	4.187E-03	3.000E+00	0.965	1.264E-02	1.000E+00	8.655E-03	1.000E+00	0.967
	Average R^2			0.983				0.993			0.978					0.984
42.3	CFU-GM	1.925E-02	1.332E-14	0.978	2.097E-02	1.332E-14	-5.383E-08	0.982	2.013E-02	1.517E-01	0.980	1.164E+00	1.039E-02	1.159E+00	8.850E-01	0.987
42.5	CFU-GM	2.268E-02	1.834E-04	0.995	9.439E-03	5.139E-04	-1.827E-06	0.998	5.723E-02	3.731E-02	0.998	1.189E+00	1.842E-02	1.131E+00	2.963E-01	0.998
	CHO	1.109E-02	1.056E-04	0.997	1.249E-02	6.911E-05	2.139E-07	0.997	3.080E-02	3.389E-02	0.993	2.338E+00	3.318E-03	2.275E+00	7.494E-01	0.996
	CHO	0.000E+00	3.955E-05	0.981	1.565E-03	-2.120E-06	1.609E-07	0.989	4.697E+01	1.825E-06	0.977	7.062E-02	1.237E-03	5.551E-15	1.240E-11	0.978
	Average R^2			0.991				0.995			0.989					0.991
43	CFU-GM	1.602E-02	7.614E-04	0.995	5.347E-11	1.519E-03	-8.067E-06	0.997	1.227E-01	2.698E-02	0.997	1.196E+01	2.254E-03	1.114E+01	1.193E-01	0.994
	CHO	1.207E-02	3.778E-04	0.995	5.415E-10	7.022E-04	-1.945E-06	0.997	1.129E-01	1.332E-02	0.997	2.824E+00	3.686E-03	2.586E+00	5.000E-01	0.996
	HeLa	1.506E-02	7.327E-14	0.993	1.197E-02	4.084E-05	-1.082E-07	0.999	1.508E-02	3.000E+00	0.992	6.411E-02	1.198E-01	4.965E-02	1.000E+00	0.993
	CHO	2.548E-03	3.489E-04	0.993	-9.882E-03	8.471E-04	-4.380E-06	0.999	8.833E-02	1.126E-02	0.995	1.706E-01	5.122E-03	5.000E-10	7.780E-11	0.994
	Average R^2			0.994				0.998			0.995					0.994
43.5	CHO	2.011E-02	1.012E-03	0.994	7.946E-04	2.020E-03	-1.182E-05	0.996	1.431E-01	3.210E-02	0.996	3.268E+00	3.201E-02	3.124E+00	1.000E-12	0.996
44	CFU-GM	8.774E-02	2.848E-03	0.972	1.539E-09	1.111E-02	-1.744E-04	0.981	2.369E-01	1.233E-01	0.978	5.000E+01	5.735E-03	4.911E+01	1.426E-01	0.974
	CHO	2.131E-02	1.558E-03	0.998	1.959E-02	1.665E-03	-1.492E-06	0.998	2.098E-01	2.872E-02	0.998	3.991E+00	7.904E-03	3.543E+00	3.364E-01	0.998
	HeLa	3.187E-02	3.503E-05	0.986	4.444E-02	-1.639E-04	6.824E-07	0.989	4.043E-02	1.062E-01	0.985	3.192E-01	3.656E-02	2.821E-01	1.000E+00	0.984
	Average R^2			0.985				0.989			0.987					0.985
44.5	CHO	5.083E-02	3.389E-03	0.994	1.360E-02	7.276E-03	-9.113E-05	0.996	2.307E-01	8.873E-02	0.996	4.688E+00	1.125E-02	4.166E+00	1.000E+00	0.995
45	Cal27	1.302E-02	1.052E-03	0.993	-4.542E-03	1.753E-03	-6.185E-06	0.996	2.341E-01	1.455E-02	0.996	8.254E-01	1.464E-02	5.923E-01	1.496E-12	0.996
	HCT116	1.226E-01	1.081E-03	0.989	1.408E-01	-8.326E-06	1.425E-05	0.989	1.915E-01	2.361E-01	0.986	5.522E-01	2.367E-01	3.608E-01	1.068E-05	0.986
	CHO	2.958E-02	7.314E-03	0.996	8.854E-10	1.137E-02	-1.211E-04	0.998	5.219E-01	4.518E-02	0.998	5.472E+00	4.501E-02	4.949E+00	1.016E-12	0.998
	HeLa	7.519E-02	9.124E-05	0.999	7.998E-02	-3.126E-05	7.032E-07	0.999	8.890E-02	2.156E-01	0.999	1.671E+00	2.447E-02	1.610E+00	1.000E+00	0.998
	Average R^2			0.994				0.996			0.995					0.994
46	Cal27	3.209E-02	3.867E-03	0.992	-1.750E-02	7.909E-03	-7.248E-05	0.996	3.798E-01	3.764E-02	0.995	1.860E+00	3.751E-02	1.479E+00	1.003E-12	0.995
	HCT116	2.815E-01	1.940E-03	0.987	1.238E-01	2.072E-02	-4.900E-04	0.996	3.569E-01	5.707E-01	0.992	1.875E+00	1.448E-01	1.636E+00	1.000E+00	0.993
	Average R^2			0.989				0.996			0.994					0.994
47	Cal27	2.249E-01	1.359E-02	0.983	2.659E-10	5.142E-02	-1.379E-03	0.995	6.350E-01	2.128E-01	0.991	4.253E+00	2.128E-01	3.618E+00	1.000E-12	0.991
	HCT116	5.150E-01	8.877E-03	0.985	2.083E-01	7.856E-02	-3.544E-03	0.993	6.864E-01	9.470E-01	0.987	6.790E+00	1.678E-01	6.390E+00	3.768E-01	0.988
	Average R^2			0.984				0.994			0.989					0.990
48	Cal27	5.203E-01	4.361E-02	0.991	2.689E-01	1.271E-01	-6.039E-03	0.994	1.144E+00	5.583E-01	0.992	9.986E+00	2.982E-01	8.857E+00	5.523E-02	0.992
	HCT116	7.667E-01	1.194E-01	0.993	1.122E-01	4.258E-01	-3.204E-02	0.998	1.989E+00	6.598E-01	0.997	2.838E+01	6.601E-01	2.640E+01	2.104E-11	0.997
	Average R^2			0.992				0.996			0.994					0.995

Table SI.6. Best fitting parameters of Jung's and Umodel to clonogenic survival data from cells exposed to HT, extracted from the literature: a) from reference⁵⁹, b) from reference²⁸ and c) from reference⁶⁰. For the corresponding parameters' uncertainties and Aikake information criterion values see Table SI.9.

T[°C]	Cell line	LQ-model			LQC-model				Jungs model			Unified model					
		α [min ⁻¹]	β [min ⁻²]	R^2	α [min ⁻¹]	β [min ⁻²]	γ [min ⁻³]	R^2	r [min ⁻¹]	c [min ⁻¹]	R^2	r [min ⁻¹]	c [min ⁻¹]	Q_{max} [min ⁻¹]	k [min]	R^2	
a) 41	CCD-18Lu	1.104E-03	-5.878E-08	0.989	1.251E-03	-1.085E-07	3.598E-12	0.992	6.488E-04	3.500E-01	0.846	1.360E-03	1.667E+00	1.811E-03	4.800E+03	0.993	
	WiDr	3.042E-04	-1.213E-08	0.878	4.507E-04	-6.068E-08	3.466E-12	0.903	2.098E-04	3.500E-01	0.827	4.758E-03	6.731E-03	4.628E-03	2.141E+01	0.898	
	A-549	6.017E-04	-2.998E-08	0.932	9.215E-04	-1.400E-07	8.011E-12	0.983	3.701E-04	3.500E-01	0.824	9.724E-03	3.790E-03	9.558E-03	2.790E+01	0.978	
	U-87MG	1.023E-03	2.649E-08	0.927	2.669E-03	-8.774E-07	1.100E-10	0.993	1.150E-03	3.500E-01	0.924	6.981E-03	1.667E+00	5.970E-03	1.825E+01	0.933	
	Average R^2			0.931				0.968			0.855					0.950	
a) 43	CCD-18Lu	1.690E-02	-1.450E-05	0.998	1.667E-02	-1.450E-05	0.000E+00	0.997	1.131E-02	3.500E-01	0.939	2.598E-02	3.692E-02	3.287E-02	2.198E+02	0.998	
	WiDr	1.517E-02	-1.614E-05	0.986	1.320E-02	-2.009E-06	-2.119E-08	0.988	8.906E-03	3.500E-01	0.872	6.704E-02	1.156E-02	7.521E-02	4.429E+01	0.995	
	A-549	2.401E-02	-2.173E-05	0.998	1.646E-02	2.660E-05	-7.120E-08	0.987	1.562E-02	3.500E-01	0.928	9.815E-02	1.942E-02	9.821E-02	2.480E+01	1.000	
	U-87MG	3.803E-02	-3.956E-05	0.999	1.586E-02	1.029E-04	-2.114E-07	0.958	2.270E-02	3.500E-01	0.885	5.522E-02	6.053E-02	7.186E-02	1.982E+02	0.997	
	Average R^2			0.995				0.982			0.906					0.998	
a) 45	CCD-18Lu	7.479E-02	-1.405E-04	0.991	5.547E-02	2.301E-04	-1.524E-06	0.992	5.604E-02	3.500E-01	0.961	5.259E-01	2.181E-02	5.498E-01	9.812E+00	0.995	
	WiDr	5.640E-02	6.050E-04	0.989	5.815E-02	4.730E-04	1.453E-06	0.990	1.433E-01	4.858E-02	0.982	1.157E+00	1.426E-02	1.000E+00	2.466E+00	0.985	
	A-549	1.166E-01	-9.716E-05	0.995	1.122E-01	1.513E-04	-2.040E-06	0.999	1.103E-01	3.500E-01	0.984	1.006E+00	3.142E-02	1.000E+00	4.760E+00	0.999	
	U-87MG	2.368E-01	-1.044E-03	0.981	3.170E-01	-7.261E-03	8.531E-05	0.998	2.018E-01	3.500E-01	0.979	7.644E-01	1.667E+00	5.922E-01	2.782E-01	0.996	
	Average R^2			0.989				0.995			0.976					0.994	
b) 41.5	CHO	1.310E-03	-1.005E-06	0.769	1.243E-03	-6.750E-07	-3.413E-10	0.770	7.241E-04	6.300E+00	0.684	2.198E-02	4.595E-03	2.286E-02	1.331E+01	0.801	
	42	CHO	3.894E-03	-3.617E-06	0.961	4.499E-03	-6.503E-06	2.958E-09	0.968	1.774E-03	6.300E+00	0.659	5.258E-02	1.353E-02	5.327E-02	6.349E+00	0.973
	42.5	CHO	1.924E-02	-1.392E-05	0.956	1.366E-02	1.315E-05	-2.797E-08	0.967	1.110E-02	6.300E+00	0.884	9.794E-02	4.640E-03	1.308E-01	1.338E+02	0.987
	43	CHO	0.000E+00	3.175E-04	0.961	0.000E+00	3.175E-04	0.000E+00	0.961	1.500E+01	4.241E-05	0.961	4.595E-01	1.609E-03	2.191E-01	2.660E+02	0.950
	43.5	CHO	8.936E-11	8.202E-04	0.966	8.936E-11	8.202E-04	0.000E+00	0.966	1.500E+01	1.097E-04	0.965	1.221E+00	2.450E-03	5.040E-01	4.385E-05	0.960
	44	CHO	2.898E-14	2.866E-03	0.921	1.099E-01	-8.012E-03	2.118E-04	0.998	1.500E+01	3.838E-04	0.921	2.504E+00	4.704E-03	1.219E+00	3.348E-12	0.916
	45.5	CHO	0.000E+00	1.234E-02	0.979	0.000E+00	1.234E-02	0.000E+00	0.979	1.500E+01	1.664E-03	0.978	2.559E+01	3.289E-03	1.792E+01	3.348E-12	0.978
	c) 42.2	CHO	1.502E-02	-1.472E-05	0.983	1.093E-02	1.090E-05	-3.573E-08	0.989	9.180E-03	2.100E+01	0.886	8.300E-02	5.457E-03	1.048E-01	8.000E+01	0.995
		42.3	CHO	1.706E-02	-1.772E-05	0.985	1.692E-02	-1.681E-05	-1.274E-09	0.985	9.822E-03	2.100E+01	0.861	9.401E-02	7.441E-03	1.082E-01	4.780E+01
42.4		CHO	1.929E-02	-1.779E-05	0.988	1.902E-02	-1.614E-05	-2.287E-09	0.988	1.204E-02	2.100E+01	0.922	1.043E-01	8.016E-03	1.161E-01	4.316E+01	0.991
42.5		CHO	3.143E-02	-3.348E-05	0.989	3.332E-02	-4.399E-05	1.326E-08	0.989	1.687E-02	2.100E+01	0.804	1.104E-01	9.998E-03	1.349E-01	7.999E+01	0.991
Average R^2				0.950				0.925			0.930					0.978	

Table SI.7. Best fitting parameters of the LQ, Jung's and Umodel to clonogenic survival data from cells exposed to RT, extracted from literature. For the corresponding parameters' uncertainties and Aikake information criterion values see Table SI.9.

Cell line	LQ-model			LQC-model				Jungs model			Unified model				
	α [Gy ⁻¹]	β [Gy ⁻²]	R^2	α [Gy ⁻¹]	β [Gy ⁻²]	γ [Gy ⁻³]	R^2	r [Gy ⁻¹]	c [Gy ⁻¹]	R^2	r [Gy ⁻¹]	c [Gy ⁻¹]	Q_{max} [Gy ⁻¹]	k [Gy]	R^2
Huh-7 ⁶²	1.900E+00	-1.287E-01	0.936	6.771E+00	-6.218E+00	1.535E+00	0.626	1.613E+00	1.691E+01	0.912	4.948E+01	6.441E+01	4.831E+01	2.824E-03	0.972
PLC 12C ⁶²	1.564E+00	-8.278E-02	0.992	1.873E+00	-2.603E-01	2.034E-02	0.990	1.390E+00	1.691E+01	0.983	4.949E+01	6.441E+01	4.831E+01	1.070E-03	0.998
Hep-G2 12C ⁶²	1.732E+00	-1.676E-01	0.861	5.534E+00	-4.411E+00	1.012E+00	0.905	1.338E+00	1.691E+01	0.823	4.908E+01	6.441E+01	4.831E+01	4.003E-03	0.943
Hep-G2 16C ⁶²	1.312E+00	-8.920E-02	0.997	1.695E+00	-5.129E-01	1.006E-01	0.995	1.116E+00	1.691E+01	0.985	2.345E+01	6.441E+01	2.249E+01	1.890E-03	0.998
SW1353 ⁶³	1.418E+00	-6.179E-02	0.999	1.000E+00	1.791E-01	-3.138E-02	0.995	1.181E+00	1.691E+01	0.987	1.862E+00	6.441E+01	1.066E+00	7.274E-01	1.000
HDF ⁶³	1.241E+00	-1.334E-02	0.996	9.592E-02	7.832E-01	-1.156E-01	0.990	1.207E+00	1.691E+01	0.996	1.943E+00	1.730E+00	2.576E+01	9.936E+01	1.000
XRS5 ⁶⁴	3.273E+00	-5.834E-01	0.977	1.256E+00	4.286E+00	-2.543E+00	0.977	2.759E+00	1.691E+01	0.953	5.061E+00	5.938E+00	4.829E+01	1.360E+01	0.982
Average R^2			0.950				0.925			0.930					0.978

Table SI.8. Exponential behavior of the sublethal damage accumulation rate. Parameters and coefficient of determination for all the cell models of this study. Below the line results for data sets extracted from literature are listed.

Cell line	b [min ⁻¹]	T _g [min]	R ²
Cal33	0.480	40.2	0.999
FaDu	1.783	44.5	0.998
HSC4	0.516	40.1	0.997
SAS	0.452	41.5	1.000
UT-SCC-5	0.518	39.7	0.998
UT-SCC-14	0.478	39.5	1.000
UT-SCC-60A	0.558	39.8	0.998
XF354	0.591	41.7	1.000
A549 ⁵⁹	1.160	41.5	1.000
Cal27	0.830	45.2	1.000
CFU-GM	2.587	42.3	0.953
CHO ²⁵	0.339	40.0	1.000
CHO ⁶⁵	1.764	44.0	1.000
CHO ²⁸	1.822	42.9	0.988
CHO ⁶⁰	0.960	44.8	0.975
HCT116	1.311	45.5	0.999
HeLa	1.629	44.7	1.000
U87MG ⁵⁹	1.173	41.8	0.995
WiDr ⁵⁹	1.373	41.9	1.000
18Lu ⁵⁹	1.489	42.7	1.000

Table SI.9. Parameters' uncertainties and Aikake information criterion values for the fits reported in the tables above: a) Table SI.3, b) Table SI.7, c) Table SI.2, d) Table SI.5, e) Table SI.6.

Cell line	LQ-model			LQC-model				Jungs model			Unified model				
	$\alpha[\Delta\%]$	$\beta[\Delta\%]$	<i>AIC</i>	$\alpha[\Delta\%]$	$\beta[\Delta\%]$	$\gamma[\Delta\%]$	<i>AIC</i>	$r[\Delta\%]$	$c[\Delta\%]$	<i>AIC</i>	$r[\Delta\%]$	$c[\Delta\%]$	$Q_{max}[\Delta\%]$	$k[\Delta\%]$	<i>AIC</i>
Cal-33	1.800E+01	2.054E+01	12.287	8.848E+01	4.555E+01	7.372E+01	6.974	5.943E+00	1.792E+01	4.979	5.451E+03	1.103E+02	3.718E+04	2.106E+07	8.979
FaDu	1.142E+01	3.916E+01	-15.391	1.665E+01	1.466E+01	1.797E+01	-36.659	2.457E+00	1.594E+01	-32.092	3.810E+03	3.807E+03	3.846E+03	1.684E+02	-25.269
HSC4	1.745E+01	1.241E+01	2.469	8.179E+01	3.760E+01	7.775E+01	-9.919	6.897E+00	1.536E+01	-10.316	2.385E+03	2.467E+03	2.867E+03	6.797E+02	-10.038
SAS	8.956E+00	1.288E+01	-16.643	2.443E+01	2.840E+01	5.294E+01	-22.872	3.081E+00	1.097E+01	-24.077	5.134E+03	5.391E+03	5.191E+03	9.440E+02	-25.397
UT-SCC-5	1.759E+01	1.162E+01	3.951	8.681E+01	1.396E+01	2.420E+01	-19.265	3.900E+00	8.369E+00	-17.411	NAN	NAN	NAN	NAN	-13.411
UT-SCC-14	5.733E+00	6.071E+00	-8.830	8.289E-01	6.022E+00	4.574E+00	-40.091	1.085E+01	3.047E+01	6.016	6.162E+02	2.407E+03	6.333E+02	6.040E+03	4.373
UT-SCC-60A	1.898E+01	1.620E+01	-18.365	3.787E+01	1.225E+04	1.151E+02	-19.176	1.846E+01	4.311E+01	-12.203	1.363E+03	3.159E+03	1.461E+03	9.900E+03	-11.429
XF354	8.669E+00	2.579E+02	5.067	2.936E+01	1.214E+02	1.287E+02	7.750	2.025E+00	1.868E+01	7.178	1.200E+03	8.561E+02	1.740E+03	3.874E+03	5.796

Cell line	LQ-model			LQC-model				Jungs model			Unified model				
	$\alpha[\Delta\%]$	$\beta[\Delta\%]$	<i>AIC</i>	$\alpha[\Delta\%]$	$\beta[\Delta\%]$	$\gamma[\Delta\%]$	<i>AIC</i>	$r[\Delta\%]$	$c[\Delta\%]$	<i>AIC</i>	$r[\Delta\%]$	$c[\Delta\%]$	$Q_{max}[\Delta\%]$	$k[\Delta\%]$	<i>AIC</i>
Huh-7	2.920E+01	1.644E+02	5.011	2.378E+01	4.527E+01	5.667E+01	9.890	1.489E+01	4.345E+02	7.844	1.020E+04	3.764E+02	1.044E+04	1.923E+04	0.660
PLC ¹² C	1.043E+01	7.515E+01	-1.273	3.132E+01	4.564E+02	1.918E+03	4.947	6.561E+00	2.028E+02	3.464	1.567E+02	2.990E+02	1.606E+02	3.203E+02	19.621
Hep-G2 ¹² C	3.672E+01	1.452E+02	54.227	3.523E+01	9.018E+01	1.298E+02	47.848	2.001E+01	5.293E+02	56.666	4.104E+03	2.316E+03	4.167E+03	7.572E+03	46.828
Hep-G2 ¹⁸ O	6.752E+00	3.797E+01	33.920	3.239E+01	2.191E+02	3.682E+02	32.209	6.243E+00	1.762E+02	39.462	3.050E+03	1.212E+03	3.179E+03	5.815E+03	28.173
SW1353	2.608E+00	1.384E+01	15.739	6.084E+01	1.471E+02	1.164E+02	3.706	7.280E+00	3.666E+02	23.563	1.945E+01	3.924E+02	2.887E+01	1.145E+02	20.039
HDF	8.709E+00	1.883E+02	64.041	1.878E+02	2.207E+01	2.803E+01	63.013	4.423E+00	2.398E+02	58.427	2.103E+02	2.709E+02	1.957E+04	3.214E+04	36.436
xrs5	9.536E+00	4.523E+01	-33.219	3.050E+01	2.757E+01	3.009E+01	-31.106	7.849E+00	1.186E+01	-25.194	1.583E+02	2.287E+02	3.835E+03	6.748E+03	-31.462

T[°C]	Cell line	LQ-model			LQC-model				Jungs model			Unified model				
		$\alpha[\Delta\%]$	$\beta[\Delta\%]$	<i>AIC</i>	$\alpha[\Delta\%]$	$\beta[\Delta\%]$	$\gamma[\Delta\%]$	<i>AIC</i>	$r[\Delta\%]$	$c[\Delta\%]$	<i>AIC</i>	$r[\Delta\%]$	$c[\Delta\%]$	$Q_{max}[\Delta\%]$	$k[\Delta\%]$	<i>AIC</i>
42.5	Cal-33	1.534E+01	2.118E+01	-1.605	7.381E+01	5.663E+01	9.377E+01	-5.764	7.750E+00	2.496E+01	-7.437	2.363E+03	2.957E+03	2.379E+03	4.094E+02	-2.257
	FaDu	2.780E+01	3.173E+01	2.456	2.622E+02	7.134E+01	1.058E+02	-3.947	1.360E+01	3.987E+01	-5.310	NAN	NAN	NAN	NAN	-6.749
	HSC4	3.540E+01	6.309E+01	14.546	7.910E+01	3.002E+01	3.866E+01	-7.229	1.715E+01	6.083E+01	4.490	NAN	NAN	NAN	NAN	-2.725
	SAS	1.716E+01	1.755E+01	-14.073	1.010E+02	4.522E+01	7.585E+01	-18.982	7.696E+00	2.078E+01	-23.245	NAN	NAN	NAN	NAN	-21.250
	UT-SCC-5	3.576E+01	4.876E+01	21.759	6.498E+01	2.603E+01	3.405E+01	12.464	1.740E+01	5.528E+01	17.747	1.565E+02	3.975E+03	1.609E+02	3.984E+03	25.656
	UT-SCC-14	5.084E+01	7.973E+00	-2.624	2.027E+11	3.673E+01	1.202E+02	-6.038	3.287E+01	4.192E+01	-7.576	NAN	NAN	NAN	NAN	-5.553
	UT-SCC-60A	2.982E+02	2.261E+01	0.523	5.239E+01	9.470E+01	5.303E+01	1.194	5.639E+00	1.590E-02	2.765	3.310E+04	2.594E+03	3.530E+04	4.058E+04	2.916
	XF354	2.406E+01	1.529E+01	-5.412	1.021E+02	1.179E+01	2.033E+01	-31.251	9.123E+00	1.885E+01	-18.548	4.654E+00	8.679E+01	4.759E+00	9.879E+05	-16.535
	Cal-33	1.498E+01	4.250E+01	-6.864	4.319E+01	4.971E+02	8.589E+02	-4.742	7.472E+00	4.678E+01	-7.410	4.803E+03	9.731E+02	4.850E+03	4.417E+03	-5.329
44.5	FaDu	1.924E+01	1.726E+01	10.795	7.936E+01	7.066E+01	1.665E+02	12.648	1.124E+01	2.869E+01	12.533	NAN	NAN	NAN	NAN	16.147
	HSC4	1.608E+01	8.162E+01	-10.769	7.735E+01	3.615E+01	3.988E+01	-24.389	6.429E+00	4.458E+01	-18.669	3.509E+02	5.387E+02	3.524E+02	2.570E+02	-11.928
	SAS	2.975E+01	2.313E+01	1.466	3.906E+02	5.383E+01	8.527E+01	-0.385	1.456E+01	3.480E+01	-2.521	NAN	NAN	NAN	NAN	-0.521
	UT-SCC-5	1.056E+01	7.048E+01	18.685	2.562E+01	2.399E+02	1.596E+02	21.538	5.758E+00	7.877E+01	14.620	1.745E+02	8.143E+02	1.748E+02	1.433E+03	15.850
	UT-SCC-14	1.306E+01	9.175E+01	-0.618	4.616E+01	2.900E+02	1.987E+02	-1.574	1.083E+01	1.193E+03	-3.067	6.456E+03	5.235E+03	6.442E+03	2.502E+03	-2.991
	UT-SCC-60A	2.543E+01	7.672E+01	8.446	1.382E+02	2.547E+01	3.158E+01	4.874	1.061E+01	5.244E+01	6.855	NAN	NAN	NAN	NAN	8.855
	XF354	2.185E+01	4.563E+01	21.340	1.271E+02	7.136E+01	9.353E+01	18.262	8.863E+00	3.963E+01	16.311	NAN	NAN	NAN	NAN	18.311
	Cal-33	INF	2.458E+01	-12.692	3.669E+01	4.358E+01	3.163E+01	-35.433	2.323E+01	2.729E+01	-18.996	1.287E+03	2.497E+01	1.592E+03	2.225E+06	-16.248
	FaDu	INF	2.089E+01	-8.854	8.101E+01	9.536E+01	7.584E+01	-11.822	7.910E+02	7.793E+02	-10.766	NAN	NAN	NAN	NAN	-3.674
46.5	HSC4	INF	1.810E+01	-33.938	5.946E+01	7.919E+01	5.083E+01	-46.602	3.153E+01	3.027E+01	-36.123	NAN	NAN	NAN	NAN	-29.273
	SAS	4.425E+01	1.094E+02	-5.805	6.518E+01	5.498E+01	5.681E+01	-11.001	3.078E+01	1.043E+02	-6.290	1.166E+00	2.438E+03	1.660E+01	6.620E+08	-4.309
	UT-SCC-5	2.343E+15	1.314E+01	-2.756	8.519E+01	6.390E+01	8.619E+01	25.545	1.614E+02	1.617E+02	15.000	NAN	NAN	NAN	NAN	4.017
	UT-SCC-14	3.141E+01	2.922E+01	-23.428	3.891E+02	9.973E+02	4.379E+03	-21.471	2.398E+01	4.734E+01	-23.082	4.441E+03	2.963E+03	4.573E+03	8.546E+03	-21.257
	UT-SCC-60A	2.482E+11	2.157E+01	-11.764	2.711E+01	3.045E+01	2.536E+01	-21.051	1.274E+03	1.229E+03	-11.702	NAN	NAN	NAN	NAN	-9.444
	XF354	3.313E+01	4.455E+01	-18.407	1.751E+02	3.799E+02	2.891E+02	-15.933	2.430E+01	5.865E+01	-18.338	1.215E+03	1.332E+04	1.197E+03	2.078E+04	-16.392

T[°C]	Cell line	LQ-model			LQC-model			Jungs model			Unified model					
		$\alpha[\Delta\%]$	$\beta[\Delta\%]$	AIC	$\alpha[\Delta\%]$	$\beta[\Delta\%]$	$\gamma[\Delta\%]$	AIC	r[Δ%]	c[Δ%]	AIC	r[Δ%]	c[Δ%]	$Q_{max}[\Delta\%]$	k[Δ%]	AIC
40	CHO	3.934E+00	1.348E+01	113.797	NAN	NAN	NAN	110.172	1.181E+01	8.086E+03	132.485	4.684E-02	8.377E+01	4.914E-02	7.791E+01	109.335
	CHO	1.121E+01	1.998E+02	127.040	NAN	NAN	NAN	127.958	5.784E+00	1.803E+02	127.183	2.204E+02	2.531E+03	2.210E+02	3.171E+03	126.775
41	HeLa	3.117E+01	7.530E+01	-8.728	NAN	NAN	NAN	-7.637	3.620E+01	5.965E+05	-5.299	1.977E+06	4.212E+06	3.130E+06	2.585E+06	-5.624
41.5	CHO	6.266E+01	6.941E+00	129.582	2.242E+02	2.038E+01	8.824E+01	129.483	4.230E+01	5.080E+01	127.803	2.177E+03	6.232E+02	2.217E+03	4.564E+03	128.667
41.8	CFU-GM	3.195E+01	6.159E+01	41.049	1.365E+02	1.827E+02	2.568E+02	43.897	1.668E+01	7.027E+01	41.792	2.181E+03	1.593E+02	2.238E+03	1.067E+04	40.969
42	CFU-GM	5.192E+00	2.788E+01	11.467	1.463E+01	6.847E+02	3.251E+02	18.016	4.886E+00	1.159E+00	35.781	1.261E+03	2.847E+02	1.294E+03	1.459E+03	15.646
	CHO	3.425E+01	1.983E+01	147.631	4.780E+01	4.919E+02	9.815E+01	152.755	3.179E+01	5.895E+01	149.959	4.050E+03	1.947E+03	4.129E+03	4.109E+03	147.377
	HeLa	2.464E+01	6.806E+03	-9.368	1.804E+01	3.520E+01	3.076E+01	-18.193	1.411E+01	1.801E+03	-9.331	7.722E+02	1.844E+04	1.138E+03	5.370E+03	-9.336
42.3	CFU-GM	NAN	NAN	46.379	NAN	NAN	NAN	37.727	7.007E+00	1.364E+02	49.219	1.108E+03	1.357E+03	1.129E+03	6.031E+02	38.929
42.5	CFU-GM	1.844E+01	2.111E+01	31.588	8.708E+01	3.689E+01	5.663E+01	17.380	2.278E+00	9.302E+00	18.736	NAN	NAN	NAN	NAN	20.556
	CHO	1.365E+01	1.433E+01	138.170	3.525E+01	1.551E+02	2.972E+02	139.854	1.218E+01	3.360E+01	150.942	1.239E+03	3.578E+03	1.236E+03	4.288E+03	143.183
	CHO	INF	3.036E+01	-3.525	2.452E+02	2.752E+03	1.190E+02	-5.652	7.884E+00	5.067E-03	-2.241	NAN	NAN	NAN	NAN	1.369
43	CFU-GM	3.146E+01	1.207E+01	28.315	2.186E+10	3.387E+01	6.678E+01	30.268	1.820E+01	2.990E+01	25.839	NAN	NAN	NAN	NAN	38.193
	CHO	3.117E+01	1.013E+01	189.032	1.461E+09	2.772E+01	5.863E+01	190.970	1.798E+01	2.805E+01	187.998	NAN	NAN	NAN	NAN	185.167
	HeLa	NAN	NAN	-11.294	1.035E+01	3.852E+01	3.961E+01	-16.159	6.682E+00	6.147E+04	-11.355	NAN	NAN	NAN	NAN	-10.904
	CHO	1.291E+02	1.412E+01	-12.147	2.958E+01	1.586E+01	3.006E+01	-25.239	5.591E+01	7.289E+01	-14.120	NAN	NAN	NAN	NAN	-9.830
43.5	CHO	3.672E+01	1.460E+01	155.641	2.296E+03	4.400E+01	8.703E+01	151.030	2.032E+01	3.472E+01	150.356	NAN	NAN	NAN	NAN	150.327
44	CFU-GM	3.438E+01	3.771E+01	69.083	5.668E+09	6.867E+01	8.994E+01	64.409	1.766E+01	4.956E+01	65.795	2.604E+03	4.404E+03	2.611E+03	3.762E+03	68.230
	CHO	2.767E+01	8.974E+00	126.848	9.584E+01	6.551E+01	1.008E+03	127.783	2.471E+01	3.734E+01	115.483	3.282E+03	2.629E+02	3.830E+03	3.191E+03	120.493
	HeLa	1.652E+01	8.439E+01	4.805	3.118E+01	1.250E+02	1.037E+02	3.226	7.873E+00	1.061E+02	6.387	2.883E+03	3.867E+02	3.266E+03	1.161E+03	6.816
44.5	CHO	2.743E+01	1.646E+01	154.719	2.511E+02	4.570E+01	8.443E+01	143.006	1.446E+01	2.956E+01	138.226	1.906E+03	2.671E+03	1.955E+03	2.257E+03	148.017
45	Cal27	5.195E+01	1.003E+01	-18.167	9.118E+01	1.265E+01	3.976E+01	-28.821	2.808E+01	3.898E+01	-26.964	NAN	NAN	NAN	NAN	-24.902
	HCT116	1.412E+01	3.487E+01	14.563	2.878E+01	2.640E+04	1.986E+02	20.443	6.650E+00	5.187E+01	0.187	2.570E+03	5.494E+02	3.939E+03	1.019E+07	2.278
	CHO	3.428E+01	6.837E+00	231.136	7.291E+09	2.020E+01	5.378E+01	222.460	1.781E+01	2.445E+01	221.574	NAN	NAN	NAN	NAN	221.475
	HeLa	5.444E+00	4.354E+01	-13.781	1.838E+01	1.131E+03	2.866E+02	-12.349	3.370E+00	5.680E+01	-6.667	7.934E+02	1.124E+03	8.243E+02	1.975E+03	-5.032
46	Cal27	4.356E+01	1.137E+01	-16.002	6.566E+01	1.560E+01	3.801E+01	-29.552	2.235E+01	3.382E+01	-23.382	NAN	NAN	NAN	NAN	-21.440
	HCT116	1.258E+01	7.944E+01	26.270	3.723E+01	2.408E+01	2.613E+01	9.558	4.731E+00	4.372E+01	12.462	4.732E+02	2.163E+01	5.675E+02	7.997E+02	14.330
	Cal27	2.382E+01	2.461E+01	-0.734	1.754E+10	2.403E+01	3.193E+01	-13.311	1.019E+01	2.788E+01	-7.866	NAN	NAN	NAN	NAN	-5.867
47	HCT116	1.507E+01	7.566E+01	-12.970	7.014E+01	3.918E+01	4.355E+01	3.883	7.228E+00	5.885E+01	6.309	2.172E+03	4.913E+03	2.430E+03	1.427E+03	5.761
	Cal27	1.483E+01	2.200E+01	52.911	6.649E+01	1.935E+01	6.547E+01	48.832	7.920E+00	2.693E+01	50.632	3.338E+03	6.475E+02	3.750E+03	6.642E+03	52.373
48	HCT116	1.865E+01	2.108E+01	-12.054	1.712E+02	1.966E+01	2.697E+01	-20.755	6.867E+00	2.062E+01	-22.422	NAN	NAN	NAN	NAN	-20.428

T[°C]	Cell line	LQ-model			LQC-model			Jungs model			Unified model					
		$\alpha[\Delta\%]$	$\beta[\Delta\%]$	AIC	$\alpha[\Delta\%]$	$\beta[\Delta\%]$	$\gamma[\Delta\%]$	AIC	r[Δ%]	c[Δ%]	AIC	r[Δ%]	c[Δ%]	$Q_{max}[\Delta\%]$	k[Δ%]	AIC
41	CCD-18Lu	4.235E+00	9.770E+00	-33.180	7.366E+00	2.617E+01	5.633E+01	-35.290	1.277E+01	1.902E+05	-4.048	2.127E+01	2.071E+04	2.178E+01	1.043E+02	-36.217
	WiDr	1.903E+01	5.838E+01	-26.368	2.888E+01	6.521E+01	8.067E+01	-26.667	1.600E+01	2.902E+04	-22.852	6.860E+03	5.363E+03	7.048E+03	8.664E+03	-26.114
	A-549	1.023E+01	2.522E+01	-31.825	7.577E+00	1.545E+01	1.934E+01	-47.774	1.182E+01	2.369E+05	-19.508	8.427E+02	2.274E+02	8.562E+02	3.883E+04	-44.512
	U-87MG	4.391E+01	3.441E+02	-1.716	1.494E+01	2.307E+01	2.209E+01	-14.238	1.831E+01	4.641E+04	-1.537	4.296E+03	6.698E+05	5.030E+03	5.272E+03	-0.217
43	CCD-18Lu	2.970E+00	8.429E+00	-33.517	3.833E-08	4.687E+01	INF	-28.064	1.489E+01	9.578E+01	-8.015	5.356E+01	1.176E+01	2.197E+01	2.145E+02	-31.638
	WiDr	7.811E+00	1.787E+01	-21.498	2.452E+01	1.074E+03	1.510E+02	-20.453	2.179E+01	2.176E+02	-6.026	4.917E+01	6.652E+02	5.762E+01	7.583E+02	-27.030
	A-549	2.957E+00	7.960E+00	-28.700	1.284E+01	1.464E+02	8.080E+01	-12.283	1.601E+01	1.607E+03	-2.424	1.580E+02	9.332E+01	1.566E+02	2.480E+02	-43.643
	U-87MG	2.057E+00	4.820E+00	-27.323	4.115E+01	1.004E+02	6.913E+01	0.755	1.966E+01	3.420E+03	5.805	9.388E+01	2.195E+02	2.364E+01	1.246E+02	-17.010
45	CCD-18Lu	5.776E+00	2.075E+01	-22.823	7.365E+00	5.486E+01	4.566E+01	-21.837	7.841E+00	6.179E+02	-6.242	2.963E+02	2.086E+02	2.524E+02	3.050E+02	-27.951
	WiDr	8.542E+00	1.703E+01	-13.281	1.248E+01	8.256E+01	2.833E+02	-12.237	1.615E+01	4.590E+01	-9.326	9.228E+02	2.987E+03	1.597E+02	5.946E+03	-9.024
	A-549	3.318E+00	6.146E+01	-15.363	4.404E+00	1.306E+02	7.630E+01	-25.189	6.996E+00	1.926E+02	-6.496	NAN	NAN	NAN	NAN	-25.104
	U-87MG	1.325E+01	8.497E+01	-2.626	1.172E+01	3.592E+01	4.124E+01	-10.988	1.200E+01	1.802E+02	-2.050	3.885E+04	2.531E+04	5.011E+04	5.726E+04	-8.183

41.5	CHO	3.118E+01	6.729E+01	-38.112	7.240E+01	5.723E+02	9.745E+02	-36.126	2.865E+01	5.926E+04	-35.292	2.671E+03	2.155E+03	2.599E+03	1.907E+03	-39.462
42	CHO	8.255E+00	1.466E+01	-42.628	1.460E+01	4.291E+01	8.726E+01	-42.431	2.252E+01	5.826E+04	-23.090	7.172E+01	5.437E+01	7.106E+01	1.482E+02	-45.985
42.5	CHO	1.204E+01	2.747E+01	-8.252	3.142E+01	1.397E+02	6.656E+01	-9.328	1.344E+01	3.347E+04	2.502	2.770E+02	9.014E+02	3.541E+02	5.173E+02	-21.257
43	CHO	INF	3.121E+01	-6.178	INF	4.109E+02	INF	-4.178	1.060E+05	5.443E+04	-6.156	1.007E+04	8.871E+03	1.710E+04	4.545E+04	-4.447
43.5	CHO	2.146E+10	2.796E+01	-3.713	7.498E+10	2.516E+02	INF	-1.713	1.513E+04	1.459E+04	-3.662	9.690E+07	5.950E+03	2.348E+08	7.780E+08	-2.650
44	CHO	1.857E+14	5.572E+01	-4.542	3.028E+01	2.669E+01	1.584E+01	-28.180	7.641E+05	1.515E+04	-4.499	NAN	NAN	NAN	NAN	-4.041
45.5	CHO	INF	1.621E+01	-15.111	INF	4.899E+01	INF	-13.111	2.313E+03	2.248E+03	-14.837	NAN	NAN	NAN	NAN	-14.575

42.2	CHO	7.589E+00	1.879E+01	-22.394	2.586E+01	1.534E+02	7.739E+01	-24.154	1.632E+01	2.436E+02	-7.210	4.137E+02	1.055E+02	3.669E+02	1.465E+02	-29.516
42.3	CHO	7.764E+00	1.762E+01	-18.595	NAN	NAN	NAN	-16.598	2.007E+01	1.303E+05	-3.169	1.491E+03	1.211E+01	1.323E+03	1.797E+03	-18.534
42.4	CHO	7.513E+00	1.945E+0													

Table SI.10. Parameters a) and uncertainties b) of the Umodel, applied to arginine deprivation experiments shown in Fig. 6 on the main text.

Cell line	LQ-model			LQC-model				Jungs model			Unified model				
	$\alpha[\text{Gy}^{-1}]$	$\beta[\text{Gy}^{-2}]$	R^2	$\alpha[\text{Gy}^{-1}]$	$\beta[\text{Gy}^{-2}]$	$\gamma[\text{Gy}^{-3}]$	R^2	$r[\text{Gy}^{-1}]$	$c[\text{Gy}^{-1}]$	R^2	$r[\text{Gy}^{-1}]$	$c[\text{Gy}^{-1}]$	$Q_{\max}[\text{Gy}^{-1}]$	$k[\text{Gy}]$	R^2
a) SAS control	2.223E-01	1.832E-02	0.999	1.559E-01	3.895E-02	-1.438E-03	1.000	4.885E-01	5.433E-01	0.999	4.025E+01	1.582E-02	3.965E+01	3.553E-01	1.000
SAS -Arg	6.757E-01	8.169E-11	0.997	5.709E-01	3.529E-02	-2.583E-03	0.999	7.156E-01	2.415E+00	0.995	3.959E+01	7.476E-02	4.026E+01	1.794E-01	0.999
SAS -Arg+Cit	6.829E-01	-8.958E-03	0.999	6.330E-01	4.342E-03	-8.111E-04	0.999	6.464E-01	2.415E+00	0.990	4.026E+01	8.052E-01	3.978E+01	6.919E-03	0.998
Average R^2			0.998				0.999			0.995					0.999
FaDu control	3.499E-01	1.209E-02	0.996	1.886E-01	6.221E-02	-3.493E-03	1.000	5.168E-01	1.026E+00	0.999	3.624E+01	1.473E-02	4.026E+01	1.168E+00	0.999
FaDu -Arg	2.886E-01	2.419E-02	1.000	3.369E-01	9.198E-03	1.045E-03	1.000	6.381E-01	5.433E-01	0.995	4.026E+01	6.041E-02	3.936E+01	6.072E-02	0.998
FaDu -Arg+Cit	4.059E-01	1.078E-02	0.998	5.338E-01	-2.895E-02	2.769E-03	1.000	5.236E-01	2.415E+00	0.993	3.240E+01	8.051E-01	3.189E+01	2.457E-03	0.993
Average R^2			0.998				1.000			0.996					0.997
Cell line	LQ-model			LQC-model				Jungs model			Unified model				
	$\alpha[\Delta\%]$	$\beta[\Delta\%]$	AIC	$\alpha[\Delta\%]$	$\beta[\Delta\%]$	$\gamma[\Delta\%]$	AIC	$r[\Delta\%]$	$c[\Delta\%]$	AIC	$r[\Delta\%]$	$c[\Delta\%]$	$Q_{\max}[\Delta\%]$	$k[\Delta\%]$	AIC
b) SAS control	8.956E+00	1.288E+01	-16.643	2.443E+01	2.840E+01	5.294E+01	-22.872	2.396E+00	8.904E+00	-24.077	2.973E+03	3.026E+03	3.005E+03	3.965E+02	-25.397
SAS -Arg	NAN	NAN	-6.444	6.481E+00	3.995E+01	4.463E+01	-14.710	4.022E+00	1.656E+01	-1.180	2.975E+03	2.535E+03	2.996E+03	9.442E+02	-8.339
SAS -Arg+Cit	4.246E+00	4.879E+01	-9.202	1.322E+01	5.595E+02	2.062E+02	-7.535	5.709E+00	3.564E+01	2.560	NAN	NAN	NAN	NAN	-3.529
FaDu control	1.142E+01	3.915E+01	-15.392	1.666E+01	1.466E+01	1.797E+01	-36.658	2.457E+00	1.594E+01	-32.093	1.045E+04	1.024E+04	1.051E+04	5.977E+02	-25.270
FaDu -Arg	5.497E+00	7.773E+00	-26.309	1.027E+01	1.093E+02	6.623E+01	-20.618	7.339E+00	2.612E+01	-2.078	7.370E+02	2.262E+03	7.404E+02	4.669E+03	-6.002
FaDu -Arg+Cit	8.218E+00	3.668E+01	-13.177	7.820E+00	4.188E+01	3.014E+01	-25.009	4.939E+00	2.244E+02	-10.968	1.249E+03	1.498E+03	1.270E+03	3.642E+02	-4.407

Table SI.11. Umodel fitting parameters to clonogenic survival data for different cell lines exposed to TRT: a) SAS and b) FaDu. For each cell line q_{\max} and k are kept constant at a) $q_{\max} = 2.465\text{E-}07 \text{ Gy}^{-1}$ and $k = 1.242 \text{ Gy}$, b) $q_{\max} = 0.4555 \text{ Gy}^{-1}$ and $k = 0.596 \text{ Gy}$.

	T[°C]	HT time [min]	$r_{\text{new}} [\text{Gy}^{-1}]$	$c_{\text{new}} [\text{Gy}^{-1}]$	TER = $\frac{r_{\text{new}}}{r_{\text{old}}}$	R^2
a) SAS	40.5	0.0	0.525	0.623	1.000	0.999
		15.0	0.547	0.515	1.040	0.996
		17.5	0.548	0.569	1.043	0.997
		20.0	0.549	0.560	1.045	0.981
		30.0	0.568	0.540	1.081	0.997
	42.5	0.0	0.525	0.623	1.000	0.999
		15.0	0.778	0.476	1.482	0.986
		17.5	0.835	0.552	1.591	0.992
		20.0	0.867	0.552	1.650	0.972
		30.0	1.030	0.552	1.961	0.971
	44.5	0.0	0.525	0.623	1.000	0.992
		15.0	1.405	0.144	2.676	0.988
		17.5	1.551	0.152	2.953	0.991
		20.0	1.701	0.171	3.239	0.962
	b) FaDu	40.5	0.0	1.610	0.327	1.000
15.0			2.703	0.115	1.679	0.970
17.5			2.886	0.118	1.792	0.993
20.0			3.067	0.104	1.905	0.975
30.0			3.791	0.073	2.354	0.946
42.5		0.0	1.610	0.327	1.000	0.992
		15.0	3.541	0.085	2.199	0.964
		17.5	3.888	0.093	2.414	0.992
		20.0	4.189	0.076	2.602	0.950
		30.0	5.487	0.059	3.408	0.948
44.5		0.0	1.610	0.327	1.000	0.949
		15.0	4.194	0.057	2.605	0.981
		17.5	4.624	0.064	2.871	0.990
		20.0	5.064	0.059	3.145	0.962